RODRIGO GIANNI FERREIRA

DEVELOPMENT OF 3RD GENERATION STEEL COMBINING HIGH TOUGHNESS AND STRENGTH FOR PETROLEUM AND AUTOMOTIVE APPLICATIONS

Trabalho de Conclusão de Curso apresentado à Escola Politécnica da Universidade de São Paulo para obtenção do diploma de Engenharia de Petróleo.

SANTOS

2021

RODRIGO GIANNI FERREIRA

DEVELOPMENT OF 3RD GENERATION STEEL COMBINING HIGH TOUGHNESS AND STRENGTH FOR PETROLEUM AND AUTOMOTIVE APPLICATIONS

Trabalho de Conclusão de Curso apresentado à Escola Politécnica da Universidade de São Paulo para obtenção do diploma de Engenharia de Petróleo.

Área de concentração: Metalúrgica

Orientador: Pascal Jacques

SANTOS

2021

FICHA CATALOGRÁFICA

Ferreira, Rodrigo
Development of 3rd generation steel combining high toughness and strength for Petroleum and automotive applications / R. Ferreira -- São Paulo, 2021.
96 p.

Trabalho de Formatura - Escola Politécnica da Universidade de São Paulo. Departamento de Engenharia de Minas e de Petróleo.

1.Metais 2.Aço carbono 3.Metalurgia ferrosa 4.Metalografia I.Universidade de São Paulo. Escola Politécnica. Departamento de Engenharia de Minas e de Petróleo II.t.

Abstract

Weight reduction was always an objective to the automotive industry to reduce production costs and fuel consumption. The petroleum industry is also avid for new developments as it is always looking for the cutting-edge developments on materials to be used. Thus, motivating the industry to develop new 3rd generation advanced high strength steels (AHSS) combining toughness, strength, and ductility. The obtained materials showed an outstanding potential to combine all the desired properties. It was also observed an excellent formability and interesting properties in comparison to the currently developing 3rd generation steels. The study presented here investigated the resulting microstructure on a medium manganese steel with high carbon content and silicon that was submitted to a full austenization at 1000°C and quenching, followed by Intercritical annealing at either 750°C or 700°C for 5 minutes and finally a bainitic maintain at 360°C for either 15 or 30 minutes. SEM observations were performed to observe the microstructure, succeeded by tensile tests to measure the mechanical properties Finally fractography and damage observations were made to evaluate the fracture mechanism and calculate the fracture strain. It was observed two main microstructures related to the annealing temperature, one containing ferrite, bainite and retained austenite (presenting TRIP effects) for 750°C and the other containing ferrite and cementite for 700°C. The steels presented remarkable mechanical properties such as an ultimate tensile stress up to 1327,23 MPa and uniform elongation up to 23,11%.

Keywords: AHSS, TRIP effect, medium manganese steel, microstructure, retained austenite

Resumo

A redução do peso dos materiais sempre foi um objetivo para a indústria automotiva, a fim de reduzir custos de produção e consumo de combustíveis. A indústria do petróleo também é avida por novos desenvolvimentos já que está sempre à procura de materiais de ponta para utilização. Deste modo, motivando a indústria a desenvolver os metais avançados de alta resistência de terceira geração (AHSS do inglês) combinando tenacidade, resistência e ductilidade. Tais materiais apresentam um grande potencial para combinar todas essas propriedades desejadas. Também foi observado uma excelente formabilidade e propriedades interessantes em comparação com os metais de terceira geração que estão sendo desenvolvidos. O estudo neste apresentado investigou a microestrutura resultante de um aço de médio manganês com alto conteúdo de carbono e silício, que foi submetido a uma austenização total a 1000º C e temperado, seguido por um recozimento Intercrítico a 750º C ou 700º C por 5 minutos. E finalmente uma manutenção bainítica a 360º C por 15 ou 30 minutos. Observações no MEV foram realizadas para observar a microestrutura, seguida pelo teste de tensão para medir as propriedades mecânicas do material. Finalmente a fractografia e observação dos danos para avaliar o mecanismo de fratura e calcular a deformação de fratura. Foram observadas duas principais microestruturas relacionadas a temperatura de recozimento, uma contendo ferrita, bainita e austenita retida (apresentando efeitos TRIP) para 750º C e outra contendo ferrita e cementita para 700º C. Os metais apresentaram propriedades mecânicas notáveis como uma tensão de tração máxima de até 1327,23 Mpa e um alongamento uniforme de até 23,11%.

Palavras-chave: AHSS, efeitos TRIP, aço de médio manganês, microestrutura, austenita retida

Acknowledgments

I would like to thank my thesis advisor Prof. Pascal Jacques who firstly taught me and got my interest on this subject and after guided me on the right direction. He gave me the technical support I needed, and his comments were crucial for the construction of this thesis.

I would also like to express my gratitude to Thibaut Heremans for his constant support and guidance along the whole experimental and writing process. He introduced me to the laboratory and techniques in detail, guiding me on obtaining and treating the data. Also, without his active participation and patience, this project could not have been conducted.

In addition, I would like to thank my family for their non-stop support along these years living in another continent, especially my parents Denise Gianni Ferreira and Renato Rodrigues Ferreira. This journey was only possible thanks to you.

Finally, my gratitude for both the Universidade de São Paulo and for the Université Catholique de Louvain for the opportunity to pursuit a double degree program that enriched me with more knowledge.

Rodrigo Gianni Ferreira

Contents

List of Figures

List of Tables

Chapter 1

Introduction

The weight of vehicles is directly related to fuels consumption and the emission of greenhouse gases, as reducing the weight reduces the fuel consumption on an average on 4,9% for each 10% reduction on the total weight (49). Steels are the most utilized material on cars, applied on doors, chassis, and support beans and therefore are the first target to weight reduction. But reducing the amount of steel on a vehicle comes with safety problem, a decrease of 100 kg can cause an increase of the safety risk of 3 to 4,5% (49). This incentivizes the development of more efficient steels that can stand the same load with smaller amounts of material and therefore, reduce weight while maintaining the vehicle's safety.

Improving the metal's proprieties can also be of use to the petroleum industry for many applications, such as drill pipes, drill collars, drill bits or any other application that benefits from high resistance and weight reduction. These proprieties combined could reduce costs and facilitate the maneuver of the equipment on the drilling sites. Culminating on time savings, that is a main target on the industry

The automotive industry utilizes huge amounts of steel on the manufacture of a large amount of car parts, generally on steel sheets as they are easily shaped and can be stamped. Even though steel has been utilized for decades it is now suffering from a strong competition with low density metals (**Error! Reference source not found.**). This led to the need of developing higher strength steels targeting to cause weight reduction while maintaining or improving crashworthiness of the vehicle. These steels being developed are normally named Advanced high strength steels (AHSS) and are designed to combine once contradictory properties, toughness (ductility) and strength.

Toughness and strength are generally correlated on mild steels and conventional high strength steels (HSS) and can be seen on Figure 1, with increasing elongations the metal present lower tensile strength and with increasing tensile strength the maximum elongation is reduced. This causes optimization problems as different types of steels will be best suited for each application, materials with high total elongations can be utilized on deep drawing manufacturing but the produced parts cannot be utilized for applications that demand higher toughness such car

crashes. To fulfil the need of an easy to shape steel that can also be utilized for high strength applications the AHSS can be used to optimize both once contradictory proprieties. Three AHSS family can be separated on three generations (37).

The 1st generation AHSS is includes Dual-Phase steels (DP), transformation induced plasticity steels (TRIP), complex phase steel (CP) and martensitic steel (MS). These steel types mainly present more than one phase, and its proprieties results from the combination of the advantages of each phase. This generation can be identified on Figure 1 in an imaginary curve slightly above the curve for mild steels and HSS.

The 2nd generation AHSS includes the Twinning Induced Plasticity steels (TWIP) , Nano-TWIP, Duplex and Triplex steels. These steels present outstanding mechanical properties, with both high total elongation and tensile strength. But their Mn content is very high, exceeding 15 Wt% causing then to be considerably more expensive and therefore economically unviable for the automotive industry. This generation can be observed in light blue on the top-right corner of Figure 1.

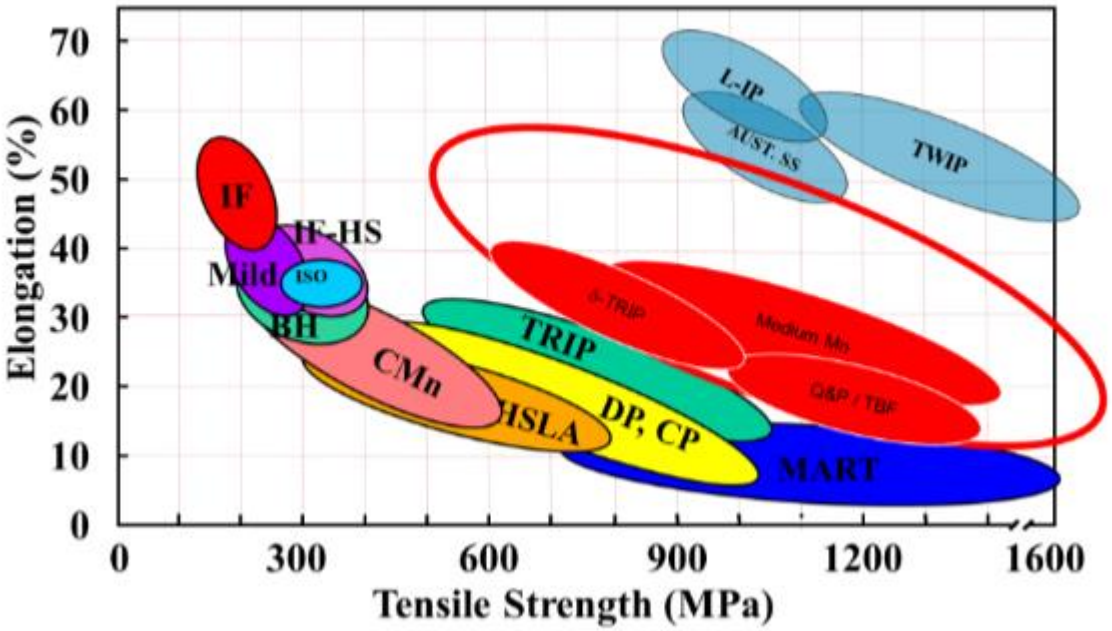

*Figure 1: Mechanical proprieties of steels with highlighted area for 3rd generation steels development (extracted from (**Error! Reference source not found.**))*

The 3rd generation of AHSS is the ongoing development and is targeting to fill the gap between the 1st and 2nd generations (Figure 1 , indicated on the circled region) while maintaining an economically viable price. The 3rd generation include the medium Mn steels, TRIP-aided Bainitic Ferrite TBF), quenching and partitioning steel

(Q&P) and δ-TRIP steels. These materials will be discussed further on Chapter 2.

Nowadays the AHSS are utilized on almost every new vehicle design and are predicted to replace 60% of the used HSS (50). They are also reported to reduce the vehicle body weight by 25 to 39% and on a five-passenger vehicle to reduce the final weight by 170 to 270 kg (50),maintaining the safety and increasing fuel efficiency. Figure 2 illustrates the used of different types of steels on a vehicle's body where HSS is present where impact absorption is important and therefore, the potential parts that can be replaced by AHSS

Figure 2: Types of steels used for each body part (50)

A growth on the consumption of AHSS is expected (50) for automotive applications, construction, and others, with the main driver being the automotive industry (Figure 3) and therefore, the defining the targeted proprieties on the developing steels.

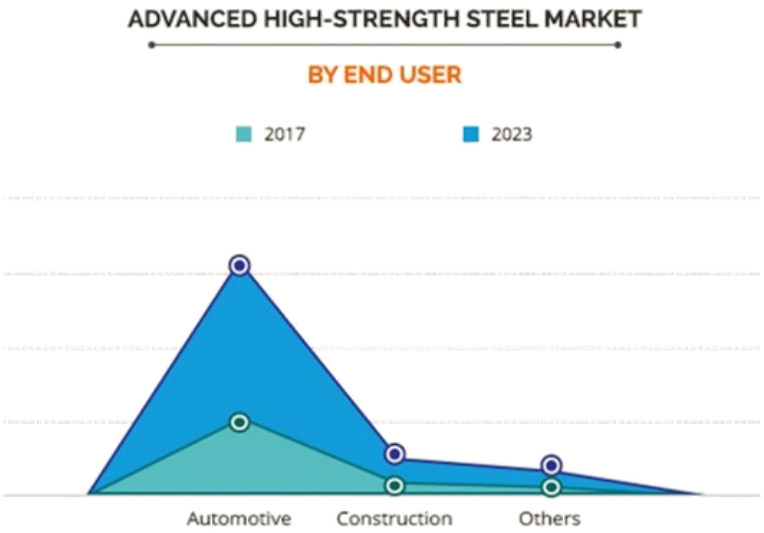

Figure 3: AHSS market in 2017 and 2023 prediction (modified from (50))

The goal of this thesis is to investigate the effects of heat treatments and compositions on final microstructure of a 3rd generation steel and its influence on the final mechanical proprieties on the steel and possibly obtain strain hardening with the aid of transformation induced plasticity (TRIP). Targeting the best compromise between toughness, ductility and strength and compare it with the existing steels being or already developed. It is desirable to identify the failure mechanism and causes for the premature failures.

Chapter 2

State of the Art

This chapter is going to discuss the actual state and knowledge about basic phase transformations on steels. Including the effect of allowing elements, basic phase transformations, different generations, and types of steels, as well as various effects such as TRIP effects and strain hardening.

2.1 Theoretical background

2.1.1 Basic phase transformations

The phase diagram illustrates the nature of the phase on the equilibrium state at a given temperature, composition, phase proportions and pressure. Figure 4 shows an example of phase diagram for iron-Carbon alloy

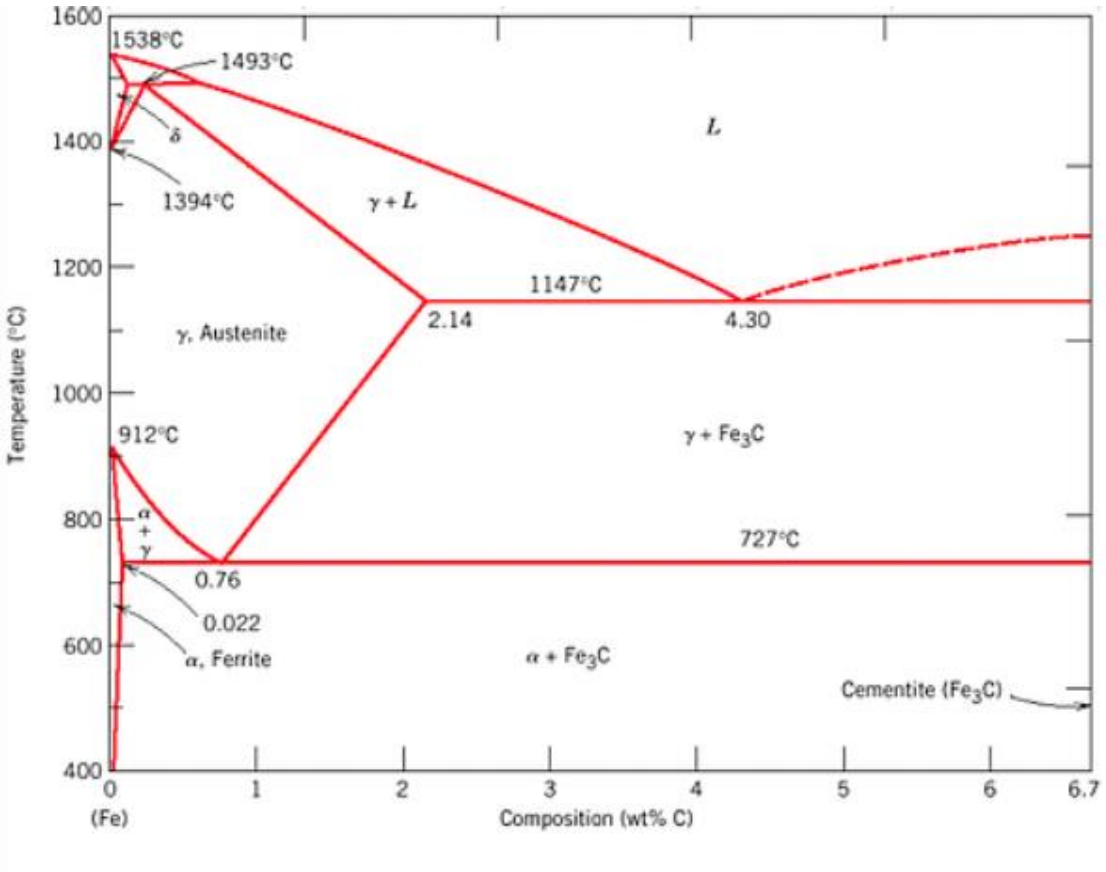

Figure 4 : Iron-Carbon phase diagram (extracted from(16))

On Figure 4 it is possible to identify the thermodynamically stable phase at each combination of composition and temperature and from that initial point trace the cooling path (considering a slow cooling) to determine the final phase on the steel being analyzed, with the phase proportions being calculated by the inverse lever rule.

One important points on this phase diagram is the eutectoid point. Found at a carbon content of 0.76% and temperature of 727 °C. At this point the steel cools from austenite, separating into layers of ferrite and cementite, this formation can be called perlite. The reverse reaction is also possible. The eutectic point at 1148°C and 4.25 weight % C is also important as the liquid solidifies into austenite and cementite.

Steels are iron alloys with a maximum carbon content of 2% in weight, on higher weight percent of the material is cast iron.

The main types of phase transformation on steels are the allotropic transformation, precipitation, eutectoid transformation, order reaction and massive transformation, being divided into reconstructive transformation and displacive transformation.

The allotropic transformation implies a change in crystalline structure, always targeting the most compact packing possible, the possible packings for pure iron are the FCC (Austenite), BCC (α-ferrite) and HCP (δ-ferrite). Due to thermal agitation, more open structures may be induced such as the FCC or the HCP, this may also be caused by contributions of the covalent bounding that imposes a directionality not compatible to the most packed structure.

Precipitation is caused by the variation of solubility with temperature, as can be seen on Figure 4. It starts on a supersaturated solid solution and from that, produces a more stable solid solution maintaining the same crystal structure and a precipitate. The massive transformation, on which the crystal structure changes without a change on composition.

Reconstructive transformations are diffusion-based processes being characterized by a total reconstruction of the lattice, with diffusion length larger than the atomic distance and with different neighboring atoms than on the initial state. An example of this type of transformations is the austenization of steels regeneration austenite grains.

Displacive transformations are diffusionless processes being characterized by coordinated displacement of atoms in an analog way of shearing a lattice where the displacement is smaller than the atomic distance and keeping the same neighboring atoms. An example of this type of transformation is the martensite transformation happening during the quenching after an austenization. The martensite transformation is a shift from an FCC lattice into a BC lattice.

It is also important to consider the cooling rate of the transformations, this is represented on the continuous cooling transformation (CCT) phase diagram, shown on Figure 5.

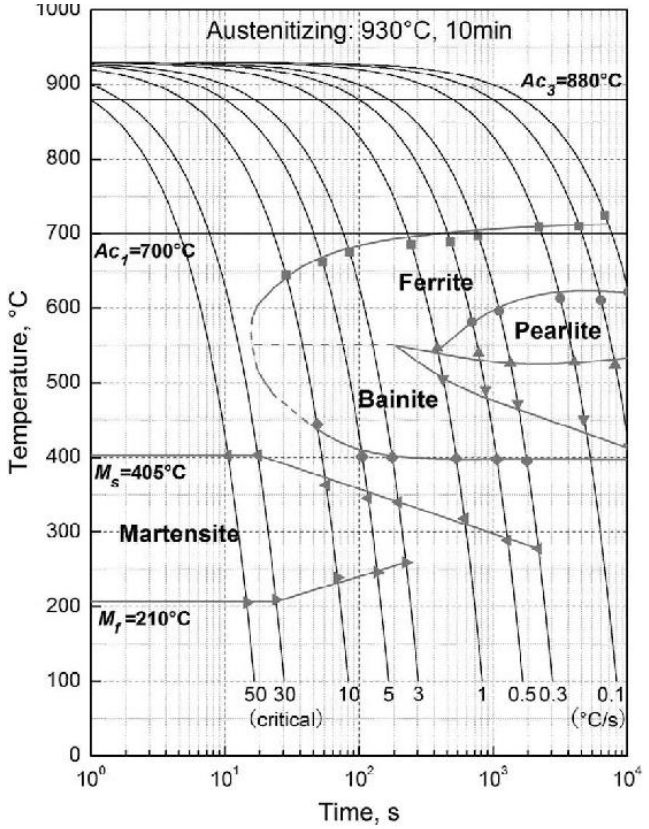

*Figure 5: CCT diagram of Fe – 0,25C – 1,5 Mn – 1,2 Ni – 0,05 Nb (mass %) extracted from (**Error! Reference source not found.**)*

By following the various cooling rate lines and the temperatures it is possible to predict the formed phase as well as the minimum cooling rate to form a martensitic structure (critical cooling rate). As one can see, the slower the cooling rates are the more difficult is for the martensite to be formed as with longer cooling periods there is more time for diffusion to occur and produce other phases.

Different results are also achieved by maintaining the metal at a constant temperature for a period, represented by the Time Temperature transformation (TTT) phase diagram, as is shown on Figure 6.

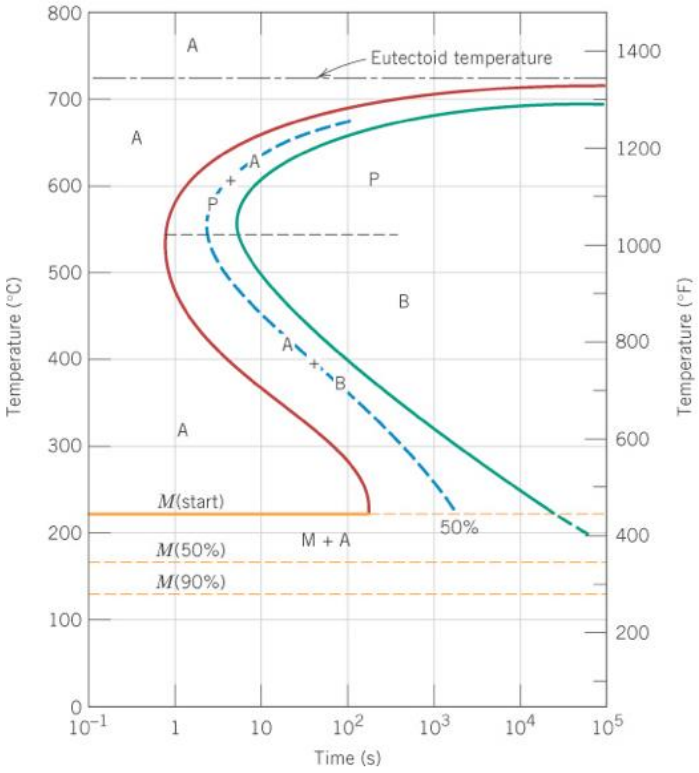

Figure 6: TTT diagram of carbon steel with eutectoid composition extracted from (21)

By setting a fixed temperature and with a specific holding time, it is possible to predict the final phases of the metal by using the TTT diagram, and it can be also utilized to identify the temperature that martensite start be formed by maintaining that temperature. By holding the temperature, different transformations can occur by various mechanisms such as diffusion, producing phases like bainite and pearlite.

2.1.2 TRIP effects

TRIP stands for Transformation Induced Plasticity, consisting of the transformation of metastable austenite into martensite during plastic deformation (14) (Figure 7). This transformation of the retained austenite into high carbon martensite can occur on room temperature and increases the strain-hardening rate and the overall strength of the steel while postponing the occurring of necking. During this transformation, the steel's ductility can either be maintained or increase even with the higher strength (14).

TRIP steels present a microstructure with austenite with enough instability to be transformed into martensite but stable enough to be present on the microstructure at the end of the heat treatments as retained austenite. Generally, the retained

austenite is contained inside a hard phase matrix, such as, ferrite or bainite.

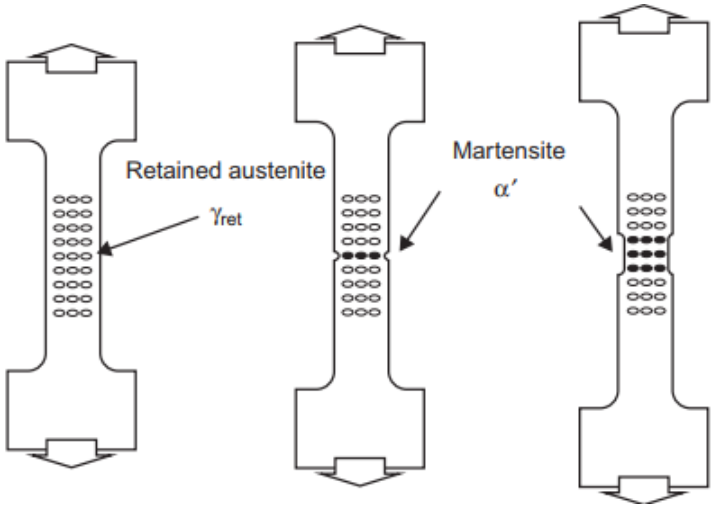

*Figure 7: Schematic of TRIP mechanisms during a tensile test (extracted from (**Error! Reference source not found.**))*

To provide stability for the retained austenite, high carbon contents are utilized as well as γ- stabilizers, such as, manganese, as illustrated on Figure 8 with increasing amounts of Mn the phase transformations change, increasing the maximum temperature for the Intercritical domain and mainly reducing the minimum temperature to reach the Intercritical domain. The stability of the retained austenite is also a parameter influencing the strain level at which the austenite begins to transform into martensite.

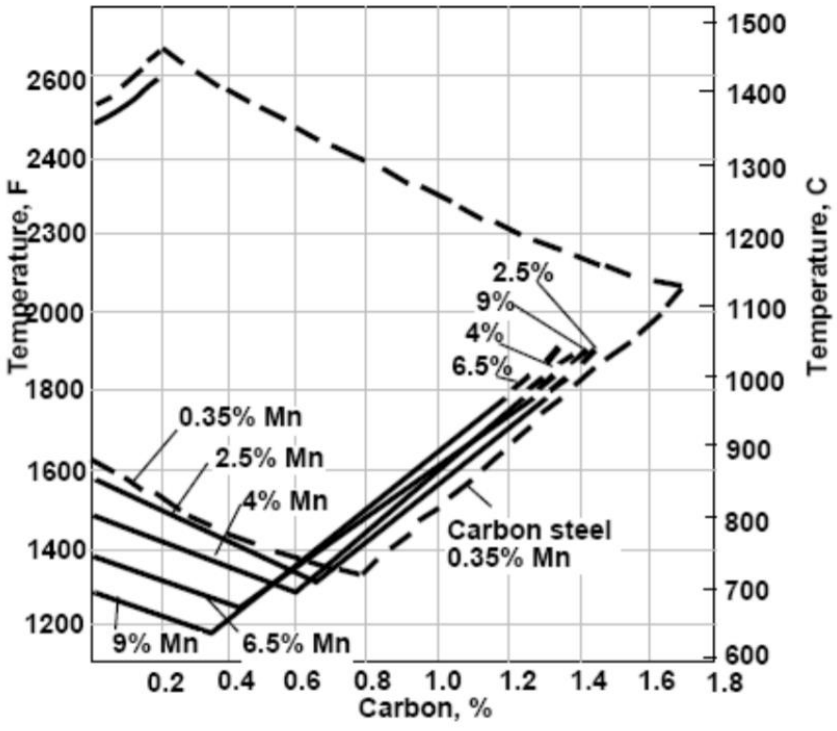

Figure 8: Manganese influence on the γ-phase field by weight (extracted from (15))

To balance the phase proportions on the final steel, silicon and/or aluminum may be added as α-stabilizers, with opposite effect as the Mn, increasing the minimum temperature to reach the Intercritical domain, to promote and speed up the formation of ferrite and bainite while avoiding the formation of carbides on the bainite ensuring good stability of the retained austenite.

The transformation from austenite to martensite is a diffusionless shear transformation following the displacive mechanism and can be of three different types (14):

- Athermal martensitic transformation.
- Stress-assisted martensitic transformation.
- Strain-induced martensitic transformation.

The Athermal transformation is only temperature dependent with starting temperature M_s. The stress-assisted transformations occur at temperatures above M_s with the presence of a mechanical driving force. And the stain-induced occurs above M_s with a presence of a deformation on the steel.

For the TRIP effects the transformation of austenite to martensite is caused by both stress and strain (14) as illustrated on Figure 9. Under M_s the transformation happens athermally and with increasing temperatures over M_s the stress needed to perform the transformation increases until the yield stress of austenite and corresponds to the stress-assisted transformation (illustrated on part I). Part II represents the strain-induced transformation preceded by plastic deformation. Over the maximum temperature limit M_d, the austenite is no longer capable of transforming into martensite by plastic deformation.

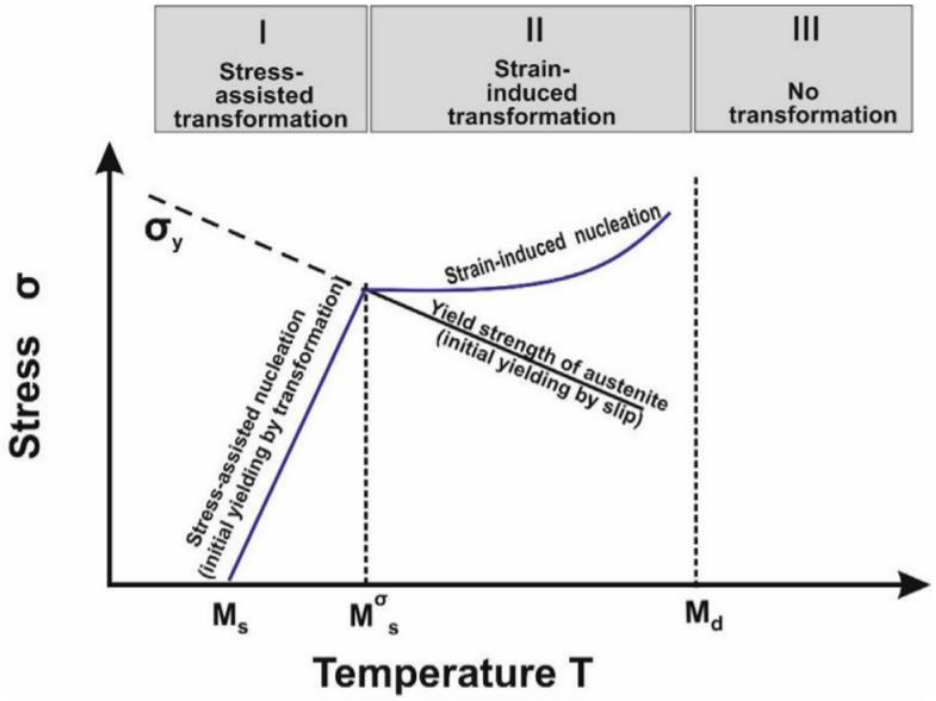

Figure 9: Critical stress to initiate the martensitic transformation as a function of temperature (extracted from (14))

TRIP effects can be observed on various types of steels, such as, DP steels, meta-stable austenitic steels, low carbon steels, high and medium manganese steels and quenching and partitioning steels. All of then presenting good proprieties and different heat treatments to achieve high strength while keeping high ductility.

2.1.3 Fracture

To better understand fracture on metals, it is important to know how the fracture can develop on the material. The two big fracture families are ductile and brittle fracture (both with many subgroups), each one of them with different mechanisms. But it can be also caused by creep fracture, crack propagation, cleavage and many more (**Error! Reference source not found.**)

The ductile fracture is the target for steels with high toughness and strength, as this mechanism is characterized by an extensive plastic deformation and therefore the damage can be noticed before the material's failure. This type of fracture can be divided into two mechanisms , void growth, and plastic localization.

Ductile fracture by void growth starts after necking, where the deformation concentrates at a single part on the metal and proceeds to void nucleation, void

growth, void coalescence to form a crack and ending on the material's fracture (Figure 10).

Void nucleation generally nucleates at the secondary phase particles, by either decohesion, a fracture on the matrix-particle interface or a fracture on the particles, if the particles on the matrix concentrate the stresses that can be high enough to drive void nucleation. The void nucleation by decohesion can be imagined as a particle inside a matrix, where the matrix is elongation, but the particle elongates less, therefore generation a gap between then and that is called the void, with this it is possible to understand also why the critical strain for nucleation is decreases with decreasing particle size, similar analogy can be made for the fracture of the particle mechanism. On the scenario the material has no secondary phase particles the voids tend to nucleate at the grain boundaries or triple points.

Void growth is the step where the created voids will enlarge by plastic grown, this is a result of the plastic deformation of the surrounding material around the void. Voids grown they tend to coalesce and form larger voids; this is the void coalescence. When the space between the voids is small, the material solid ligaments behave like tensile specimens and plasticity gets localized and present a mechanism that is like the necking mechanism. On this stage new smaller voids will be generated but will grow on a perpendicular direction with the main strain axis and the ligament then fail due to a crack propagation between the main voids. This coalescence process will be repeated with larger voids that will form a crack that finally fracture the material.

The ductile fracture can be identified using a scanning electron microscope and observing the dimples formed during the process. The dimples are simply the leftovers of the generated voids that may still contain the particle it was formed around. It is also possible to identify the mode that the force was applied by the size distribution of the voids or dimples, in tensile tests the bigger voids will be on the center and reducing in size near the edge, in tearing the larger voids will be on the starting edge and on shearing the voids will be distorted on the shearing direction.

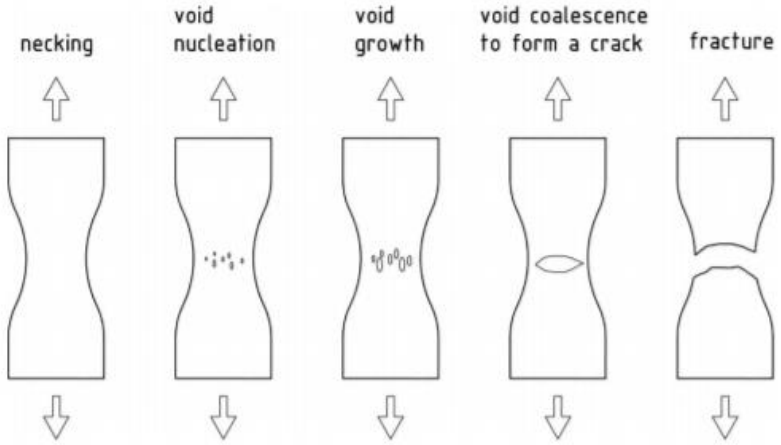

*Figure 10: Illustration of Ductile fracture by void growth mechanism (extracted from (**Error! Reference source not found.**))*

Ductile fracture by plastic localization is mostly the necking formation and those can be either a diffuse neck or a localized band (with an approximate angle of 45º).Generally, both the plastic localization and void growth mechanism coexist, and this combination is the origin of the cup and cone shape that is common on tensile tests. The combined mechanism starts with the voids nucleating and propagation by coalescence on the center of the neck, forming a crack. When the crack is close enough to the edges to create a plane stress condition that increases the shear component, it induces a localization of the deformation in a shear band, this causes the crack to propagate on the direction of the shear bands at 45º with the tensile stress axis.

The brittle fracture is generally not desirable on steels as it fails very rapidly with little or no plastic deformation and with a crack propagating at high speed, therefore, being difficult to recognize it before failure. Brittle materials such as martensitic steels can be applied on applications where the main desired property is the hardness, examples of applications are on pumps, valves, bearings, and many other applications that involvers wear.

The brittle fracture mechanism is globally cleavage along the crystallographic planes when the stress is higher than the critical stress for the separation of the atomic planes. Therefore, the brittle fracture is a stress-controlled mechanism. The main stages of this mechanism are a concentration of dislocations along slip planes by plastic deformation, followed by the nucleation of microcracks caused by the shear stress where the dislocations are blocked and the crack propagation until fracture.

This kind of fracture is characterized by flat fractures perpendicular to the

stress axis, shiny surface with a grainy finish, chevron patters pointing to where the fracture began are also common (Figure 11), this patter can present secondary ridges coming from the main chevron ridges . The main factors that can contribute to a brittle fracture are low temperature, high loading rate or a rapid loading rate and a triaxial stress, the later implies that certain geometries are more susceptible to brittle fracture than others. Defects such as porosity and pre-existing cracks also contribute to the brittle fracture but reducing the grain size increases the toughness.

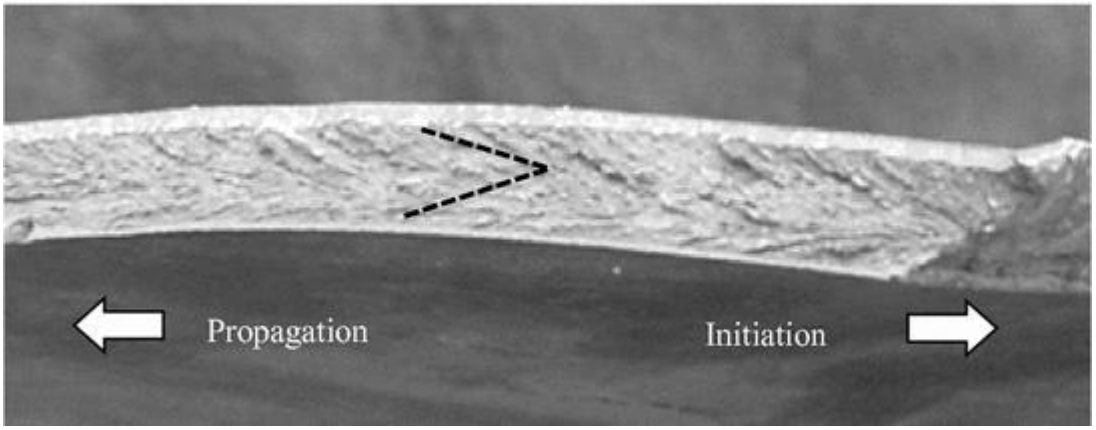

Figure 11: Chevron patters point to initial fracture point (extracted from (22))

Cracks can propagate by different means on materials, the main ones are the cohesive zone mechanics which act in the material ahead of the physical crack tip, being more common for metals and the bridging zone mechanisms which act on the crack faces in the wake of the crack tip that are more common for composites, ceramics, and polymers. Therefore, the cohesive zone mechanics are the ones being considered for metals.

The cohesive zone mechanics examples are:

- Cleavage along crystal planes
- Nucleation, growth, and coalescence of voids
- Localized necking in thin plates
- Grain boundary damage
- Microcracking
- Stress corrosion and chemical damage in aggressive environments
- Cracking accompanied by phase transformation.

Metal also has a differentiation for crack propagation on brittle and ductile materials that will each one follows a different mechanism in response to the high stress applied on the crack tip due to its stress intensity factor.

Brittle metals will present brittle particles breaking near the crack tip due to the high stress, the speed of this small crack is very high as to reach the matrix and do not allow dislocations to operate in the matrix and therefore, the crack propagates by cleavage on the matrix and cross the grain boundaries to join the main crack. The described mechanism is named crack injection. This happens when the crack tip reaches a distance equal to the average space between two brittle sites, according to the Ritchie Knott and Ric model (RKR model). A similar mechanism can also be observed, but is less frequent, when the separation of grain along grain boundaries is more favored than the cleavage through the grain, this mechanism is called intergranular brittle fracture.

On ductile metals the mechanism is the same as the one discussed for the ductile fracture, with the increased plastic deformation caused by the stress caused by the crack , voids near the crack will nucleate, be enlarged, and coalesce with the main crack with the resulting surface being also consisting of small dimples (Figure 12). The fracture toughness will decrease with increasing temperature but will increase with decreasing grain size, increasing bond strength between the particles and the matrix and by hardening with less brittle particles.

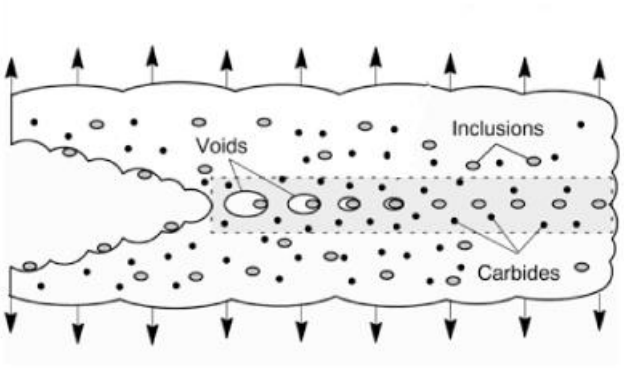

Figure 12: Ductile crack propagation illustration (modified from (43))

BCC and HCP can present either ductile or brittle fracture and therefore, there is a transition between both behaviors. This is called the Ductile-Brittle transition. BCC and HCP are strain rate sensitive, implying that the yield strain decreases with increasing temperature because the movement of dislocations is strongly related to

the temperature, such an effect is not so prominent on FCC metals.

This transition occurs because at low temperatures at the brittle region the fracture toughness increases with temperature and then when a critical temperature is reached, at which the critical stress does not reach the critical stress to initiate the crack injection mechanism, with this void start to nucleate and grow and coalesce, after the transition the fracture toughness decreases slowly with temperature. The temperature at this transition occurs is called the Ductile-Brittle transition temperature and the region around this temperature characterizes the mixed mode-fracture region. This happens because these metals the development of the plastic zone is a temperature dependent process, at high temperatures the thermal energy in the crystal structure is sufficient to aid the movement of dislocations under one applied stress, allowing the fracture to proceed as ductile. The opposite behavior is observed at low temperatures and therefore, causes that metal to have a brittle fracture.

The Ductile-Brittle transition temperature depends on various factors such as, yield stress evolution, stress state and velocity of cracking or even grain size or composition. Therefore, for each material tests are necessary to identify its critical temperature, most commonly Charpy or Izod tests to measure the absorbed energy as a function of the temperature.

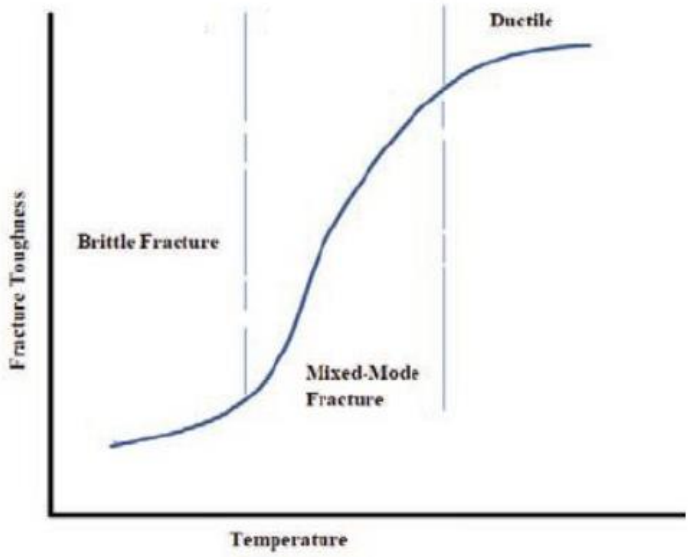

Figure 13: Ductile-Brittle transition with Brittle, ductile and mixed-mode regions (modified from (42))

As the fracture toughness is much higher on the ductile fracture it is desirable to keep the metal on temperature above the Ductile-Brittle transition temperature to prevent sudden failure of a metal part or structure.

2.1.4 Strain hardening

Strain hardening is also known as cold working or work hardening, on this process the metals are made stronger and harder via permanent deformation. By hindering the movements of dislocations on a metal the elastic limit is increased and therefore the material is hardened, many obstacles can block the dislocations movement, such as, grain boundaries, precipitates, or even other dislocations. Keeping in mind that dislocations can block other dislocations moving on other planes, this causes and agglomeration of dislocations that is called dislocation entanglement. The dislocation entanglement prevents deformation on the grain it is present, unless a larger energy is utilized. After this hardening, the material's strength is increased for further loadings.

Annealed crystals present dislocation sources known as Frank and Read sources between pinned dislocation nodes, when a stress over the minimum stress for activating a dislocation source is applied, the source generates dislocations following the Frank and Read multiplication mechanism. The combination of many active dislocation sources will generate the dislocations entanglement or cause the dislocations to pile up on barriers, hardening the material.

The hardening exponent (n) is utilized to characterize the capability of a material to strain harden, and this value is applied on the Hollomon's equation :

$$\sigma = k\varepsilon^n \tag{1}$$

Where σ is the true stress, K is the strength coefficient (determined by the material), ε is the true strain and n is the strain hardening exponent. Values for n varies from 0 (perfectly plastic) to 1 (perfectly elastic), with most metals presenting values between 0,1 and 0,5.

Considerer's criterion states that the strain at the onset of necking is equal to the strain hardening exponent, this is valid when the Hollomon's equation is applicable to describe the material's behavior.

The strain hardening can be undone, this process is called recovery. One of the types of recovery is the dynamic recovery, that is a thermally activated process. With the multiplication of dislocations and their pinning, while the material suffers

strain hardening it also suffer from an increase on the internal stresses that is the driving force for recovery.

During dynamic recovery, with sufficiently high stresses combined with thermal activity, the dislocations can move away from the obstacles hindering its movement, targeting a lower energy configuration. The mechanism for these movements is generally by cross-slip of the screw dislocations to other slip planes with later dislocation annihilation and dipole formation. Therefore, as dislocations multiply and recover by different methods, this causes the hardening capacity of the material to be set by the tendency of recovery because it sets the dislocation density and consequently the strength.

Grain boundaries are efficient barriers to dislocations and the internal stress built on then can cause the multiplication of dislocations on the neighboring grain. In consequence, smaller grain sizes present higher resistance for dislocations to move and therefore more strain hardening capability and higher elastic limit. The grain boundaries also act as dislocation sources that also contribute to the strain hardening. According to Marek Opinela et al 30), if the grains are very small, the strain hardening rate is very high on the initial deformation and decreases very fast with increasing strain, consequently, the best combination of toughness and strength will be at intermediate grain sizes. Different grain sizes can be achieved during the heat treatment by controlling various parameters, such as, the initial microstructure, the austenization temperature and the holding time during austenization.

It is also important to notice that TRIP effects can also induce a strain hardening behavior as the austenite to martensite transformation affect the hardening of the material. Two mechanisms for this are currently proposed **Error! Reference source not found.**). One states that the volumetric expansion accompanied by the martensitic transformations generates local plasticity in the matrix phase around the formed martensite leading to an increase on the dislocation activity in the matrix and thus strain hardening. The other states that the difference on strength between the hard martensite and the soft matrix results on a stress and strain partitioning and a composite like behavior, enhancing the strain hardening as long as the martensite remains elastic.

2.2 Rolling techniques

Rolling is one of the main processes on metalworking. This is mainly utilized to produce metal sheets that are used for many applications such as on the automotive industry. Many car parts are produced from metal sheets, as illustrated on Figure 14.

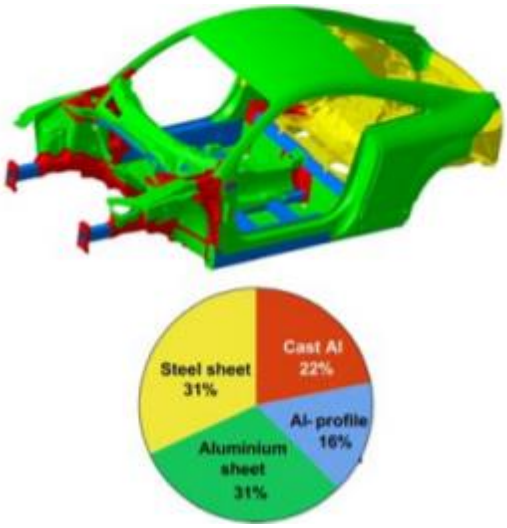

Figure 14: Illustration of base material for a car (extracted from (31))

There are two main rolling techniques , hot and cold rolling. Both are based on passing the initial metal through different pair of rolls to reduce its thickness until the desired specifications and they are classified by their process temperature.

On the hot rolling process, the temperature of the metal is above its recrystallization temperature. Therefore, after the grain's deformation during rolling, they recrystallize after each pass and maintain an equiaxed microstructure. The metal sheet is after cooled with a controlled rate (specific for each application and desired microstructure, Figure 5).

On the other way, cold rolling is defined as a rolling with temperatures below the recrystallization temperature. Consequently, the metal keeps the deformation after the rolling process with no recrystallization, this implies that the resulting microstructure will be elongated on the rolling direction and possible inclusions will be also elongated. This method also grants a better surface finish in comparison with hot rolling.

During cold rolling, strain hardening can also occur, increasing its strength up to 20%. It is possible to separate the cold rolled sheets in four groups, accordingly to the percentage of the thickness that was reduced, full-hard, half-hard, quarter-hard

and skin rolled. On full-hard rolling the thickness is reduced by 50% of its original dimensions with smaller reductions for the other groups, until the skin rolled, that present reductions of the order 1% of the thickness.

Cold rolling has a lot of application, for example, on furniture, car parts, tubing's and many more. But one disadvantage of this method is that with the strain hardening increasing the strength the toughness is reduced, making the material not favorable to be stamped and therefore, limiting the possibility of objects made with a cold rolled metal.

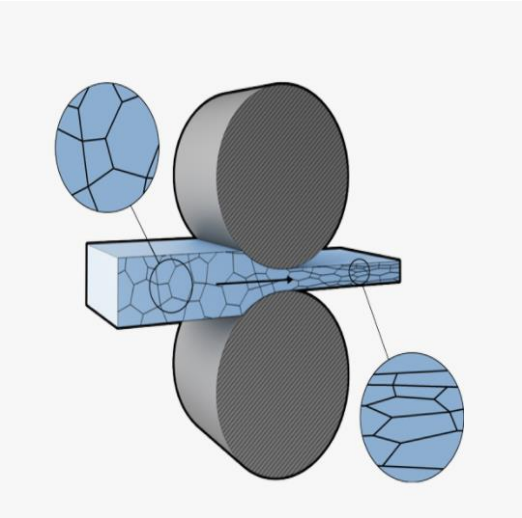

Figure 15: Cold rolling illustration and elongation of microstructure (extracted from (35))

During cold rolling, edge cracks can be formed, caused by secondary tensile stresses introduced by non-homogenous deformation (**Error! Reference source not found.**). These cracks occur by following the ductile fracture mechanisms and are dependent on the ductility of the material. As the edge cracks generate and area that is full of defects and cannot be utilized, it generates losses of material, and it is interesting to reduce it. Considering the ductile fracture that occurs an increase on the toughness of the material been rolled the edge cracks can be avoided and more useful material will be yielded by the rolling process.

According to Ejaz Ahmad *et al (*34) the cold rolled material can maintain some of its elongated microstructure even after heat treatments such as annealing (if the holding time is not enough to fully recrystallize the sample), therefore, even with a session o heat treatments, some features of the starting cold rolled metal will continue on the final product, an example of this are elongated voids or inclusions that may be formed during the cold rolling.

2.3 3rd generation steel

The 3rd generation of AHSS (Advanced High Strength Streel) have proprieties between the 1st and 2nd generations of steels, combining better proprieties then the 1st generations but lower cost compared to the 2nd generation (Figure 1). Examples of this generation are the medium-Mn steel, TBF (TRIP-aided bainitic ferrite), Q&P (quenching and partitioning) and δ-TRIP.

2.3.1 Medium Mn steel

Medium-Mn steels are characterized by having 3-12 wt% Mn on an ultrafine and grained ferritic matrix with grain sizes generally on the order of 1 micron, presenting a volume fraction of austenite up to 30 vol%.

According to Krizan et al. (**Error! Reference source not found.**), this kind of metal can have a tensile strength higher than 1000 MPa with elongations between 25% and 40%. Therefore, presenting great mechanical proprieties , but also lower cost and easier production when comparing to the high-Mn steels from the 2nd generation.

This material can be obtained by two main methods, one step heat treatment or the two step heat treatment methods. As the name implies the one step heat treatment consists of only one heat treatment, the Intercritical annealing, with the holding times in the range of minutes (continuous annealing) or hours (bath annealing), targeting to form the retained austenite. The formation of the retained austenite is helped by its stabilizers, C and Mn, as well as the low size of the retained austenite grain. This process starts with a cold worked martensite and yields a globular ferritic-austenitic microstructure after its recrystallization, where the austenite is rich in C and Mn.

The two-step heat treatment consists of an initial full austenization followed by the Intercritical annealing. Similar results can be obtained by using a cooling rate fast enough after the hot rolling to provide the martensitic structure necessary. The main difference between the two methods is mainly the shape of the grains, the one step method will present more deformed grains, but both methods yield a predominantly lamellar structure.

2.3.2 TRIP-aided Bainitic Ferrite (TBF)

Trip-aided bainitic ferrite consists of a matrix composed of bainitic ferrite with retained austenite as interlath films, that will transform into martensite after the TRIP effects occur. This kind of metal is generally produced with the addiction of alloying elements, such as, carbon, manganese, and silicon, with 0,1 – 0,6 wt% C, 1,5 wt% Mn and 1,5 wt% Si **Error! Reference source not found.**).

To produce this material, the first step is a full austenization of the metal to fully homogenize it, this is followed by a cooling to a temperature in which the isothermal bainitic transformation takes place, at this stage the Si present on the steel favors a carbide-free retained austenite and therefore the austenite can be enriched in C with decreasing grain size. Intercritical annealing is possible in between steps but may cause a deterioration of the tensile strength (**Error! Reference source not found.**).

The minimum tensile strength expected on a TBF is 980 MPa (**Error! Reference source not found.**) with high elongations due to its soft matrix. Therefore, being very useful on forming operation with globally distributed deformation.

2.3.3 Quenching and Partitioning steel (Q&P)

Quenching and partitioning steel consists of microstructure composed of ferrite (for partial austenization) martensite and retained austenite (enabling TRIP effects), bainite can be also present in low amounts. The most common composition for this metal is 0,15-0,3 wt% C, 1,5-3,wt% Mn and 1-2,0% Si and low amounts of Al can be present (**Error! Reference source not found.**). Silicon is present to suppress the cementite formation.

The production of this material starts with a partial or full austenization followed by a quenching between martensite start and finish temperatures, the temperature choice will determine the martensite and austenite phase proportion, this results in martensite with some retained austenite. This is the quenching part of the process.

The partitioning step is done by heating the metal to the partitioning temperature at which the Carbon on the martensite is partitioned to the austenite and

the martensite will be tempered, while some bainite can be formed. The partitioning of carbon is what causes the austenite to stabilize and produce retained austenite.

The minimum expected tensile strength for Q&P steels is 1180MPa, but presents a lower yield strength than TBF steels, and therefore, it is better for applications with localized deformation.

2.3.4 δ-TRIP aided steel

δ-TRIP steels or density reduced steels are alloys with high Aluminum content when compared to other TRIP steels and present dendritic δ-ferrite in the microstructure that is formed during the solidification process and cannot be removed by further heat treatments. The remaining microstructure is comparable to conventional TRIP assisted steels. The typical composition for this kind of metal is 3,0 – 0,4 wt% C, 2,0 – 6,0 wt% Al, 0,2 – 0,8 wt% Si and 0,5 – 1,6 wt% Mn (**Error! Reference source not found.**).

The Al is the responsible of the reduced density proprieties as it replaces the denser pure Fe for Al and because the Al expands the lattice as it has a larger atomic radius than Fe, this results in an increased lattice parameter and therefore larger volume, the larger volume causes the density to decrease. It is also important to notice that the density is also related to the Young's modulus and with lower densities the material will have a lower Young's modulus, consequently the later will be reduced with increasing aluminum content. This is the reason why Mn and Si are usually added to Fe-Al alloys, to increase the Youngs modulus and compensate the amount lost by Al addition. Al is also related to the formation of a substantial amount of δ-ferrite dendrites during solidification. Some portions of δ-ferrite can resist the transformation into austenite (**Error! Reference source not found.**) due to its allowing elements. Mayr et al. (**Error! Reference source not found.**) also demonstrated that δ-ferrite can be retained at room temperature with alloying elements that are not Al

The production of this material is generally an Intercritical annealing followed by reducing the temperature for an over-ageing , transforming the austenite into a mixture of bainite and retained austenite rich in carbon. With this, TRIP effect will be possible.

Generally, δ-TRIP metal present tensile strength up to 900 MPa and elongations up to 40% (41), the tensile strength is lower than the other 3rd generation steels but having lower density it is applicable on lightweight applications on the automotive industry and safety parts (**Error! Reference source not found.**).

Chapter 3

Materials and Methods

This chapter is going to describe the material and methods utilized during the manufacturing and testing of the target metal, describing the base material, each step of the heat treatments, metallographic tests and tensile tests that were performed.

3.1 Base material

The base material received from the UCLouvain (Université catholique de Louvain) university was a medium-Mn third generation steel with high carbon content and silicon. This material was cold rolled until a blank dimension of 450 X 185 X 1 mm and later sheared into 12 parts of 15 X 4 mm and holes were drilled of the specimens to hold then on the future bainitic hold on a fluidized bed.

Table 1 : Theoretical composition of the received steel.

C [%wt]	Mn [%wt]	Si [%wt]	Fe [%wt]
0.45	1.49	0.52	Bal.

Figure 16: Cold rolled blank received.

With the offcuts of the blank an Inductively Coupled Plasma Atomic Emission Spectroscopy (ICP) to confirm the composition of the alloy was performed, yielding the following results.

Table 2: ICP results for the composition of the received steel

Cr	Cu	Fe	Mn	Ni	Si	C^{tot}
0.01	0.01	96.5	1.45	0.02	1.42	0.48

Dilatometry is a technique used to identify phase transitions on metals by measuring the change in volume associated with the phase transformations. This change in volume can be identified on the measurement of the length of the specimen with varying temperature. A dilatometry test was performed, and the received result is shown on Figure 17.

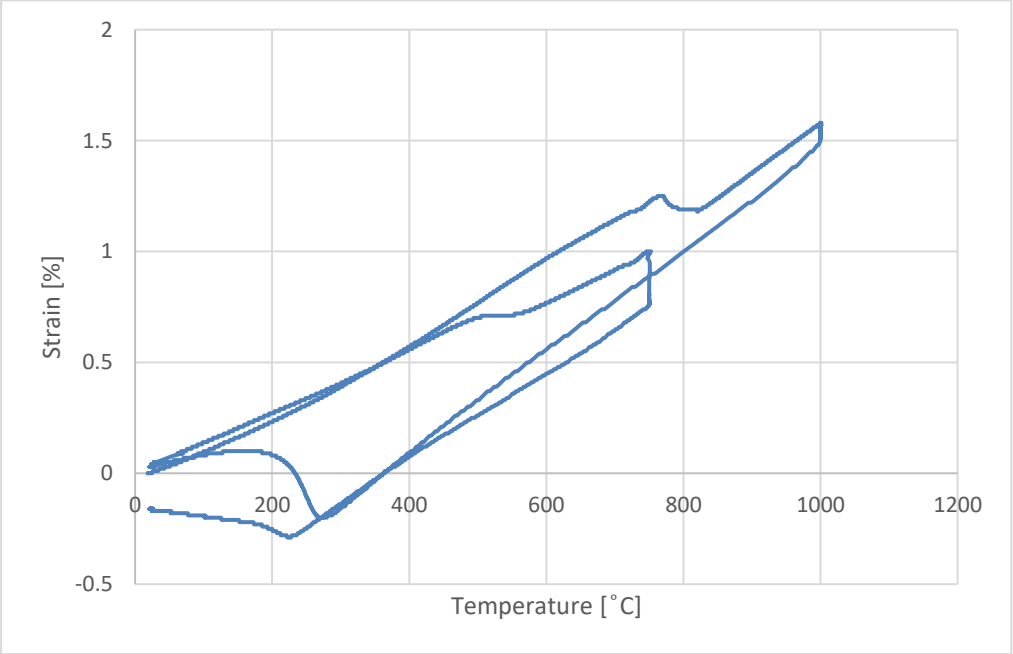

Figure 17: Dilatometry test results

It is possible to identify the main transformations on these results. The martensite start temperature at 273◦C characterizing the diffusionless transformation that does not require the atoms on the lattice to move more than one lattice spacing to change the crystal structure and produces martensite. The bainitic transformation

consists of the decomposition of the austenite on ferrite and carbides, generally cementite). The ferrite nucleation at 530° C is the decomposition of austenite into ferrite.

The complete heat treatment for the specimens is illustrated on Figure 18, the first step will be a full austenization followed by water quenching, then the Intercritical annealing with later bainitic hold. The temperatures and holding times are varying parameters that will be discussed on sections 3.2 and 3.3

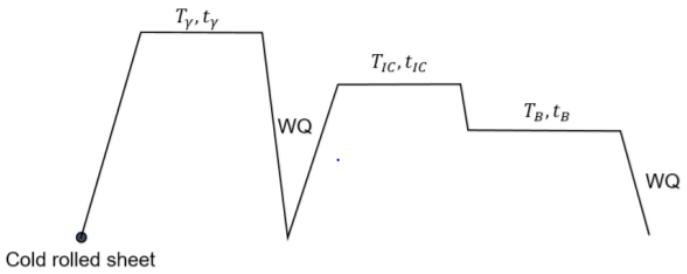

Figure 18: Planning for the heat treatments

3.2 Austenization and quenching

To produce the desired martensitic structure the 12 samples were heated to 1000° C for 5 minutes using a carbolite furnace targeting to regenerate proper austenite grains and directly quenched in water to produce a martensite substructure. For this heat treatment the use of a specially designed casing for the specimens was necessary to avoid bending and distortions that would influence the future tensile tests.

Figure 19: Specimens casings on the left part of image and austenized specimens on the right part

After the heat treatment one of the specimens broke in half (top right of Figure 19) and was later used as a control specimen for further heat treatments. The formation of oxides (mostly iron oxide is expected) was observed on all samples. Regarding bending, minor distortions were observed but not large enough to influence on further heat treatments or tensile tests.

A carbonite furnace was chosen due to its good precision with high temperatures and easiness to use.

Figure 20: Carbolite furnace used for the austenization.

3.2.1 Metallography after the first heat treatment

To perform the metallographical observation the samples needed to be

prepared by involving it in a conductive resin, polished and etched following the following steps.

- Pre-polishing
    - Sandpaper grit #80 with water as lubricant up to planarity
    - Sandpaper grit #320 with water as lubricant up to planarity
    - Sandpaper grit #800 with water as lubricant up to planarity
    - Sandpaper grit #1200 with water as lubricant up to planarity
- Polishing
    - Diamond paste (DP) with grain size 6 μm for 4 minutes
    - Diamond paste (DP) with grain size 1 μm for 3 minutes
    - Oxide particles solution (OP-S) for 1 minute
- Etching was performed using Nital 2% for 23 seconds.

Figure 21:Polished and etched sample for microstructural analysis with the flat part (left) being a sample through the length and the thin (right) a sample along the thickness.

3.2.2 Scanning Electron Microscope (SEM)

The analysis on the scanning electron microscope was made after polishing to evaluate the microstructure after the first heat treatment.

The images were obtained by using the secondary electrons signal (SE2), 15 KV of electron high tension (EHT)and magnifications between 31 and 5000 times.

The contrast is given by different lattice orientations of the martensite. Along the entire manuscript the rolling direction will be represented on the horizontal axis for any microstructure observation

On Figure 22(d) it is possible to identify the former austenite grains by grouping the needles with similar orientation, it is also possible to measure the former austenite grains that have an average size of 10 microns. Porosities are present on the structure of the sample and can be seen at Figure 22 (a) and Figure 22 (b) as black dots.

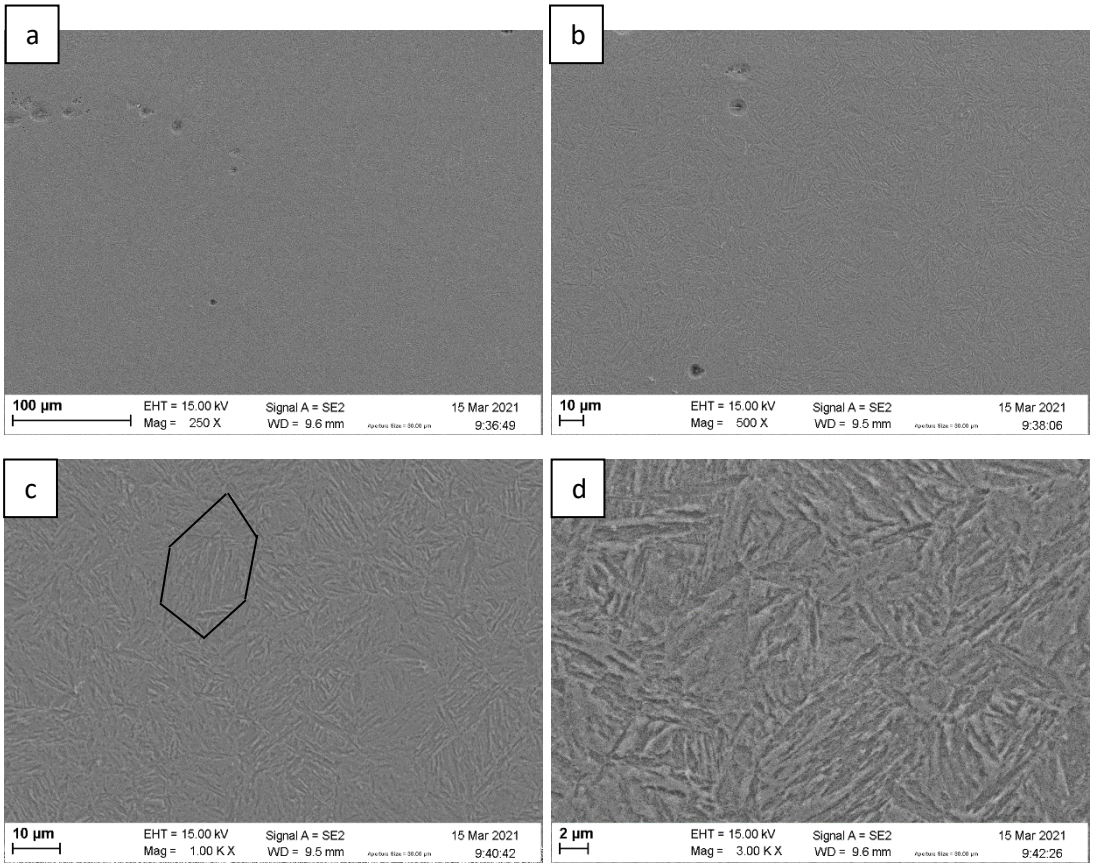

Figure 22: SEM images of the center of the sample's flat part (highlighted former austenite grain)

Figure 23 images have the rolling direction on the horizontal axis and that can be seen on the elongated voids that are present on Figure 23 (c) and Figure 23 (d).

On Figure 23 (d) Is also possible to observe an inclusion that was elongated during the rolling step and further decohesion caused a void around the elongated inclusion

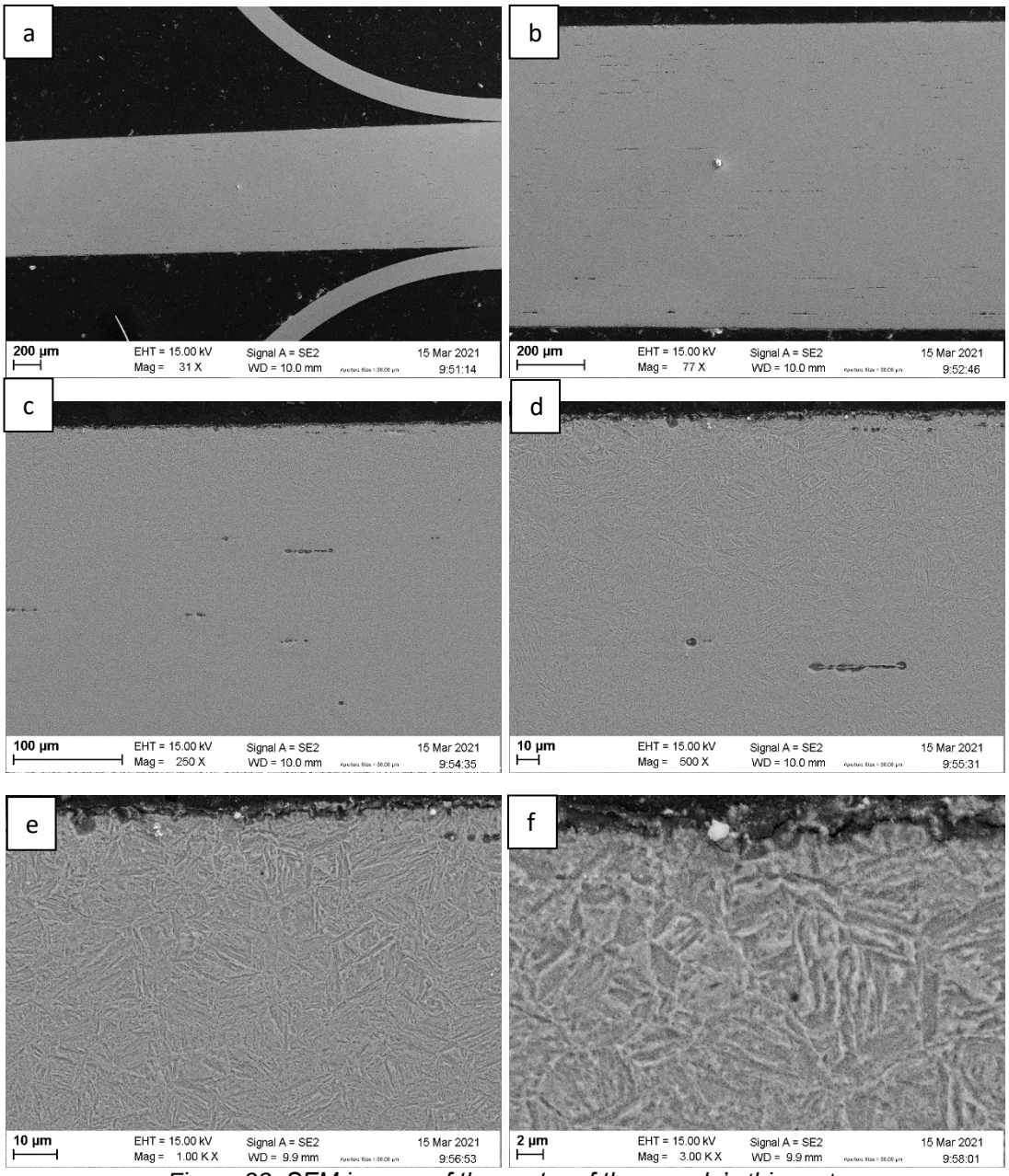

Figure 23: SEM images of the center of the sample's thin part

3.2.3 X-Ray Diffraction (XRD)

To identify the phases, present on the metal an XRD was performed using a cobalt source and angles between 26^{o} and 120^{o}. By using the database from the XRD software, the obtained curve matches the curve for martensite as can be seen on Figure 24 on all 3 peaks that corresponds to the preferential orientations of the lattice.

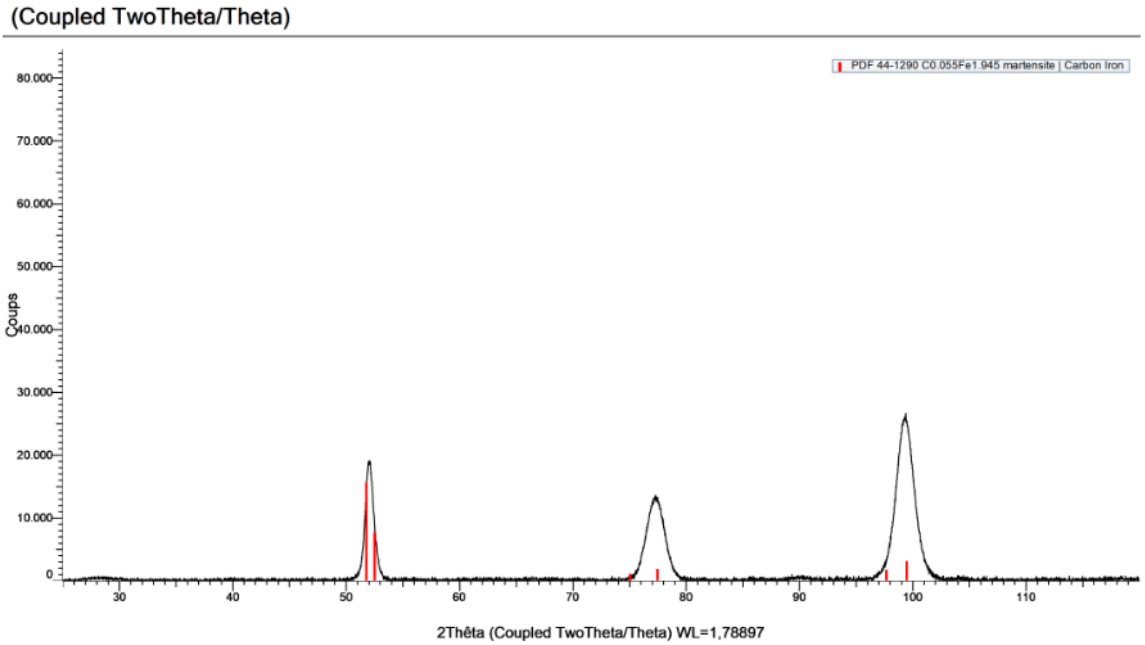

Figure 24 : XDR results of the sample with martensite fitting.

3.3 Intercritical annealing and bainitic hold.

The setup for these heat treatments is shown on Figure 25, where the fluidized bed furnace (on the left) was loaded with alumina powder and gas flow introduced on the bottom, the flow rate should be chosen according to the equipment calibration to always be at the fluidized state but low enough to not overflow the powder and potentially cause an accident. On the right is the lead bath furnace that was filled with lead, that was molten, and grinded charcoal added on the top of the liquid lead. Both furnaces were equipped with clamps on top to holt fix the sample holder and prevent large movements during the heat treatment, especially during the fluidized bed step where the turbulence can cause the sample holder to move. It was also part of the setup a thermocouple that was attached to the sample holder and a live measurement of the temperature to ensure precision on the heat treatments.

Figure 25: Fluidized bed furnace (left) and lead bath furnace (right)

The fluidized bed furnace was used for the Intercritical annealing targeting to cause austenite and ferrite to grow between the laths and still conserve the fibrous morphology. While the lead bath furnace was utilized for the bainitic hold, aiming to stabilize the austenite even further and form a microstructure composed mainly of ferrite and retained austenite to possibly present TRIP effects.

The 11 specimens were distributed on 4 groups and the broken one was used as a control after the first heat treatment. The temperatures of 750°C and 700°C on the fluidized bed furnace were chosen because the austenite martensite reversion occurs transformation occurs. Around 750° C and to evaluate the influence of the temperature on the proportions of ferrite and austenite a lower temperature of 700°C was selected expecting for it to still be on the Intercritical domain and analyze the expected smaller formation of austenite. Regarding the times for the bainitic hold, two different times were selected to evaluate the impact of the retained austenite such as, thickness and proportions.

- 6 specimens were treated at 750°C for 5 minutes at the fluidized bed furnace.
    - 3 specimens were treated 360°C for 30 minutes at the lead bath furnace.
    - 3 specimens were treated 360°C for 15 minutes at the lead bath furnace.
- 5 specimens were treated at 700°C for 5 minutes at the fluidized bed

furnace.

- 3 specimens were treated 360°C for 30 minutes at the lead bath furnace.
- 2 specimens were treated 360°C for 15 minutes at the lead bath furnace.

- 2 broken specimens
  - 1 specimen was treated 750°C for 5 minutes.
  - 1 specimen was treated 700°C for 5 minutes.

Table 3: Summary of heat treatments

Intercritical annealing temperature [°C]	Intercritical annealing holding time [min]	Lead bath temperature [°C]	Lead bath holding time [min]	Sample number	group number	Group name
750	5	360	30	1	1	750-30
		360	30	2		
		360	30	3		
750	5	360	15	4	2	750-15
		360	15	5		
		360	15	6		
700	5	360	30	7	3	700-30
		360	30	8		
		360	30	9		
700	5	360	15	10	4	700-15
		360	15	11		
750	5	---	---	13	5	750-00
700	5	---	---	14	6	700-00

Hereafter the samples will be referred by its group name.

The followings steps were followed for the performing of the heat treatments.

1. To prevent the adhesion of lead, all the samples should be coated with boron nitride as well as the sample holder and thermocouple.

2. Dry the montage using paper and air blast. Water on the fluidized bed can expand fast and cause accidents.
3. Fix the specimen on the sample holder using 2 metal wires being sure it is not too tight. The final montage is represented on Figure 26.
4. Insert the montage on the fluidized bed for the specified time for the specimen plus 1 minute and 40 seconds to allow the increase of temperature to the targeted temperature and check temperature.
5. Remove the montage from the fluidized bed and insert on the lead bath for the specified time for the specimen plus 20 seconds. Being as short as possible on the transfer to prevent the cooling of the specimen.
6. Remove the montage from the lead bath and quench on water.
7. Unmount the montage, grind the remaining lead from the components as it can cause damages on the fluidized bed furnace.
8. Proceed for the next sample.

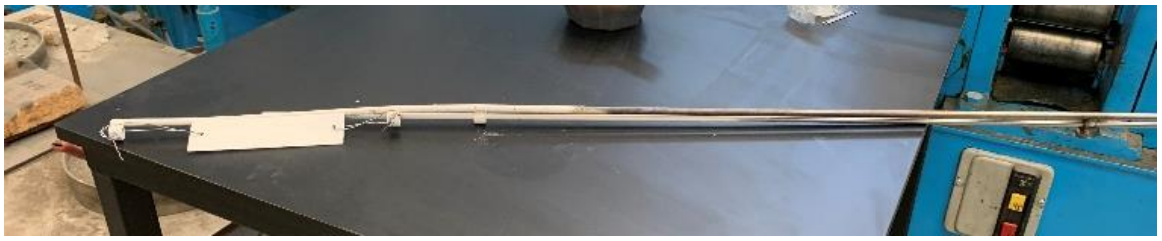

Figure 26: Specimen mounted on sample holder.

3.3.1 Metallography after the complete heat treatment

The polishing and etching were performed as described on (3.2.1). The analyzed samples were a total of 6 , one of each group described on (3.3) and images were obtained at the Scanning electron microscope.

3.4 Tensile test

To evaluate the proprieties such as, uniform elongation, ultimate tensile stress, and yield strength of the heat-treated metals, two tensile specimens from groups one to four described on (3.3) with target dimensions of 110X6X1 mm were machined as shown on Figure 27.

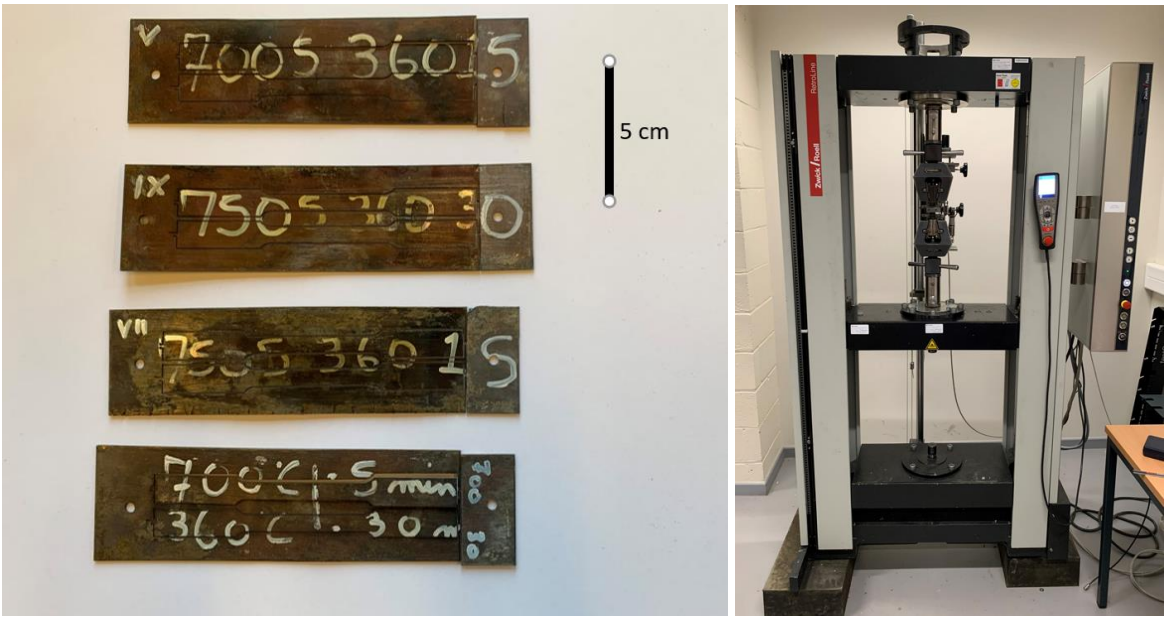

Figure 27: Machined tensile specimens (left) and tensile tester (right)

For the tensile test, a Zwick/Roell tensile tester was utilized with speed of 1 mm/min. the real dimensions of each sample were measured using a caliper by averaging the measurements at 3 different points and are shown on Table 4.

Table 4: Real dimensions of the tensile specimens

Sample group	Sample letter	Thickness [mm]	Width [mm]
750-30	A	1.02	5.98
	B	1.02	5.98
750-15	A	0.98	6.06
	B	0.99	5.98
700-30	A	1.01	5.99
	B	0.99	5.99
700-15	A	0.99	5.98
	B	1.00	5.99

After acquiring the results of the tensile tests, the fractography was performed on all the samples by using one stereoscope and evaluated on the SEM. With the obtained images it is possible to utilize the formulas below to calculate the fracture strain by using measuring the final dimensions of the samples using software such as image J and . Choosing the central areas for the measurements of width and the smallest cross section for the thickness.

$$\varepsilon_f^{22} = ln\frac{\omega_f}{\omega_0}$$

$$\varepsilon_f^{33} = \ln\frac{t_f}{t_0}$$

$$\varepsilon_f^{11} = -\varepsilon_f^{22} - \varepsilon_f^{33}$$

$$\varepsilon^{-f} = \sqrt{\frac{2}{9}\left[\left(\varepsilon_f^{11} - \varepsilon_f^{22}\right)^2 + \left(\varepsilon_f^{22} - \varepsilon_f^{33}\right)^2 + \left(\varepsilon_f^{33} - \varepsilon_f^{11}\right)^2\right]}$$

After the SEM analysis on fractography, the samples were grinded and polished until the center of its thickness to observe ,using the SEM, possible changes on microstructure due to the tensile tests, such as the expected TRIP effects.

Chapter 4

Results

This chapter targets to show the resulting microstructures before and after the tests, the materials proprieties obtained at the tensile test as well as the way the metal suffered fracture.

4.1 Microstructures

The microstructures of each group (Table 3) were analyzed on the SEM according to (3.3.1) and the results are the following.

For the samples on 750-00 (left) and 700-00 (right) that were both treated with only Intercritical annealing at 750°C and 700°C respectively:

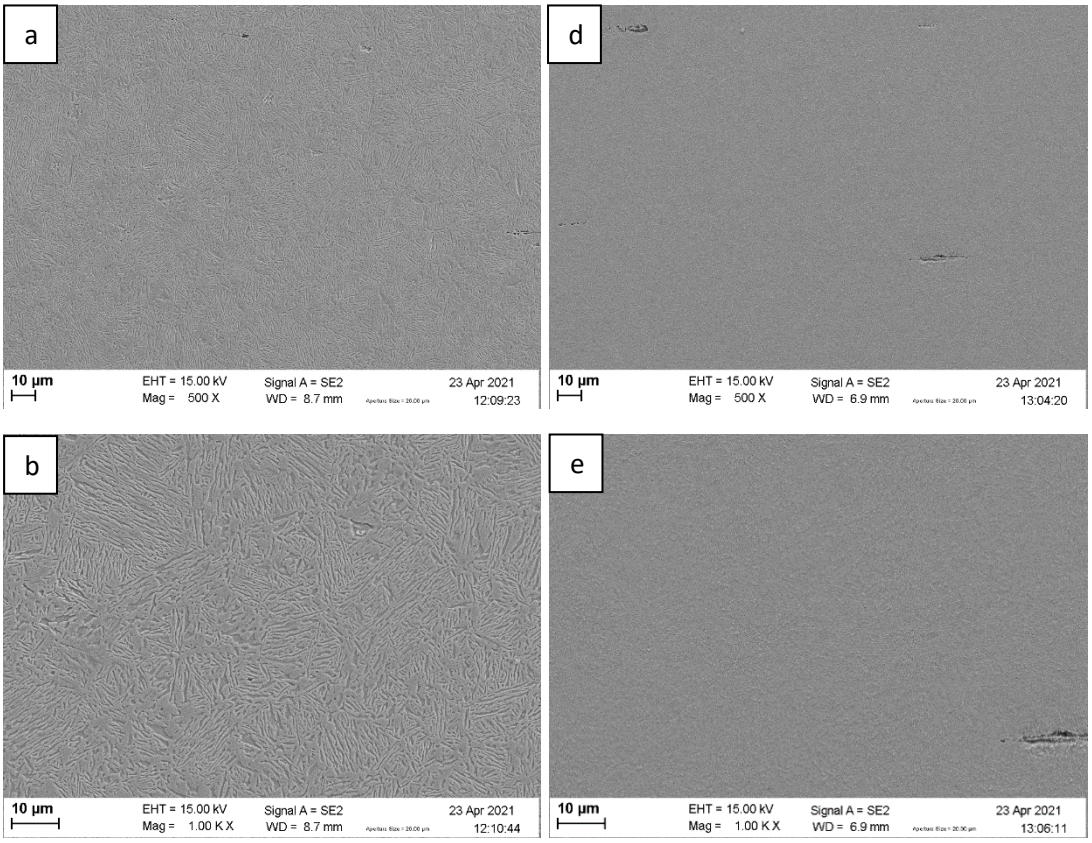

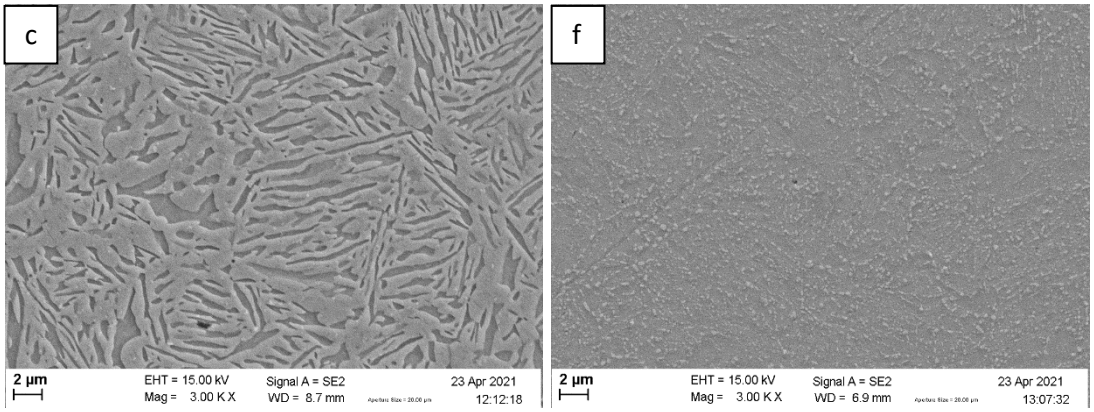

Figure 28: Microstructures for 750-00 (left) and 700-00 (right). At low and high magnifications

On Figure 28 (a) it is possible to identify some defects and porosity, that are more carefully observed on Figure 29, on (b) and (c) it is possible to identify the former austenite grains with the order of 10 microns (the same order as observed after only the austenization heat treatment) formed by lamellas oriented in the same direction.

Generally, less defects were observed on this sample in comparison with what was observed on Figure 23, this could be caused by the fact that the material used for that sample was taken for the edge of the heat-treated metal.

On the 700-00 sample, a big change in the microstructure was observed. It presents a microstructure with very small spheres in the order of nanoscale, in a plain matrix (assumed to be very small grains). The lamellar structure is lost but it is possible to trace lines with the spheres that slightly resembles the parent morphology and cold be a sign that those spheres were formed following the lamellar structure from the martensite.

A thermocalc simulation of the phase proportions as a function of the temperature, provided by Thibaut Heremans can be found on Figure 31.

Inclusions were observed in both samples (750-00 and 700-00), as shown on Figure 29. It is most likely to be Mn inclusions. To confirm this hypothesis, an EDX was performed during the SEM observations with the following parameters:

- Aperture size -120 microns
- 15K Volts
- Working distance of 6.0 mm

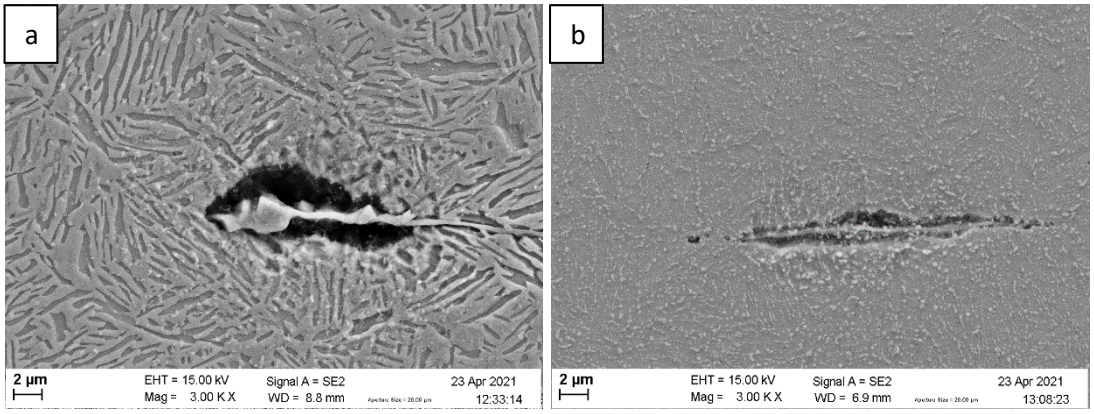

Figure 29: Mn inclusion on samples for 750-00 (left) and 700-00 (right)

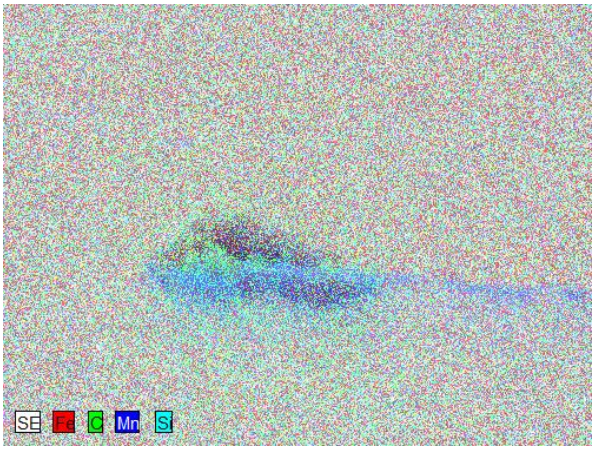

Figure 30: EDX results referent to Figure 29 (a)

The EDX confirmed that the inclusions were in fact Mn inclusions formed during the initial cold rolling and persisted both heat treatments.

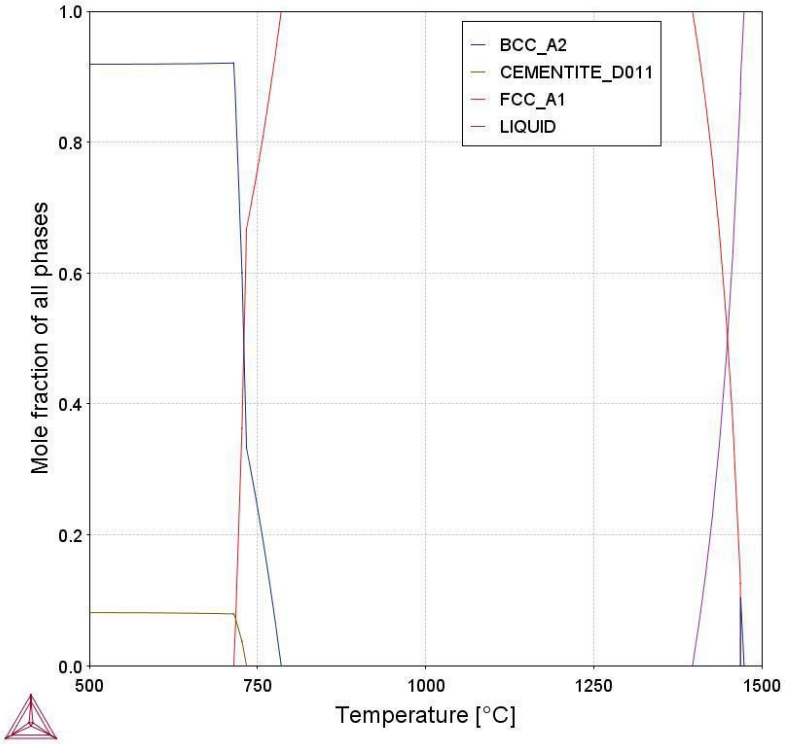

Figure 31: Thermocalc simulation of the phase proportions as a function of temperature

By using the Image J software and images from 750-00 and 700-00 it is possible to set a threshold to better separate the dark and light gray pixels (converting than on either black or white) then using the measurements built on the software to count the black pixels, one can measure that:

- the 750-00 sample has approximately 68% of Austenite and 32% of Ferrite on its structure.
- The 700-00 sample has approximately 91% of Ferrite and 9% of Cementite on its structure.

The calculated phase proportions are also in accordance with the simulation (Figure 31) which predicted 75% Austenite for 750-00 and 95% Ferrite for 700-00 .

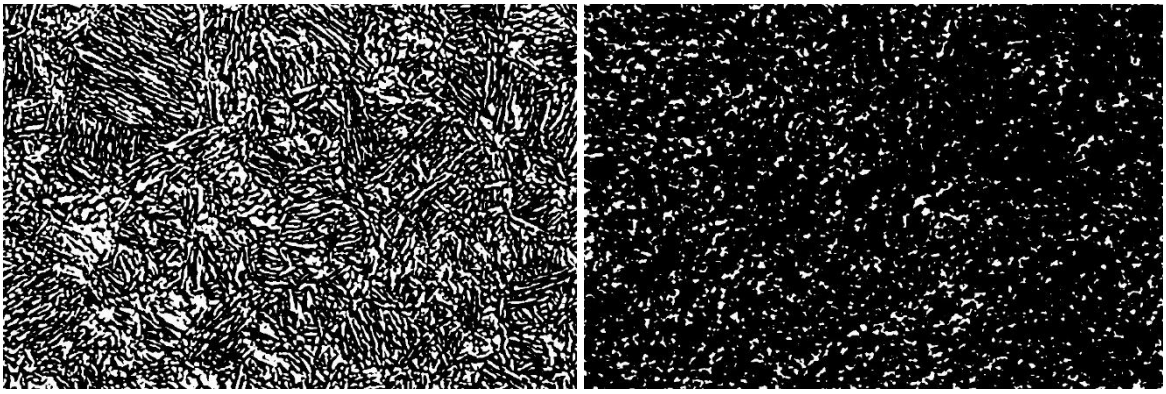

Figure 32: Image J treated images of 750-00 (left) and 700-00 (right) samples.

For the samples on 750-30 and 750-15 that were both treated with an Intercritical annealing at 750º C and bainitic maintain of 30 and 15 minutes respectively:

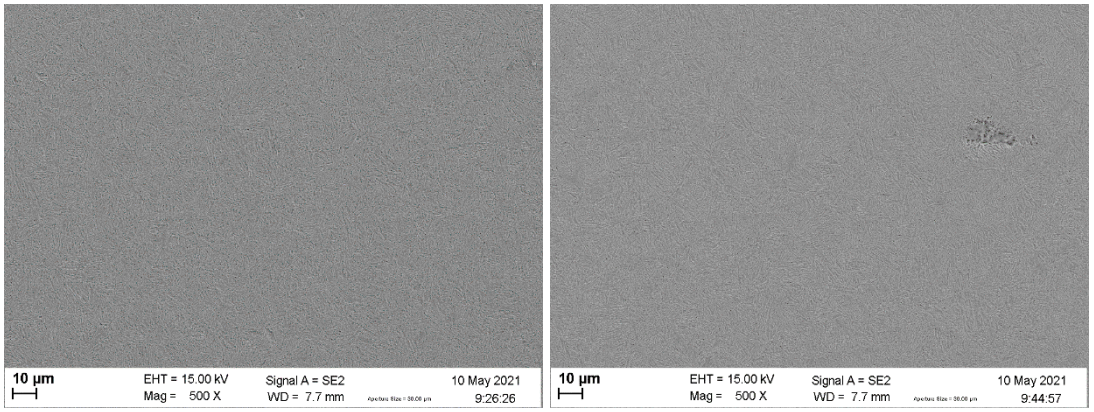

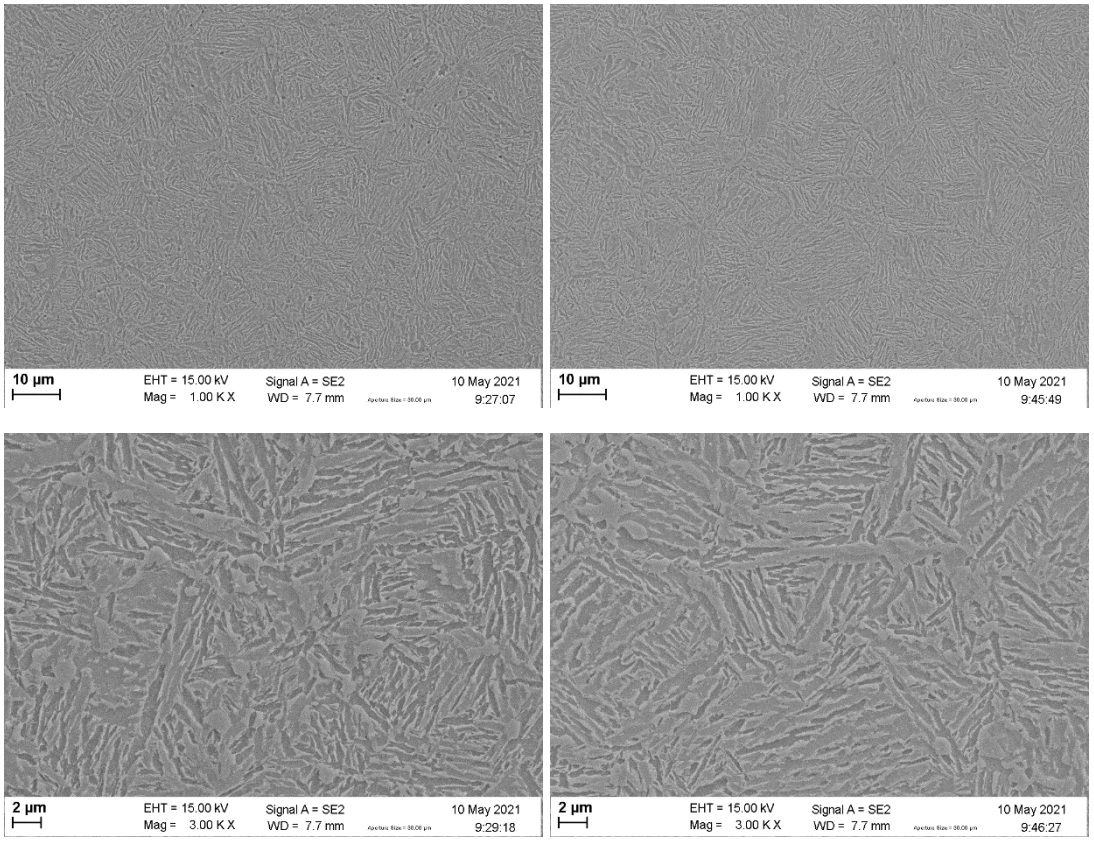

Figure 33: Microstructures for 750-30 (left) and 750-15 (right). At low and high magnifications

Both groups present a lamellar structure but comparing both groups it is possible to identify that for 750-30 the lamellas are thicker; this may be caused by the longer period that diffusion of the carbon from the austenite was allowed causing the ferrite and bainite to enlarge. Another difference is in comparison with 750-00, where the edges of the lamellas were round , but on 750-30 and 750-15 the lamellas are sharper (Figure 28 c).

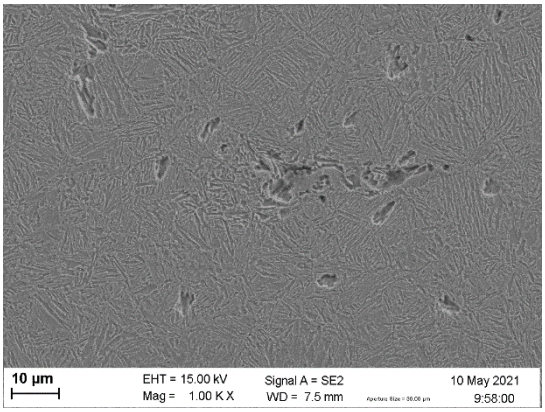

Figure 34: Decohesion on sample 750-15

This material also presented what is most likely to be decohesion, shown on Figure 34 (now filled by OP-S during the polishing step during sample preparation). It can be also noticed that the number of inclusions is reduced in comparison with both

the samples observed after only the austenization and the Intercritical annealing) and even less present on 750-30 when comparing to 750-15. This could be caused by the diffusion.

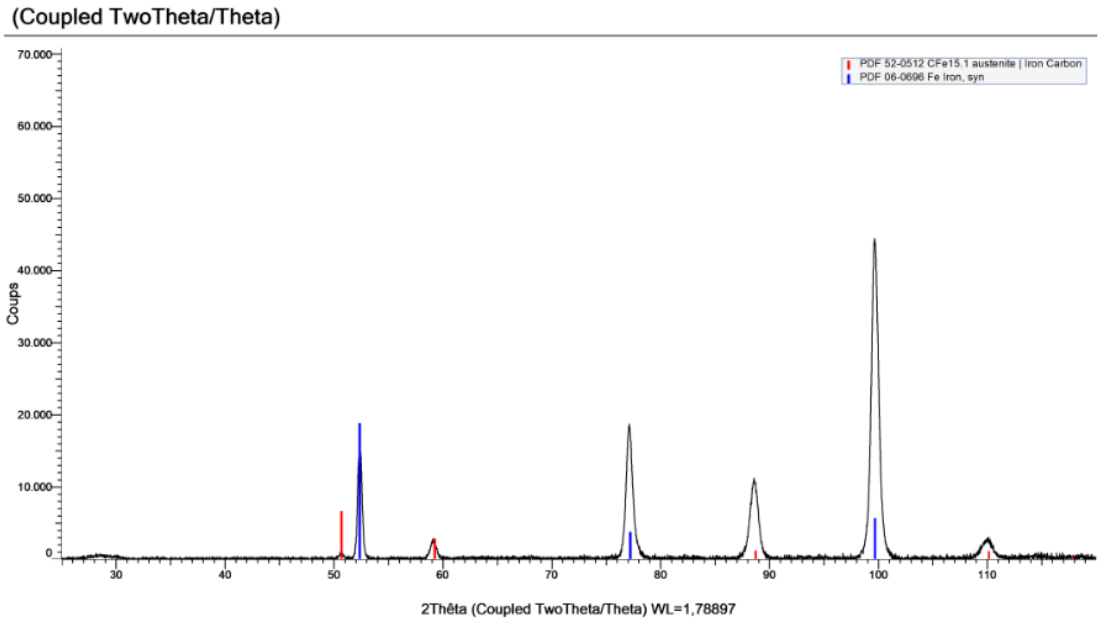

Figure 35: XDR of sample from 750-15.

To confirm the phases present, and XRD was performed on a sample from 750-15 (expected to present similar phases with 750-30). Ferrite and austenite were identified and the small peak at 2Θ = 28° can be linked to cementite 45), and consequently bainite. This supports the argument that the microstructure is comprised of mainly ferrite, bainite and retained austenite.

For the samples on 700-30 and 700-15 that were both treated with an Intercritical annealing at 700° C and bainitic maintain of 30 and 15 minutes respectively:

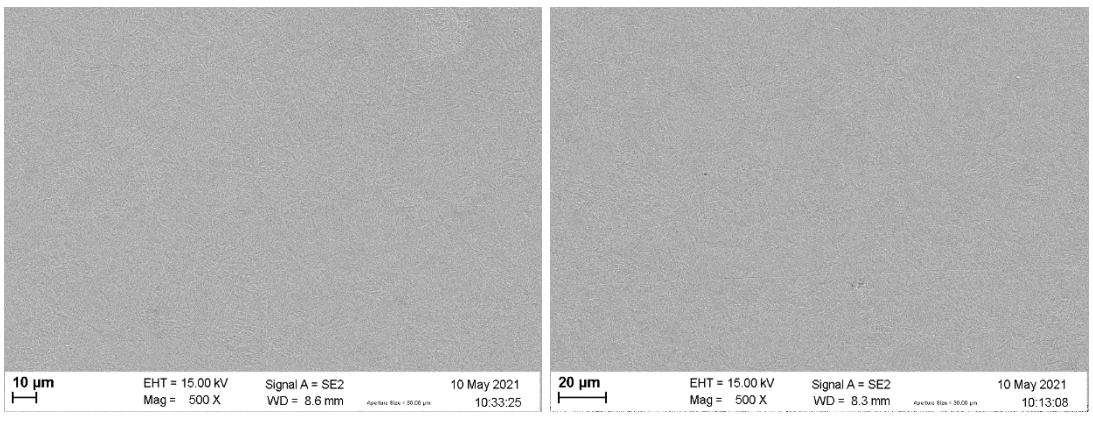

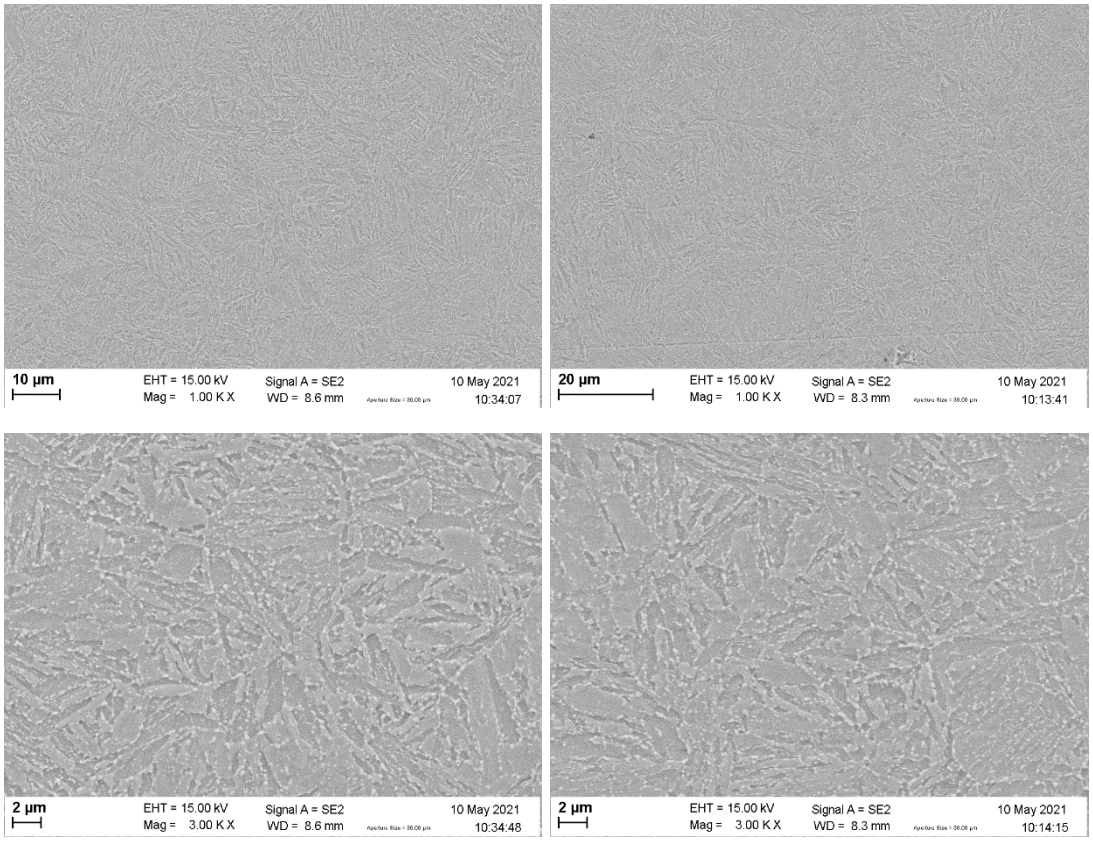

Figure 36: Microstructures for 700-30 (left) and 700-15 (right). At low and high magnifications

These groups present very similar lamellar shaped grains with grain sizes of 4 microns on average, with spheres at the grain boundaries, where 700-30 present slightly bigger spheres. When comparing to its corresponding group after only the Intercritical annealing (700-00) the spheres were formed at that stage and consequently the grains were formed during the bainitic maintain.

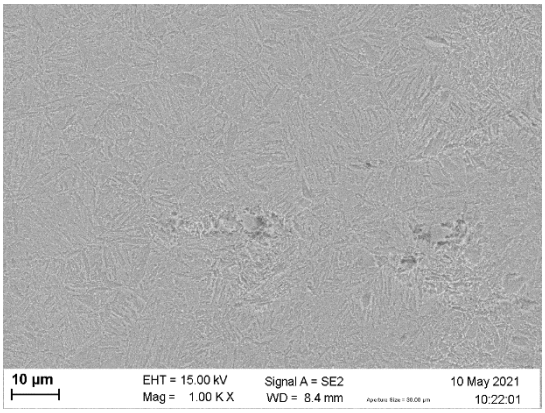

Figure 37: Mn inclusion on sample 700-15

These samples also presented structures originated from the Mn inclusions (Figure 37). These inclusions appeared filled with material (probably OP-S) and as discussed for 750-30 and 750-15, the porosity and number of inclusions was reduced after the bainitic maintain, this is possibly linked to the time during that diffusion was

allowed.

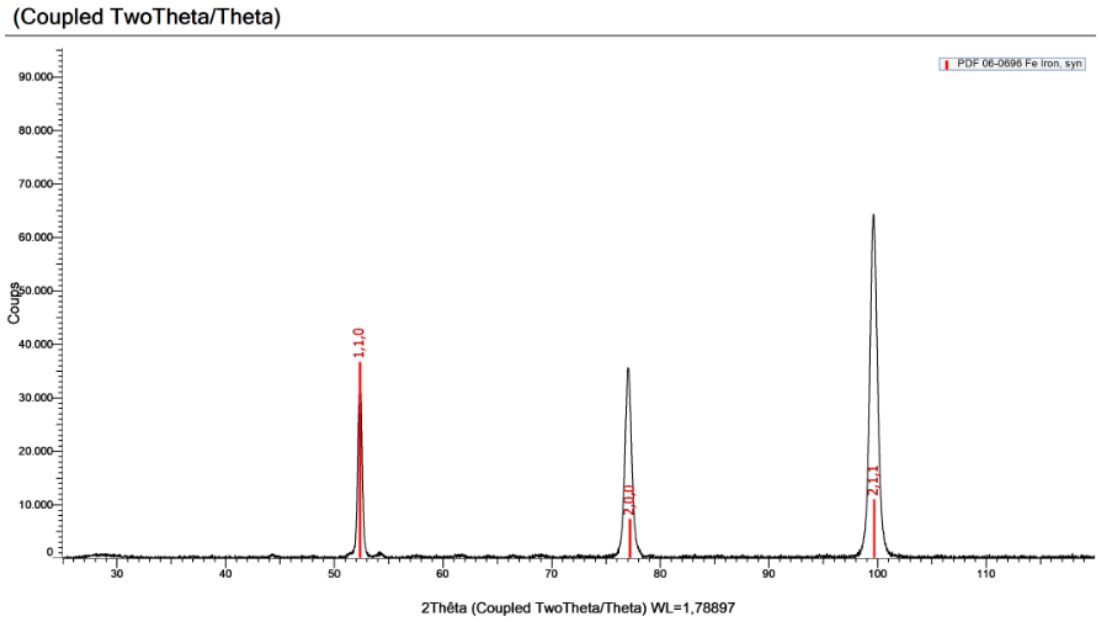

Figure 38: XDR of sample from 700-15.

By analyzing the results obtained on a XRD performed on sample 4 (expected to present similar phases with 700-30), only ferrite was identified but it also presents a small peak at 2Θ = 28º that according to 45) it represents cementite. This is an indicative that even with the different structure when comparing to 750-30 and 750-15, 700-30 and 700-15 presents a microstructure composed of ferrite and one extra phase.

4.2 Tensile tests

The information obtained during the tensile tests are plotted on Figure 39 and Figure 40 as engineering stress/strain curves and true stress/strain curves, respectively.

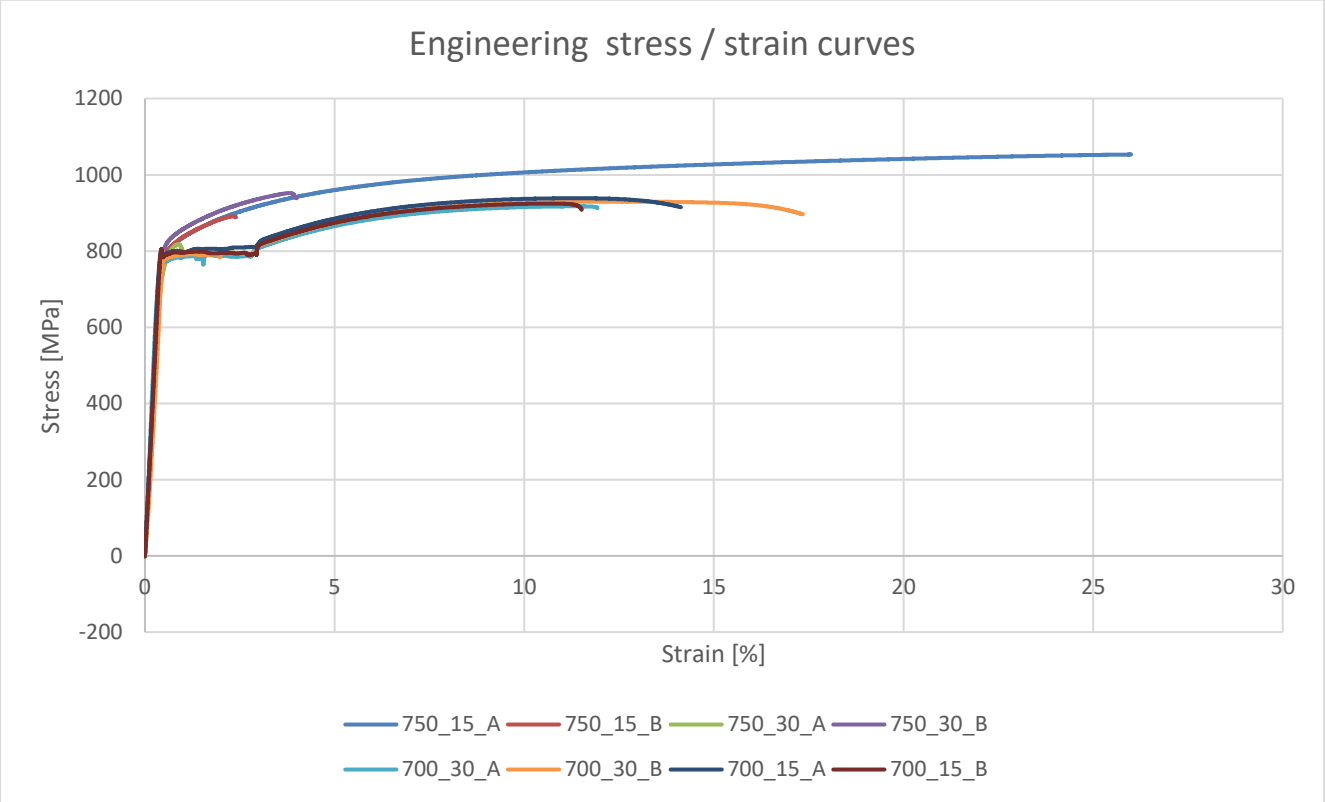

Figure 39: Experimental engineering stress-strain curves of the steels

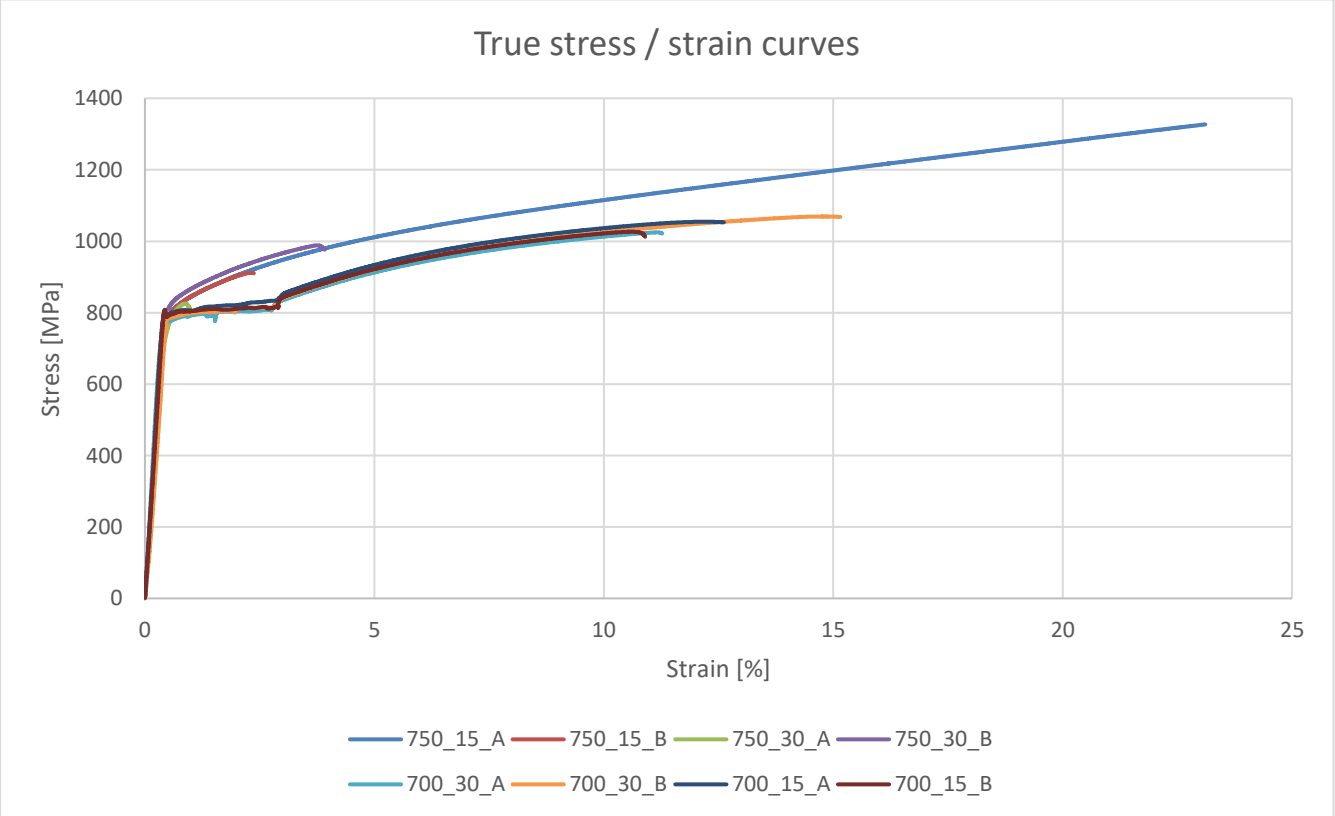

Figure 40: Experimental true stress-strain curves of the steels.

From the curves it is possible to extract some of the material properties of each sample. Ultimate tensile stress, yield strength and uniform elongations are presented on Table 5.

Table 5: Properties of tensile test samples

	ultimate tensile stress [MPa]	yield strength [MPa]	uniform elongation [%]	Product UTS X UE [Mpa . %]
750-30-A	805.21	760.81	0.99	800.68
750-30-B	976.46	811.28	3.92	3829.14
750-15-A	1327.23	799.25	23.11	30672.47
750-15-B	909.96	777.69	2.37	2157.51
700-30-A	1021.84	804.17	11.27	11514.70
700-30-B	1051.76	806.17	15.15	15938.50
700-15-A	1044.51	807.14	12.62	13178.35
700-15-B	1012.97	808.20	10.90	11041.13

For the samples on 750-30 and 750-15 , similar behaviors were observed on elastic deformation and during the beginning of plastic deformation, until the samples unexpectedly failed. Except for 750-15-A that failed at high elongations and present the highest UTS X UE product. Strain hardening can be noticed as the stress increases during plastic deformation and the strain hardening rate can be obtained from the curve by calculating the derivative and plotting it as a function of the true stress and can be observed on Figure 41.

700-30 and 700-15 also presented similar curves but with a uniform elongation that varies within the same group. Both groups' curves have a Lüders plateau for similar elongations and stresses. Strain hardening can also be observed on these groups after the Lüders plateau as the stress increases during plastic deformation.

By deriving the true stress/strain curve and plotting it against the true stress allows to compare the strain hardening on each sample and with the considerer's criterion.

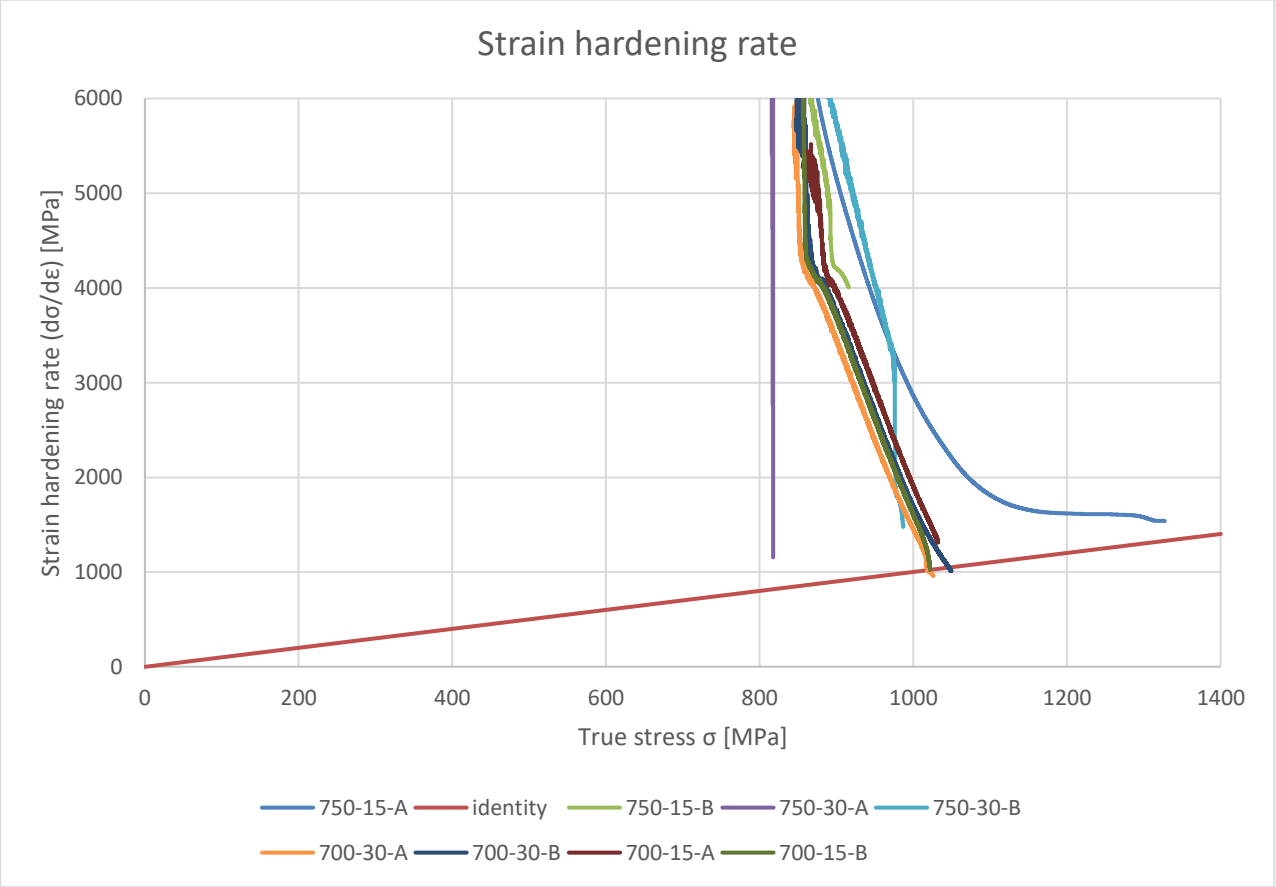

Figure 41: Stain hardening rate

On Figure 41 it is possible to compare the strain hardening rate with the n=ε curve (considerer's criterion) and identify the point at which the samples reach the considerers criterion and start the necking process. Not all the samples reached the considerer's criterion and therefore did not suffered necking. Sample 750-15-A presented an exponential decrease while the other specimens annealed at 750ºC had more linear and very different behaviors. On the other hand, samples 700-30 and 700-15 had a linear behavior with a step near the true stress of 870 Mpa. at this step the inclination was increased.

4.3 Fracture

With the aid of the SEM, it was possible to analyze the fracture surface from the samples from each group. The results are shown below.

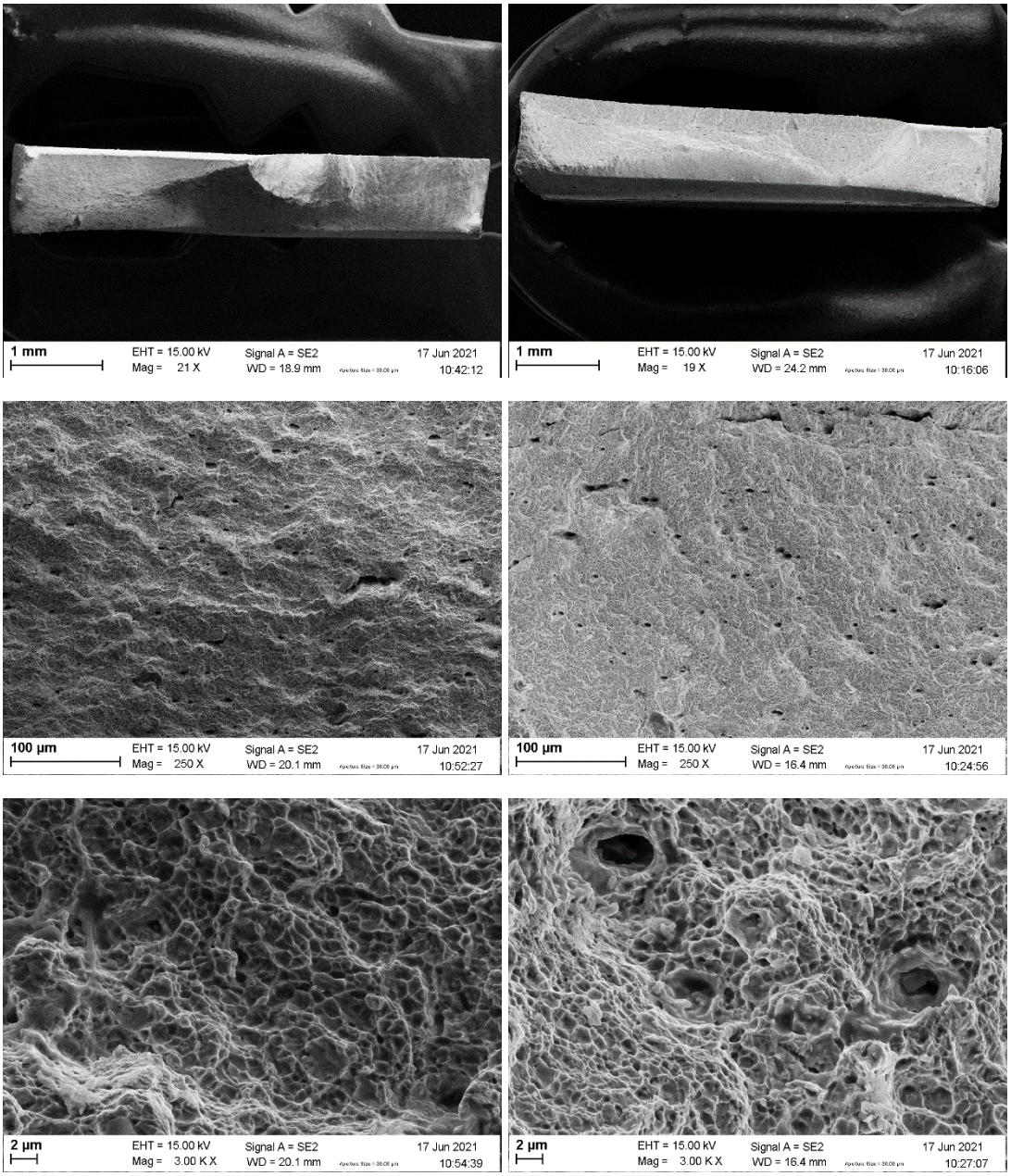

Figure 42: Fracture surface for 750-30 - A (left) and 750-30 - B (right). At low and high magnifications

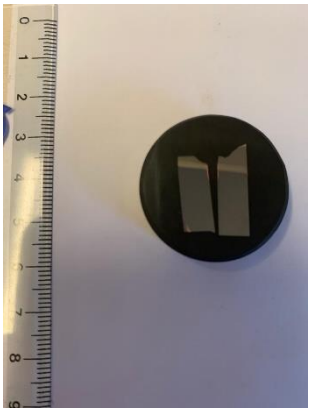

Figure 43: Macroscopic fracture surface for 750-30 - A (left) and 750-30 - B (right)

On Figure 42 it is possible to identify voids ranging from 25 to 50 microns with similar void density on the center and on the edges of the specimens. On a smaller

scale, dimples can be observed, characterizing the fracture as a ductile fracture at most of the specimen's area. The average dimple diameter on both 750-30 samples is 1 micron (coherent with the lamellas thickness). Smaller voids are also present at higher magnifications with average diameter of 4 microns, possible generated by the previously observed Mn inclusion on the metal. A flat fracture surface with a "step" was observed on sample A while a "cup" shaped surface with a 45º slant (approximately) on sample B

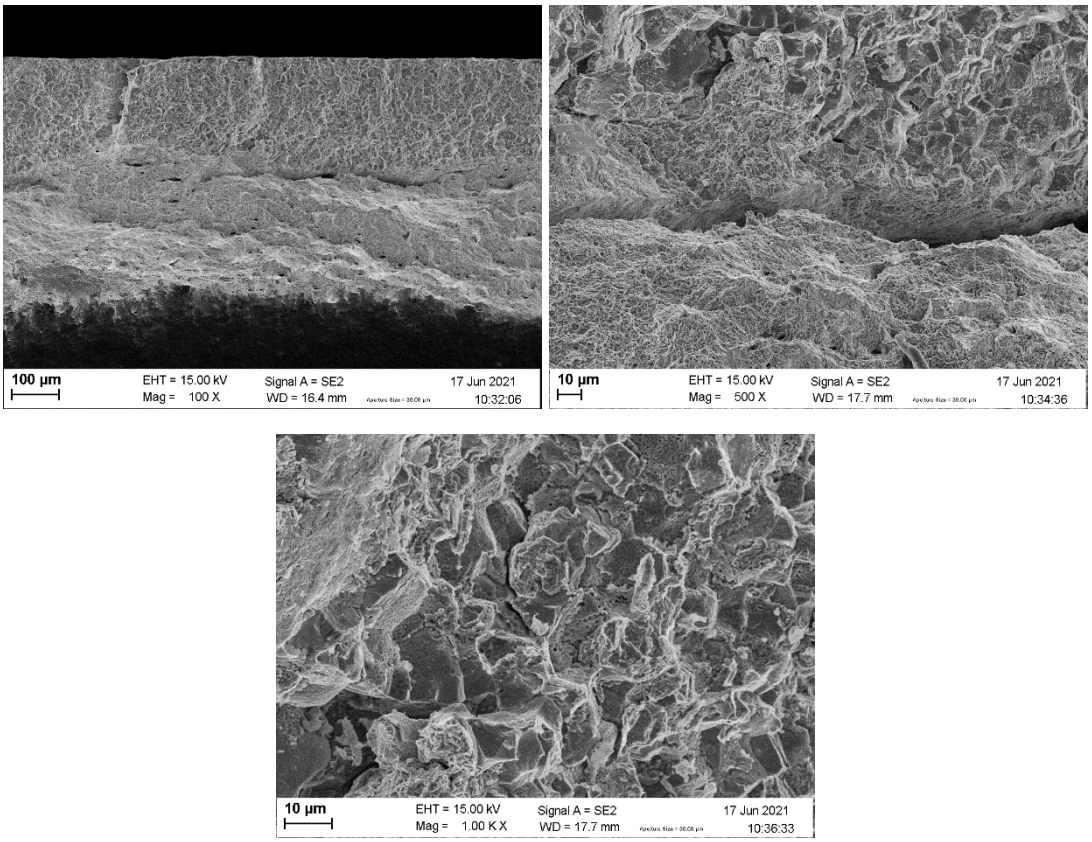

Figure 44 : Mixed fracture mechanics on 750-30- B

Sample 750-30 – B presented areas with step shaped structures (with sizes with the same order as the grains) that characterize a brittle fracture and therefore it had two different fracture mechanics separated by a large crack along the sample (Figure 44). The ductile fracture area is concentrated on the center while the brittle fracture is predominant on the sample's edges.

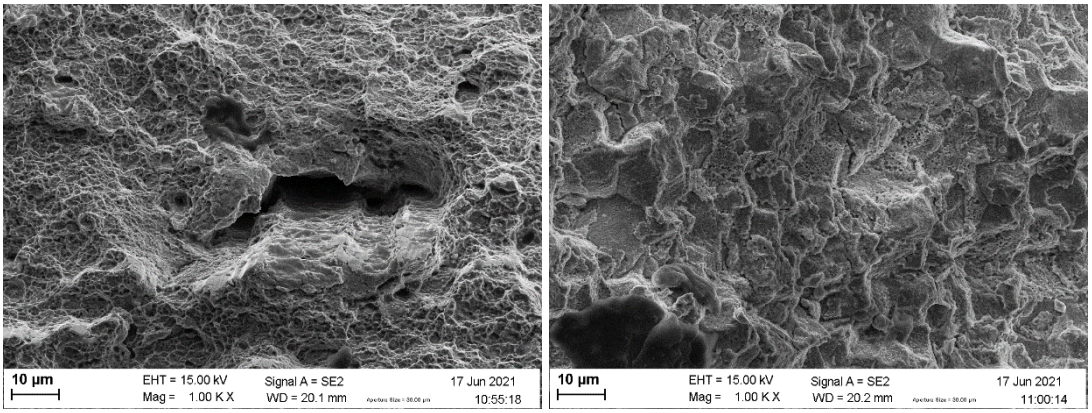

Figure 45 : Void and brittle fracture on sample on 750-30 - A

A 750-30-A sample had a brittle fracture (Figure 45), but while on sample B the brittle fracture was on the edges of the sample, sample A's brittle fracture was concentrated on only one side of the sample. This difference can be an evidence of a previously existing defect that propagated. It was also observed large voids with a maximum size of 40 microns.

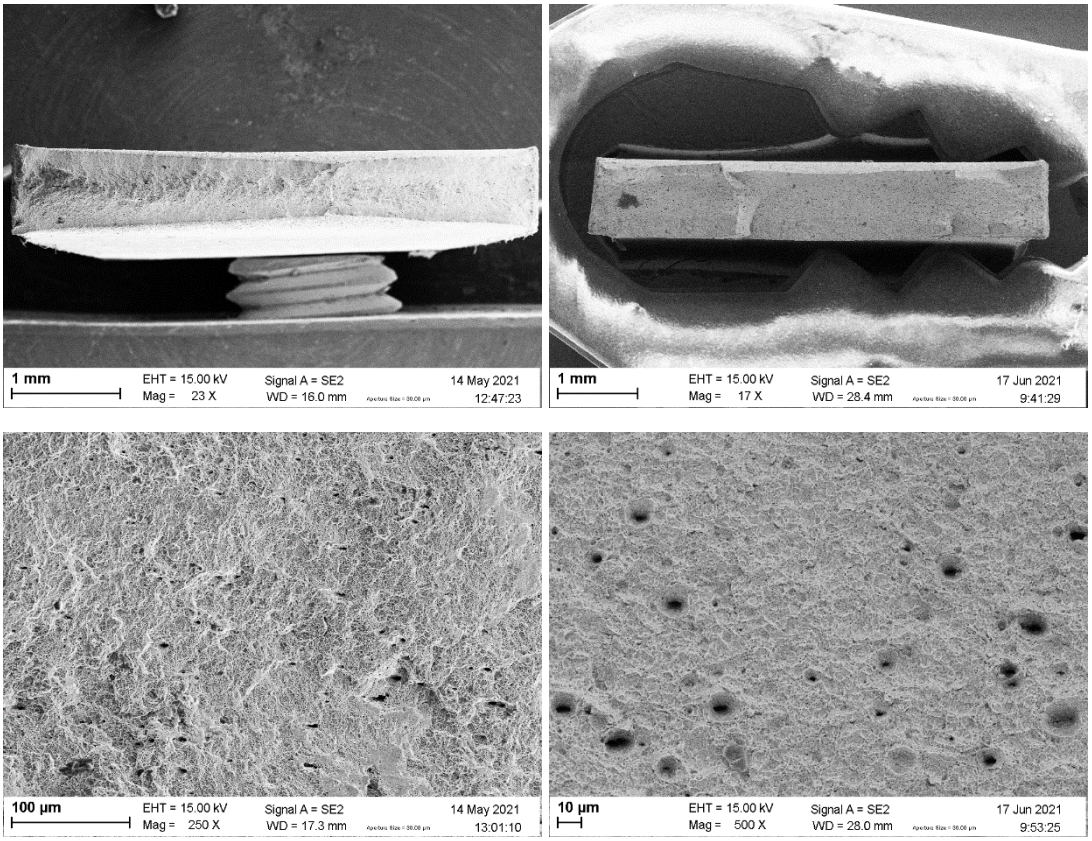

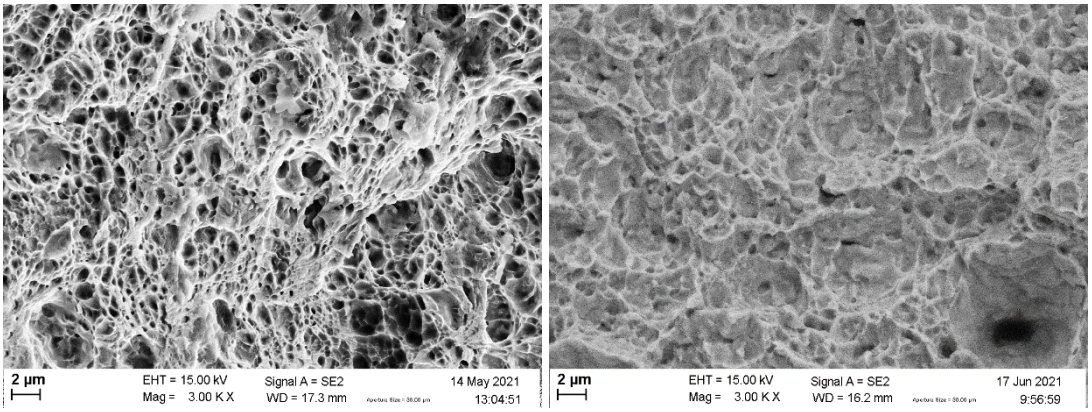

Figure 46: Fracture surface for 750-15 - A (left) and 750-15 - B (right). At low and high magnifications

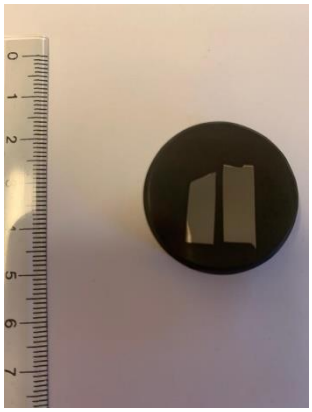

Figure 47: Macroscopic fracture surface for 750-15 - A (left) and 750-15 - B (right)

750-15–A was the best performing sample, and it can be observed that its fracture was purely ductile, with a considerable necking and a fracture creating a 45º angle slant . This sample also presents porosities that are slightly increased on the sample's center, but the samples is still consistent through the width. The observed dimples are on average 1 micron in diameter ,again consistent with the lamellas thickness. 750-15–B has slightly larger dimples and higher void concentration (Figure 46). It can be also observed a "step" on the fracture surface with an almost flat surface.

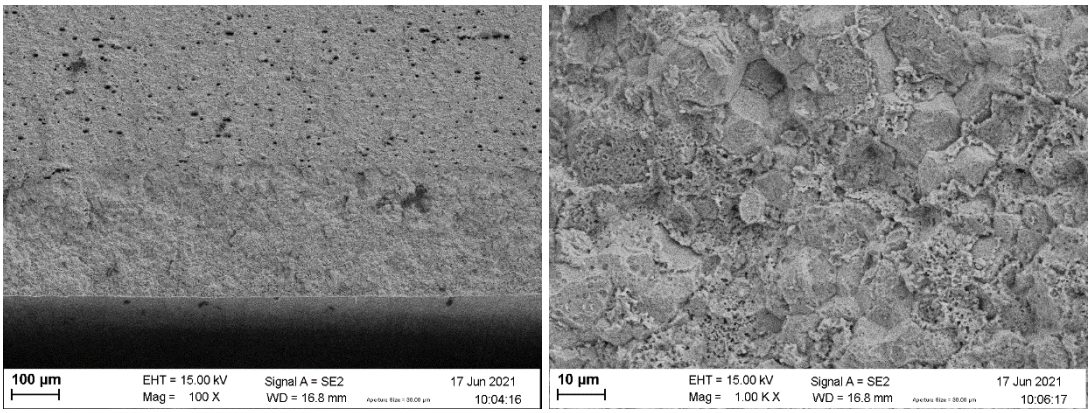

Figure 48: Mixed fracture mechanics on 750-15- B

Sample B also presented a transition from ductile to brittle fracture, as can be observed on Figure 48. This can be observed by the characteristic “steps” formed during brittle fracture (with sizes with the same order as the grains) on the edges of the sample, similar to 750-30 - B.

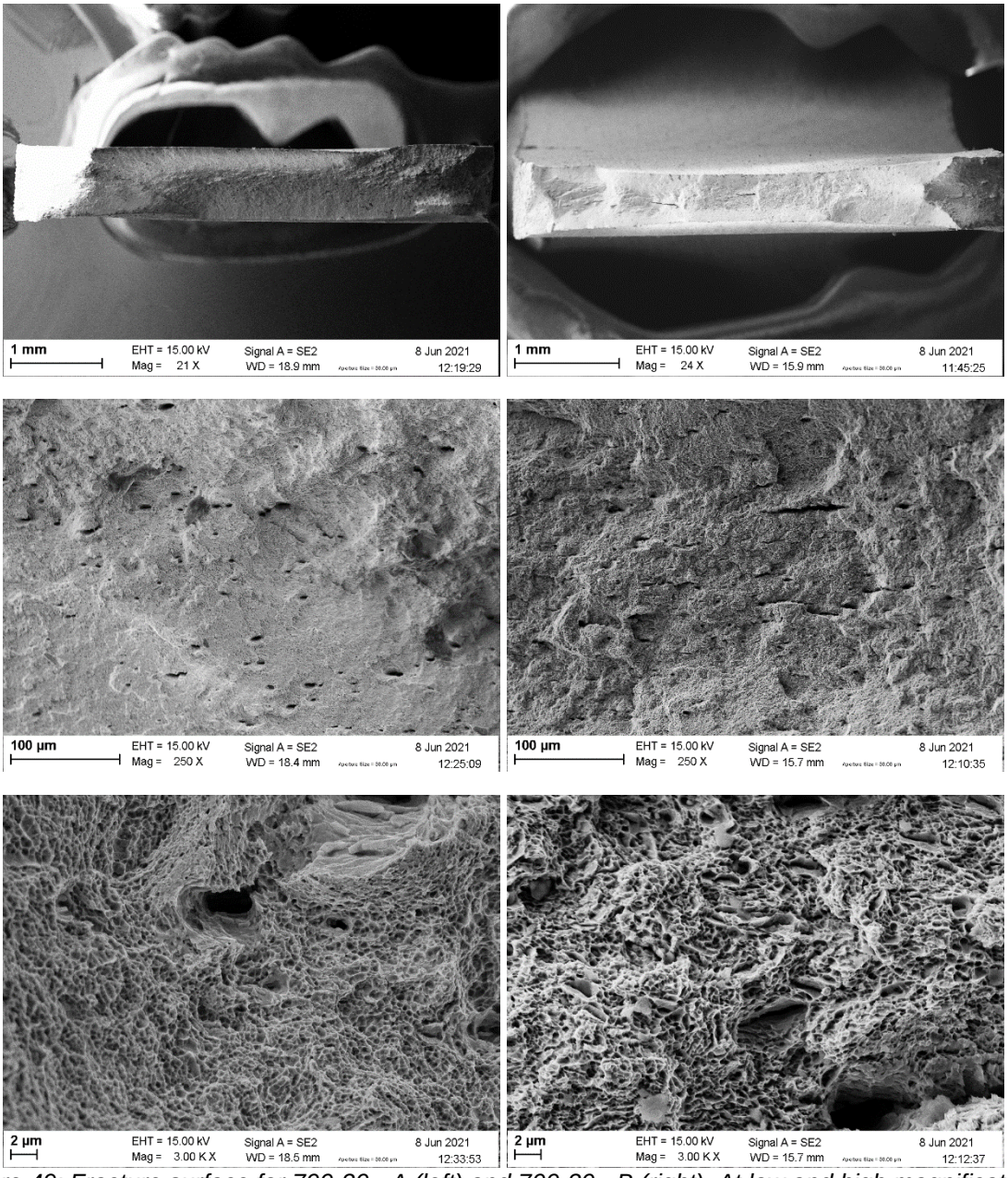

Figure 49: Fracture surface for 700-30 - A (left) and 700-30 - B (right). At low and high magnifications

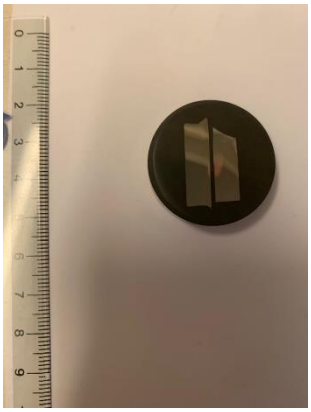

Figure 50: Macroscopic fracture surface for 700-30 - A (left) and 700-30 - B (right)

The samples from 700-30 presented similar void density and size when compared to the samples annealed at 750ºC, the main difference is on the dimples size that ate on average 0,7 microns on diameter, a lot smaller than on 750-30 and 750-15.

Sample A fracture resulted on a cup shaped surface and with no apparent cracks of the fracture surface, this characterizes the fracture mechanics as ductile.

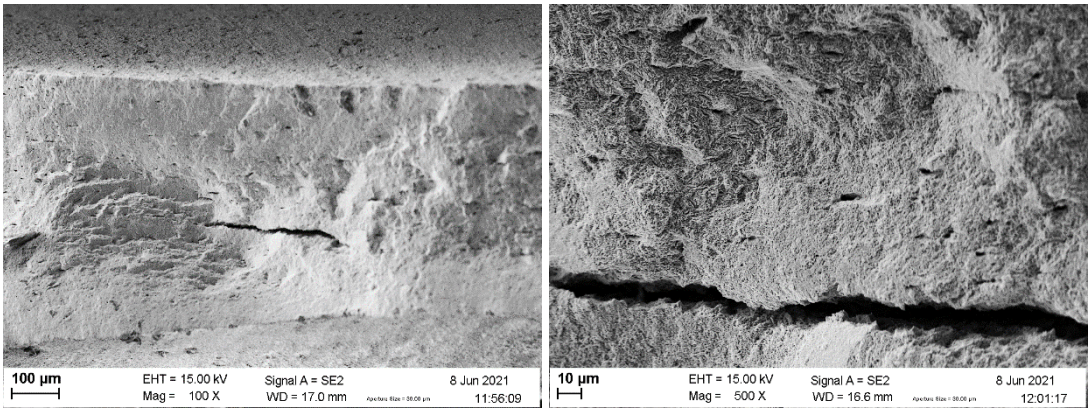

Figure 51 : Large cracks on sample from 700-30 - B

Sample B on the other hand presents large cracks and ridges along the width direction(perpendicular to the tensile direction) this could been due to pre-existing defects on the metal, it also fractured in a single 45º slant. Even with these larger structures, the sample also has dimples that indicate that the fracture mechanics continues to be ductile fracture.

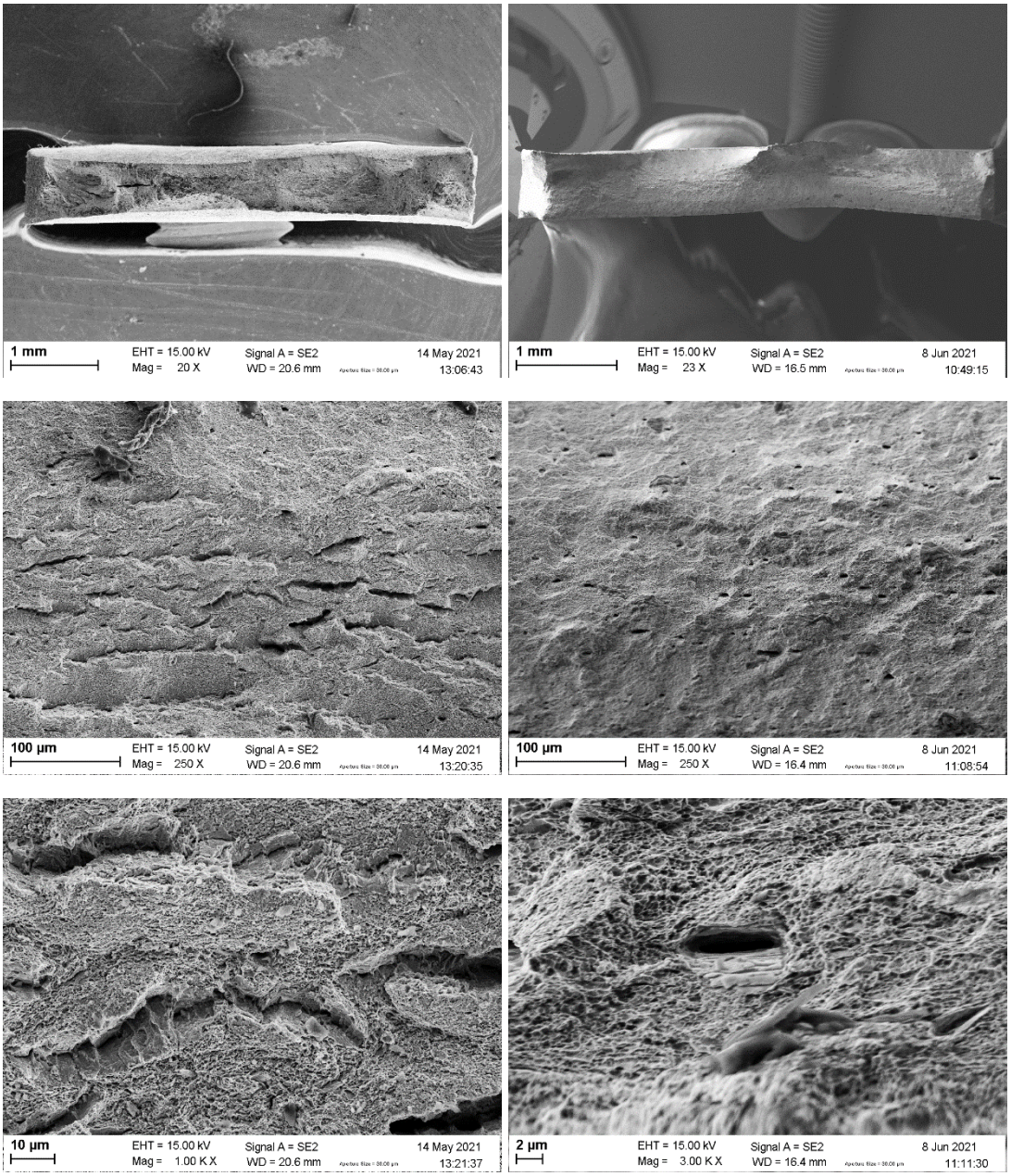

Figure 52 : Fracture surface for 700-15 - A (left) and 700-15 - B (right). At low and high magnifications

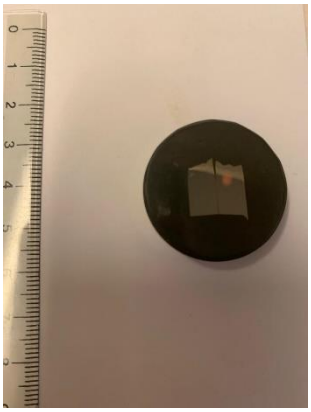

Figure 53: Macroscopic fracture surface for 700-15 - A (left) and 700-15 - B (right)

On 700-15–A different structures can be observed on low magnification (Figure 52), ridges and cracks on the width direction (perpendicular to the tensile

direction) as well as a considerable necking on the sample's center. Besides the cracks , low void density is observed, possible the voids propagated into cracks, while oval dimples are still present and with an average diameter of 0.6 microns. The fracture created is shaped as a 45ºslant.

Sample B has two 45º slants on the edges and two on the center , forming "w" shaped fracture surface. Voids are observed on a similar density as on other samples and dimples sizes are the same as on sample A.

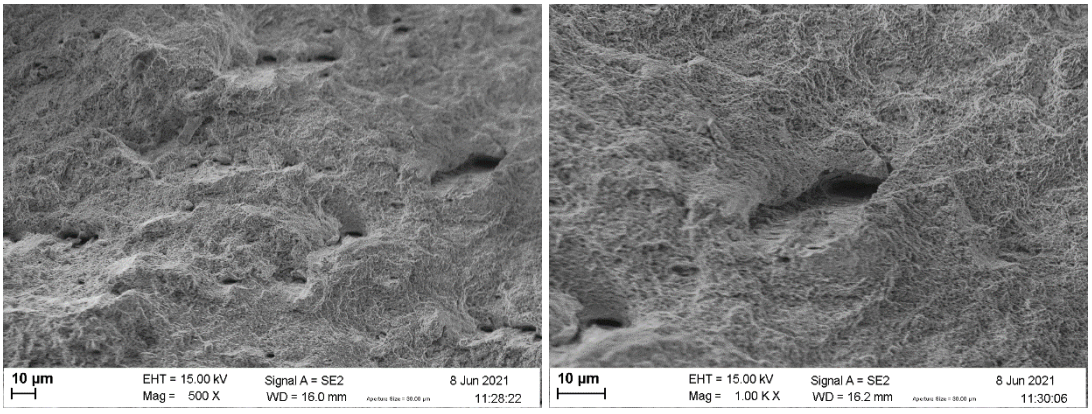

Figure 54 : Voids on sample from 700-15 -B

The observed voids on the samples are elongated on the width direction Figure 54, this could have been caused by the rolling process that flattened the Mn inclusions and while it was elongated it also increased in size on the width direction and decreased on the thickness direction.

By using the obtained images, it is possible to measure the strain on each direction on the samples and calculate the fracture strain for each sample. The measures may not be a perfect representation, because if the samples were not perfectly perpendicular to the support the image will be distorted, but it still a valid approximation.

Table 6: Measurements of initial and final width and thickness

	Wf [mm]	w0 [mm]	Tf [mm]	To [mm]
750 30 A	5.3	5.98	0.937	1.02
750 30 B	5.66	5.98	0.83	1.02
750 15 A	4.97	6.06	0.48	0.99
750 15 B	5.76	5.98	0.96	0.98
700 30 A	5.31	5.99	0.78	1.01
700 30 B	4.6	5.99	0.42	0.99
700 15 A	5.2	5.98	0.53	0.99
700 15 B	4.74	5.99	0.68	1

Table 7: Calculated parameters and fracture strain

	e22 [-]	e33 [-]	e11 [-]	Ef [-]
750 30 A	-0.12071	-0.08487	0.205588	0.206627
750 30 B	-0.055	-0.20613	0.261129	0.275322
750 15 A	-0.19829	-0.72392	0.922209	0.970858
750 15 B	-0.03748	-0.02062	0.058102	0.058912
700 30 A	-0.1205	-0.25841	0.378911	0.387187
700 30 B	-0.26404	-0.85745	1.121485	1.172651
700 15 A	-0.13976	-0.62483	0.76459	0.814265
700 15 B	-0.23405	-0.38566	0.619717	0.625868

4.4 Microstructures after tensile tests

During a tensile test, the microstructure can be affected in various ways, alignment of the grain, appearance of voids, deformation of grains and many others.

The images from the region near the fracture surface (obtained on the SEM) are shown below.

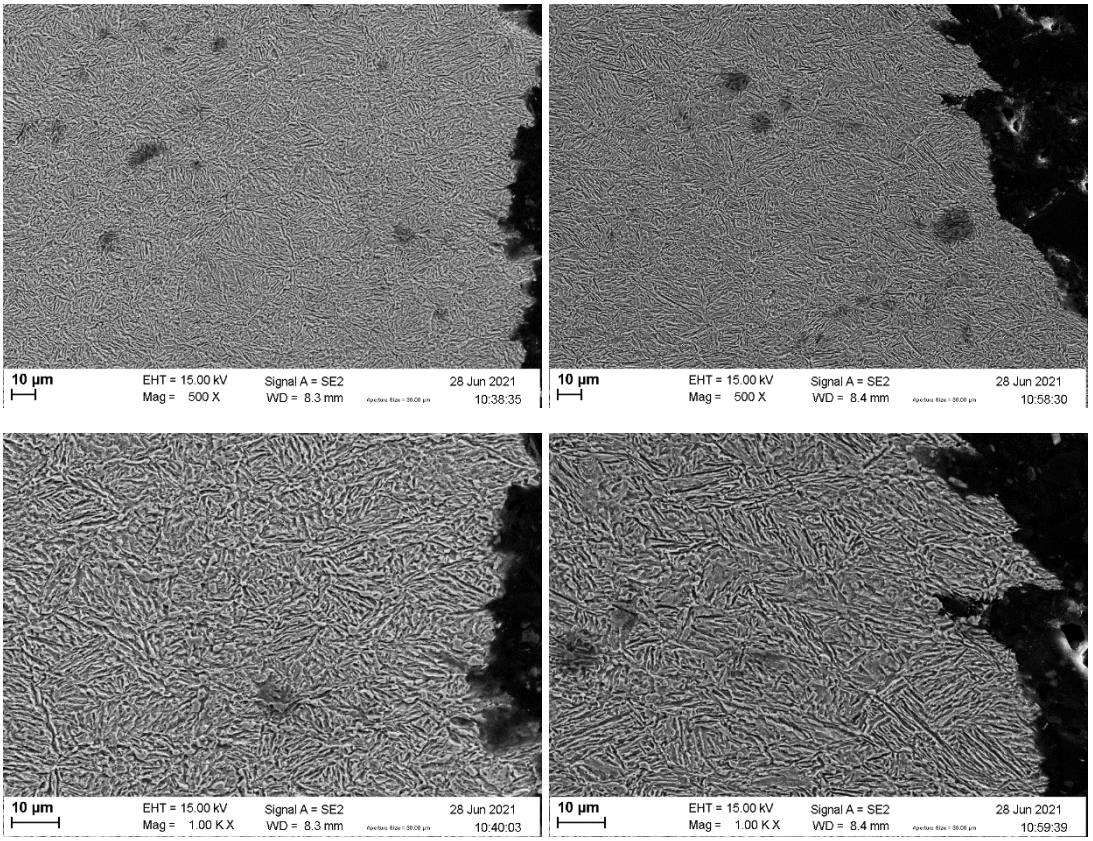

Figure 55 : Microstructures after the tensile test for 750-30 - A (left) and 750-30 - B (right). At low and high magnifications

On both samples from 750-30, almost no voids were observed near the fracture surface and the microstructure is constant through the sample. It showed no alignment of the grains or any other modification on its microstructure.

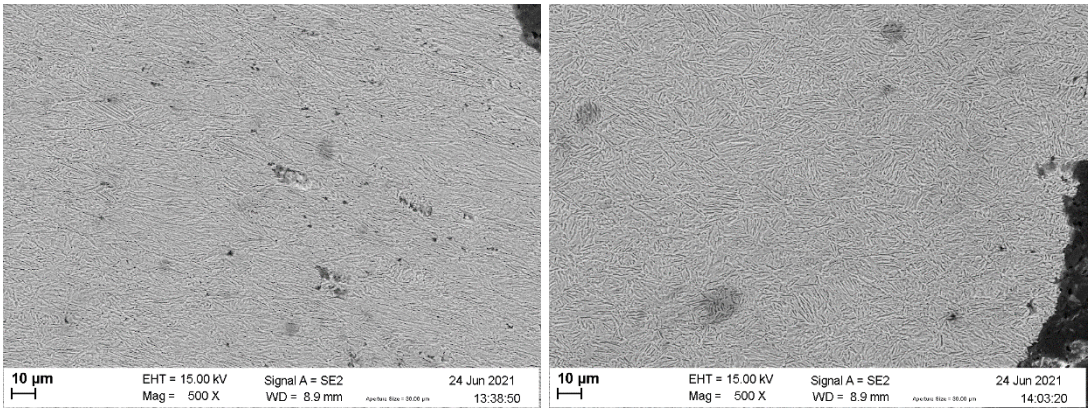

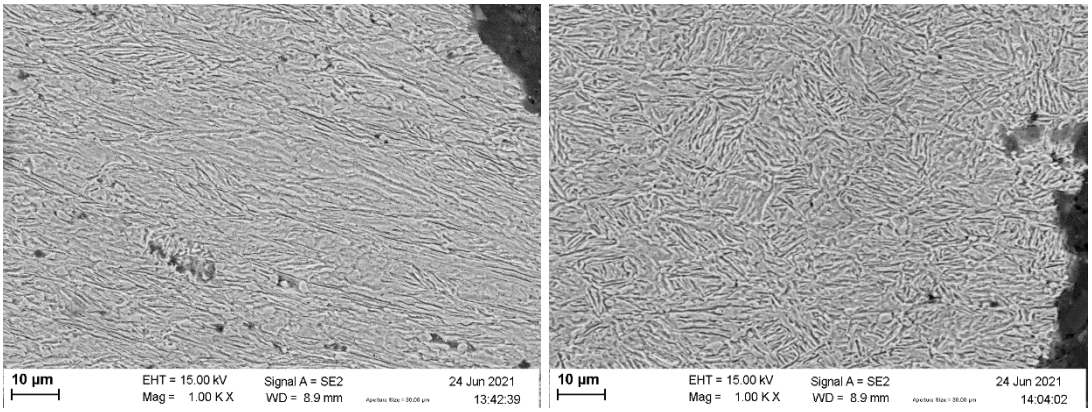

Figure 56 : Microstructures after the tensile test for 750-15 - A (left) and 750-15 - B (right). At low and high magnifications

On 750-15 , sample A presents voids nucleated near the fracture surface, that are not present far from that region, and a high grain alignment with the tensile direction. This characterizes a large change on the original microstructure. This is coherent as this is the best performing sample on the tensile test.

Sample B on the other hand did not develop a grain alignment with the tensile direction, and a smaller number of voids nucleated neat the fracture surface. As both samples had the same heat treatments and compositions, the premature fracture should have been cause by another factor, such as a pre-existing crack or another type of defect.

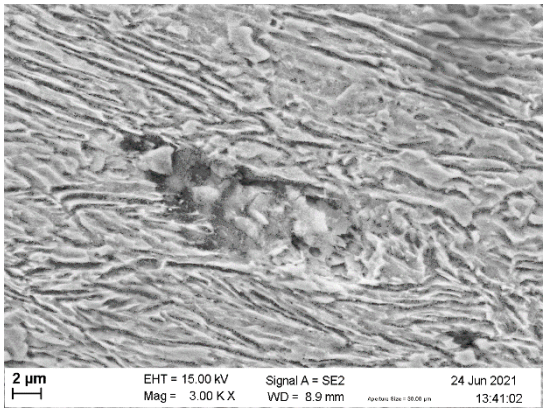

Figure 57: Inclusion near the fracture surface on 750-15 - A

The previously observed Mn inclusions are also present but are modified, appearing now with a scales pattern, a possible cause for this can be that the Mn separated from the steel structure and fragmented into this shape.

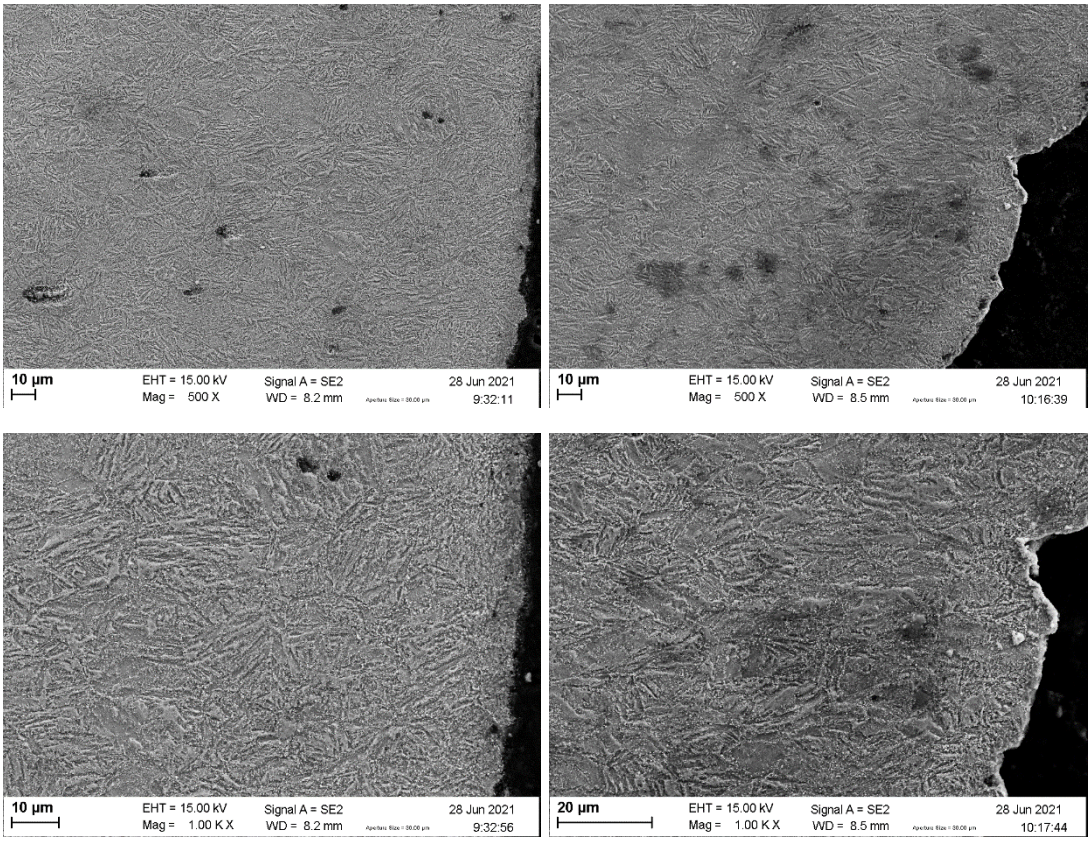

Figure 58: Microstructures after the tensile test for 700-30 - A (left) and 700-30 - B (right). At low and high magnifications

Samples A and B from 700-30 are very similar to each other . Both had voids nucleating near the fracture surface but with minor alignment of the grains with the tensile direction or changes on the microstructure.

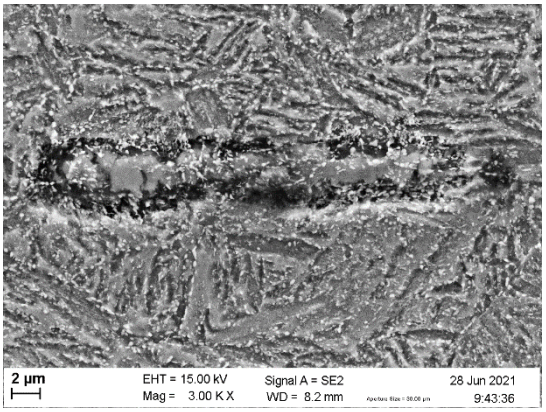

Figure 59: Inclusion near the fracture surface on 700-30 - A

Similar Mn inclusion were observed on the samples with a larger size than the ones observed on 750-15, similar origin is possible for these inclusions. On Figure 59 it is possible to observe one of the inclusions where the white dots are OP-S that was not completely removed

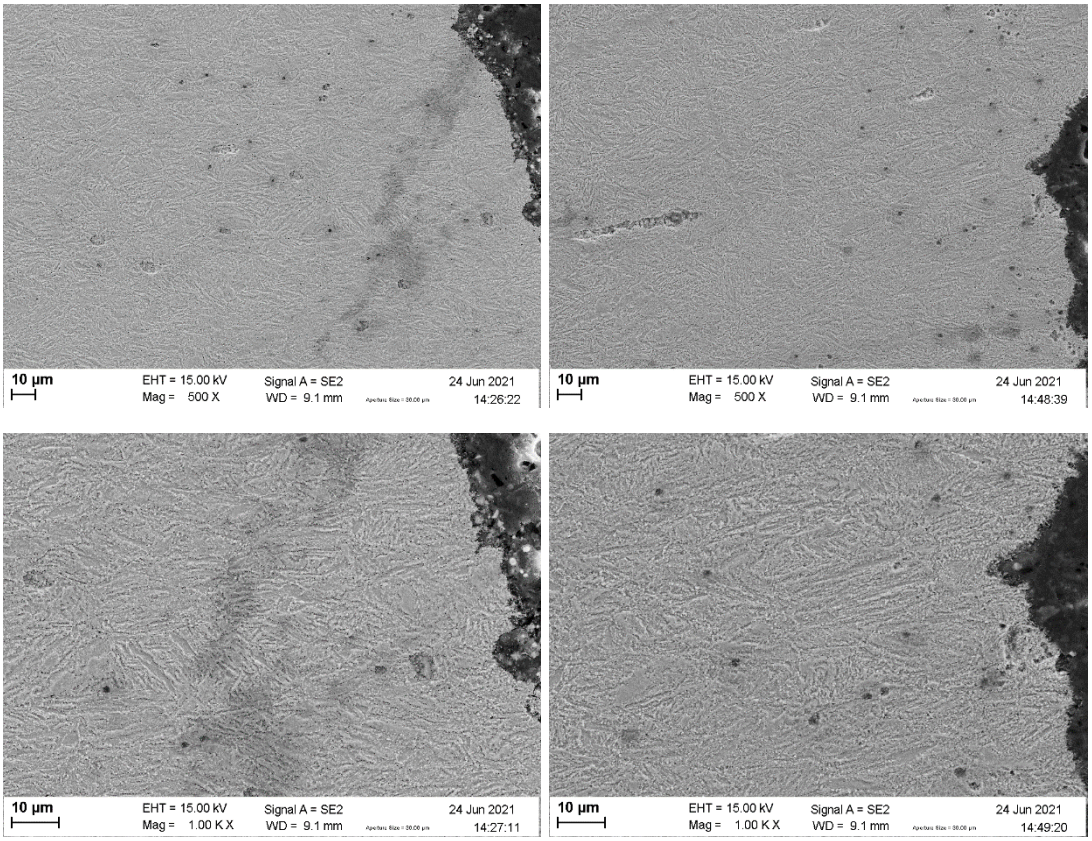

Figure 60: Microstructures after the tensile test for 700-15 - A (left) and 700-15 - B (right). At low and high magnifications

700-15 A and B are very similar near the fracture surface with voids nucleated a minor alignment of the grains with the tensile direction. In general, 700-30 and 700-15 had the same behavior.

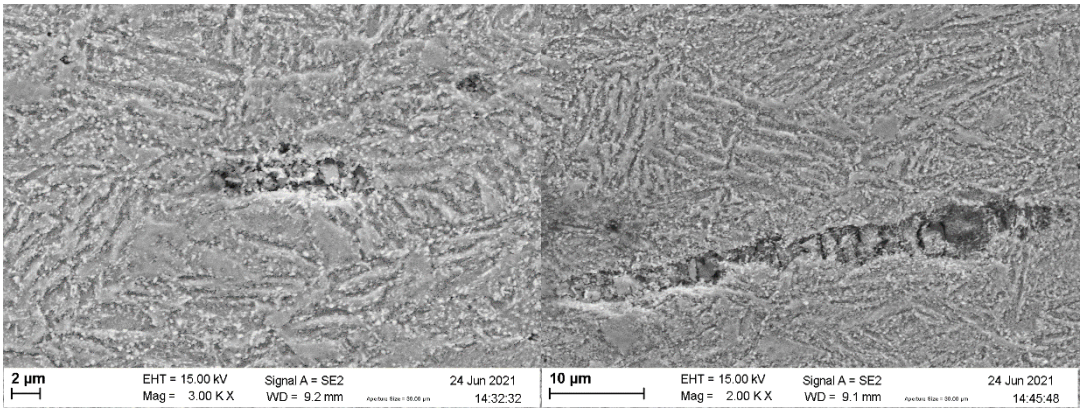

Figure 61: Inclusion near the fracture surface (for 700-15 - A (left) and 700-15 - B (right))

Mn inclusions on these samples are very similar to what was previously described, one inclusion on sample B (Figure 61) is abnormally long, with a length of more than 40 microns, with the same morphology described for 750-15 and 700-30.

Chapter 5

Discussion

This chapter targets to discuss the obtained results and correlate the mechanical proprieties to the resulting microstructure and the heat treatments, while comparing the obtained material with existing metals and metals being developed for similar applications.

Firstly, discussing the microstructures of 750-00 and 700-00, on Figure 28 (b) and (c) referring to 750-00 the composition on this sample is most likely to be ferrite and martensite as it was quenched after the Intercritical annealing, the formed austenite transformed into martensite. As the lamellas observed have the same arrangement and size as the previous martensite, it can lead to the conclusion that the lamellas were formed by it can be assumed that the austenite and ferrite were formed from the fibrous martensite parent structure.

On 750-30 and 750-15 that were annealed at 750ºC a possible route for the formation of the microstructure is that during the Intercritical annealing, ferrite and austenite were formed keeping the fibrous structure from the martensite, after that, during the bainitic maintain, the carbon present in the C-rich austenite diffuses and forms ferrite and cementite (forming the bainite) while the austenite gets its carbon content reduced, stabilizing it into retained austenite. The obtained microstructure is coherent with a medium Mn steel with the two-step heat treatment but adding the bainite phase due to the extra bainitic maintain performed.

The performed heat treatments are like what is used to produce δ-TRIP steels with an extra step of an initial full austenization and quenching to create a martensite fibrous structure that remained present until the final material. The composition on the metal differs with a δ-TRIP steel due to the common high Al content that is not present on the metal processed for this project. This correlation is still valid as the Al is used mainly to reduce the material's density.

As Al reduces the density it also reduces the young's modulus, therefore is expected that the materials developed during this project have a higher modulus than

the traditional δ-TRIP steels. By comparing the obtained microstructure with the one for δ-TRIP steels (**Error! Reference source not found.**), the present phases are the same but with a fibrous structure originated by the initial martensite structure (with the shape of former austenite hexagonal grain boundaries).

A similar heat treatment to the one for this project was performed by Yi et al. (51), with very close temperature and holding times, described below (but with no prior full austenization and quenching) and with Al on the composition (that accelerates the bainitic transformation). It was observed that lower Intercritical annealing temperatures results in slower bainitic transformations due to the higher carbon content on the austenite. With lower Intercritical temperatures and more carbon been enriched into the austenite, its stability is increased and leads to the formation of blocky austenite. During his analysis it was observed the presence of blocky and film austenite as well as bainite, ferrite and small amounts of martensite.

The obtained microstructures and stress/strain curves obtained by Yi et al. for the three heat treatments temperatures and holding times are provided for comparison, where heat treatment C is the closest to this projects metal.

- Heat treatment A consists of Intercritical annealing at 800º C for 5 minutes and isothermal transformation at 330ºC for 30 minutes
- Heat treatment B consists of Intercritical annealing at 800º C for 5 minutes and isothermal transformation at 330ºC for 90 minutes
- Heat treatment C consists of Intercritical annealing at 760º C for 5 minutes and isothermal transformation at 330ºC for 5 minutes

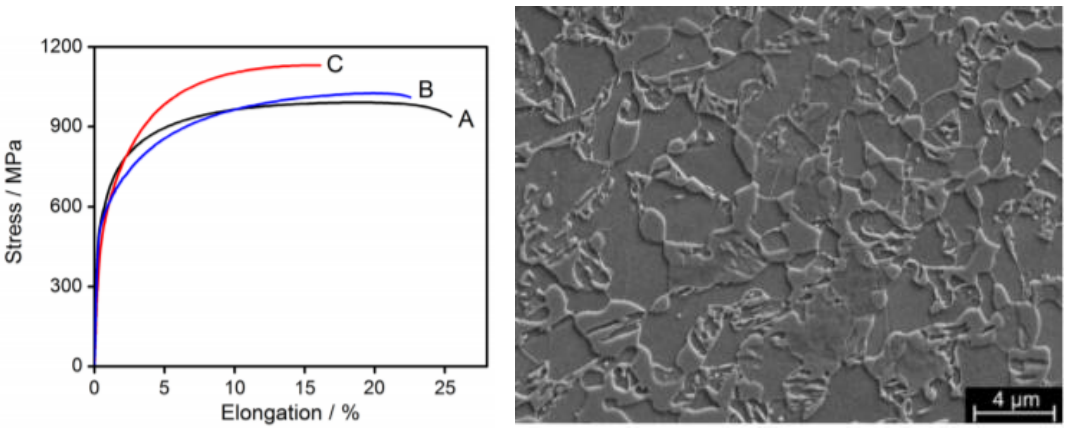

Figure 62: Stress strain curves and microstructure obtained by Yi et al (extracted from (51))

While comparing the microstructure, the encountered phases are the same but the bainite is less prominent on this project's observations. This can be related to the absence of Al on the composition, making the bainitic transformation slower in comparison. The structure itself is also different as the fibrous structure is maintained (Figure 33) and is the main difference between both samples.

This change on structure has an impact on the mechanical proprieties as the best performing sample from 750-15 has higher yield strain, ultimate tensile stress and uniform elongations when compared to all the samples evaluated by Yi et al (51). Therefore, the extra step of fully austenizing and quenching to form a martensite substructure to produce a final product with that structure can contribute for an improvement on the mechanical proprieties if the material can be produced on a manner that premature failure can be prevented.

The difference on microstructure between 750-30 and 750-15 are mainly that the 750-30 have thicker lamella. This can lead to a conclusion that thinner lamella present better mechanical proprieties than the thicker ones. But as there is no clear pattern on the samples, no conclusions can be made. The effect of the length is difficult to be evaluated as both groups present close lamellas length.

Figure 63: True stress/strain curves for 750-30 and 750-15

To prevent the premature failure the causes for it should be first identified. On Figure 42 large, elongated voids were observed that can be correlated to the previously observed manganese inclusions that may acted as nucleating voids and favored the premature crack propagation and therefore, the premature failure of the sample.

It was also observed that the dimples size matches the lamellas thickness and contribute to the conclusion that the main failure mechanism is ductile. But some samples presented regions with brittle fracture that for 750-30-B can be attributed to the large crack along the sample's width that most probably served as a stress concentration point and favored the brille fracture. While for 750-15-B it is not clear what caused the transition to brittle facture, but it is possible that during the void nucleation a defect caused it, this is indicated by the step of the fracture surface, observed on Figure 47.

On a publication of Shiri et al. (52) about the failure on Nb-micro alloyed δ-TRIP steels it found that the fracture surface was similar to what was observed on 750-30 and 750-15, a mixture of ductile and brittle fracture, with tearing and ridges on the sample's center, similar angle of the fracture surface with the tensile direction. The brittle fracture is concentrated on the edge and present "step" (or "terrace") shape structures mainly formed by cleavage. It was concluded that the soft phases such as austenite and ferrite produced the dimples' structure while hard phases as martensite produces the structures originated from cleavage.

As there is no pattern on the stress/strain curves related to the bainitic maintain holding times, a correlation with it is impossible with this number of samples and the failure is most probably related to defects present on the samples.

Analyzing the microstructure after the tensile tests, elongated voids in the tensile direction were observed on 750-15-A, indicating an early nucleation, the voids seem to be nucleated mainly by particle decohesion. This effect was observed by Karin et al. (5) that performed a close heat treatment but without the bainitic maintain, it found that the particle alignment results on a higher resistance to void nucleation increasing the fracture strain as the most propitious weak spots for void nucleation (the phases interface) are now perpendicular to the tensile direction. Combining good resistance to void nucleation and resistance to void coalesce would result in a larger

fracture strain.

on the other hand, the remaining samples from 750-30 and 750-15 develop no or a small number of nucleated voids and zero to small amounts of alignment with the tensile direction, despite having the same or similar heat treatments and compositions, contributing to the hypothesis that the failure was caused by pre-existing defects.

Regarding the strain hardening, the samples that suffered plastic deformation (all except for 750-30-A) had similar strain hardening rates until failure with no considerable difference between holding times. By comparing the curves with the Considere's criterion, it is possible to conclude that only 750-15-A reached the necking point, even though the curve did not touch the Considere's criterion line, because necking was observed on the sample, this discrepancy could have been caused by the fitting made using Table Curve 2 D . All other samples failed before reaching the necking point. The same strain hardening behavior was observed on (51) and attributed to TRIP effects, more specifically to the transformation of blocky austenite into martensite at early stages of staining and the film austenite during all the deformation, prolonging the uniform elongation. Therefore, a balance between these two morphologies is desired. On 750-15-A, the strain hardening rate decrease rapidly with the initial deformations, then, the strain hardening stabilizes at constant level (observed on the bending on the curve). This bending is most likely to be cause by the TRIP effects and the consequently increasing of the material hardening.

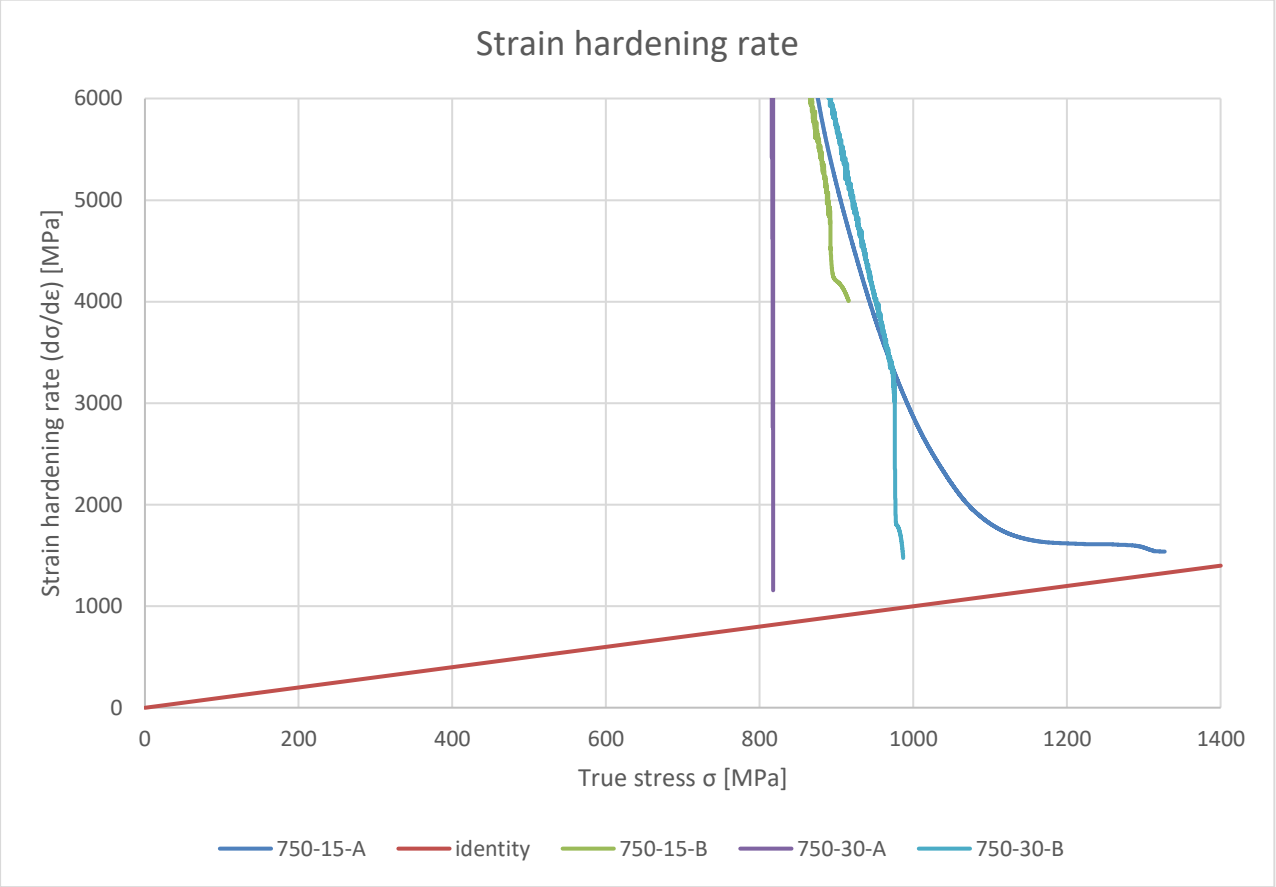

Figure 64: Stain hardening rates for 750-30 and 750-15

Summarizing 750-30 and 750-15 , great results can be obtained by refining the composition and heat treatments to reduce defects and pre-existing cracks on the material as they prevent the metal from achieving outstanding mechanical proprieties like 750-15-A, in a consistent and predictable way.

For samples from 700-30 and 700-15 that were originated from 700-00, the microstructure is completely different from the previous discussed groups as the Intercritical temperature is not reached and therefore no austenite was produced. Another conclusion is that the Intercritical temperature for this composition is between 750ºC and 700ºC.

On the intermediate 700-00, ferrite grains on the nanoscale were observed with spheres of cementite. This agrees with the thermocalc simulation of the phase proportions as a function of the temperature, provided by Thibaut Heremans (Figure 31). A possible route is that the martensite started transforming at the grain boundaries into ferrite and cementite (because the temperature was below the lower Intercritical temperature) and assumed this structure after quenching.

Wang et al. (**Error! Reference source not found.**) has similar results on a

much complex heat treatment but with same principle, several annealing processes, but with the addiction of Cr on the alloy. A microstructure composed of a ferrite matrix with undissolved spheroidized cementite was observed (similar to this project's observations), the chromium present was reported to affect the cementite dissolution. As Wang at al. concluded that Mn is highly soluble on cementite and the spheres had higher Mn content than the surrounding ferrite matrix and this can be also the case for 700-00 samples.

As no tensile test war performed on 700-00, the comparison between the mechanical proprieties is impossible. Wang et al. observed great change on mechanical properties between the samples with more annealing process and great strain hardening properties on most of the tested samples. On his paper if was found that the mechanical proprieties are mainly determined by sizes of the ferrite grain and the cementite spheres.

The cementite spheres could be observed on the fracture surface inside the dimples. Therefore, it is possible to infer that the void nucleation can be started on then (the larger number of dimples and smaller size can be correlated to larger elongations.

The microstructure observed on the samples of this project presented generally smaller cementite spheres, this is possibly due to the drastically smaller holding tome for annealing and that only one annealing treatment was done. An important remark is that on (**Error! Reference source not found.**) the cementite spheres changed in size according to each heat treatment with the smaller on being on the spheroidizing annealing.

Even though materials similar to 700-00 has found applications and developments , the objective of this project is the complete heat treatment including also the bainitic maintain and the microstructure produced by this processing.

After the bainitic maintain the microstructure was greatly modified, presenting larger ferrite grains with random orientations (where there was only nanoscale ferrite grains) with cementite spheres (Figure 36). The lower temperature of 700°C does not reach the Intercritical domain, being slightly below the lower Intercritical temperature and therefore will constitute a similar heat treatment to soft annealing. At this temperature, the martensite will transform into ferrite and spherical cementite.

After this process, during the bainitic maintain diffusion will take place and the now allowed diffusion will again form larger ferrite grains. This structure presents no austenite at all, but instead presents cementite spheres that were formed instead.

The phases present are also different from 750-30 and 750-15 , as according to Kangying et al. (**Error! Reference source not found.**), ferrite retards the formation of bainite and accelerates the martensite formation. The bainite formation was also concluded to occurs on the interface between ferrite and austenite with the percentage on the ferrite phase being inversely related to the bainite formation. Therefore, the formation of bainite on these samples are not to be expected. And on a publication of Lee et al. (**Error! Reference source not found.**) it was calculated a possibility of having ferrite austenite and cementite on the same region for a similar composition but as no austenite was identified on the XRD, no austenite presence will be considered.

As the Intercritical region was nor reached and no austenite was formed, 700-30 and 700-15 cannot be considered a δ-TRIP steel. The microstructure and composition of the final product is comparable with the Q&P steel produced by An et al. (**Error! Reference source not found.**). On the article it describes a similar steel but with the addiction of other alloying elements but mainly Ni. It was reported that Ni works to reduce the grain sizes and as a cementite destabilizer, therefore, the cementite appearance with Ni present should be reduced when compared to 700-30 and 700-15.

The observed microstructure after quenching is very similar to the one for 700-00 and 700-00, mainly martensite grains respecting the boundaries of the former hexagonal austenite grains and on variating orientations.

After the tempering at 630ºC for 1.5 hours, a ferrite matrix maintaining the martensite structure with cementite precipitates formed on the grain boundaries, either with elongated shapes or granular and discontinuous, the later similar to what was observed on the project's samples. The main difference between 700-00 and 700-30 and 700-15 was the formation of large ferrite grains , this is most likely to be caused by the last heat treatment that by maintain the nanoscale ferrite grains on a moderately high temperature causes the grains to grow.

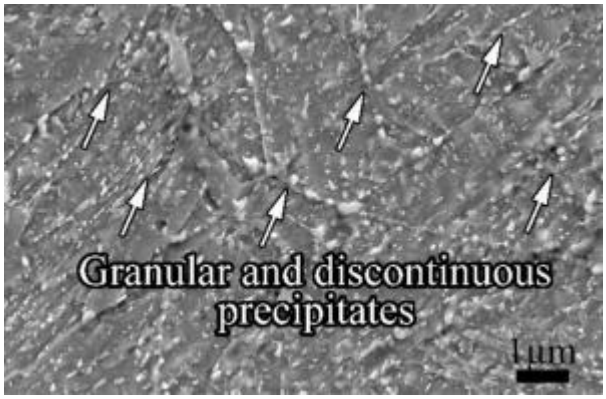

*Figure 65: Microstructure obtained by An et al. (modified from (**Error! Reference source not found.**))*

This steel can be described as a Q&P steel where the quenching temperature was not between martensite start and finish temperatures and consequently has no retained austenite on the final product, but cementite on its place as the diffusing carbon diffuses away from the martensite forming only ferrite and martensite.

To evaluate the mechanical proprieties, a comparison with the results achieved by Jia et al. (45) can be made. On this article a steel with final microstructure containing a ferrite matrix with nanoscale spheroidized cementite (Figure 66) was obtaining after obtaining a fully martensite structure by homogenizing and quenching followed by annealing at 750°C for 5 minutes and hot rolling at the same temperature and again annealed at 550°C for 5 minutes (UFG-1) and 600 °C for 5 minutes (UFG-2). The elongated pattern on the observed microstructure is due the final hot rolling. Ferrite grains on the order of 1 micron (smaller than 700-30 and 700-15).

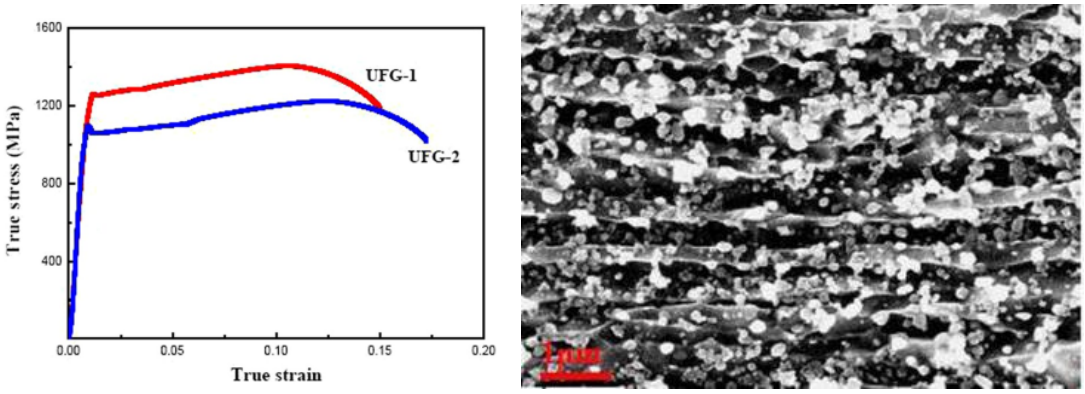

Figure 66: Stress strain curves and microstructure obtained by Jia et al (extracted from (45))

This indicates that the material from 700-30 and 700-15 is in fact ferrite and cementite, formed by annealing the martensite at temperature below the Intercritical domain. Ans also the possibility of forming very small ferrite and cementite grain sizes that can be beneficial for the mechanical proprieties.

By comparing the true strass/strain curves it is possible to identify Lüders bands on both works, the main difference is that both samples from (45) have higher ultimate tensile strengths, ranging from 1260 MPa to 1400MPa for UFG-1 and from 1080 MPa to 1200MPa for UFG-2 and from , while 700-30 and 700-15 has a maximin of 1051 MPa for the best performing sample. On the other hand, the uniform elongations are higher on 700-30 and 700-15, highlighting the compromise between toughness and ductility.

The higher ultimate tensile stresses can be caused by the warm rolling and refinement of the ferrite matrix, with the higher temperature final annealing presenting a higher ultimate tensile strength and smaller total elongation and vice versa. While the coarsening of the cementite will reduce the ultimate tensile and increase the uniform elongation.

The difference on microstructure between 700-30 and 700-15 are mainly that the 700-30 have slightly bigger cementite spheres with no apparent change on ferrite grain size. Thus, leading to the conclusion that increasing the size of cementite spheres improves the mechanical proprieties. But similarly, to the discussion of 750-30 and 750-15, there is no clear pattern to relate the sphere sizes to the proprieties, as the second-best sample is part of the 700-15 group.

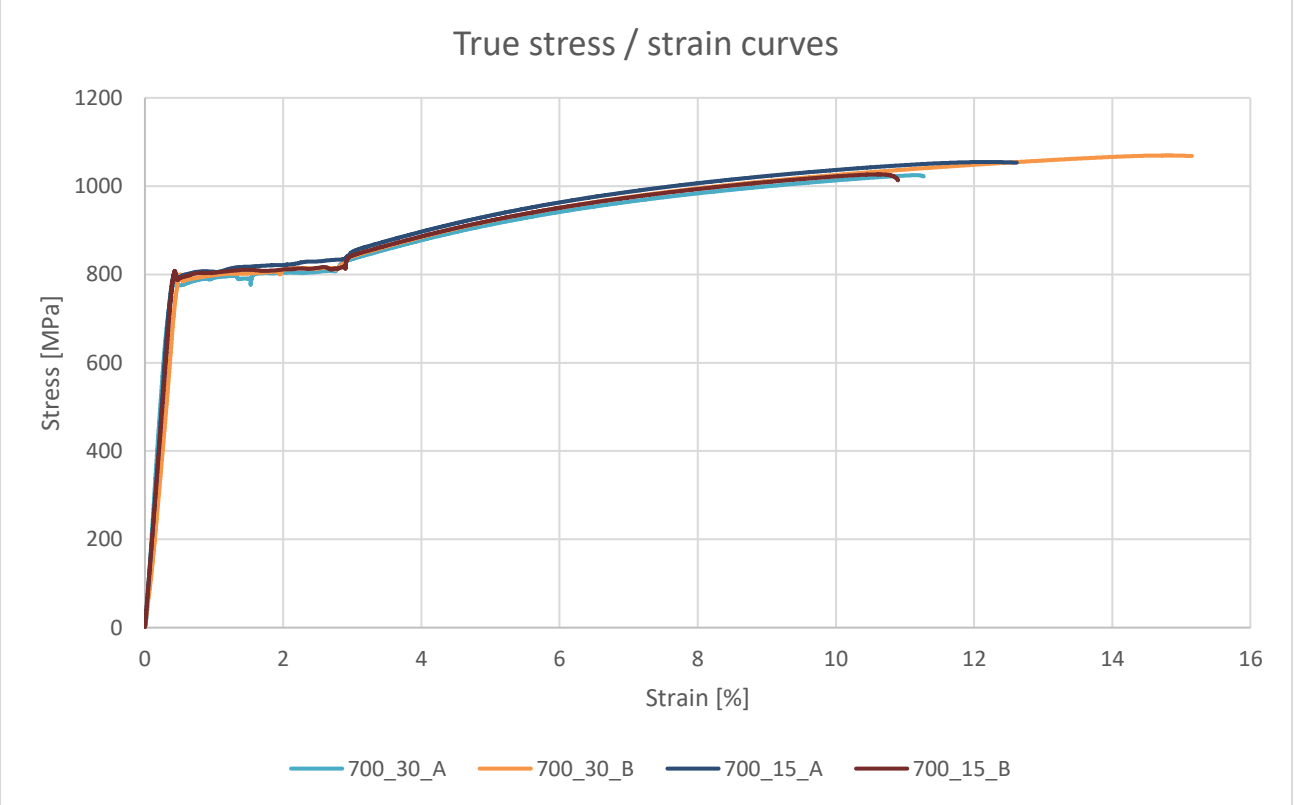

Figure 67: True stress/strain curves for 700-30 and 700-15

The observed strain hardening rates for 700-30 and 700-15 can be seen on Figure 68, it can be concluded that most samples reached the Considere's criterion and therefore reached the necking point (besides 700-15-A). The decrease on the strain hardening rate can be divided into two main linear parts. The first part is a sharp drop on the strain hardening rate that can be related to the region right after the Lüders plateau, the second on is after a step, it is still decreasing but at a slower rate.

Similar results were obtained by Gao et al. (**Error! Reference source not found.**), it was also a decrease on the strain hardening rate after the Lüders plateau, flowed by a step and a slower decrease after. On their article, it was found that the strain hardening rate can be a combination of the hardening rates of each phase. This implies that the hardening of a single phase can slow down the decrease of the total stain hardening rates of the total specimen.

Therefore, this behavior can be observed on metals with a Lüders plateau on its stress/strain curve. But no increase on the strain hardening rate could be observed for the samples annealed at 700º C. There were also not substantial differences between samples with samples of different holding times on the bainitic maintain.

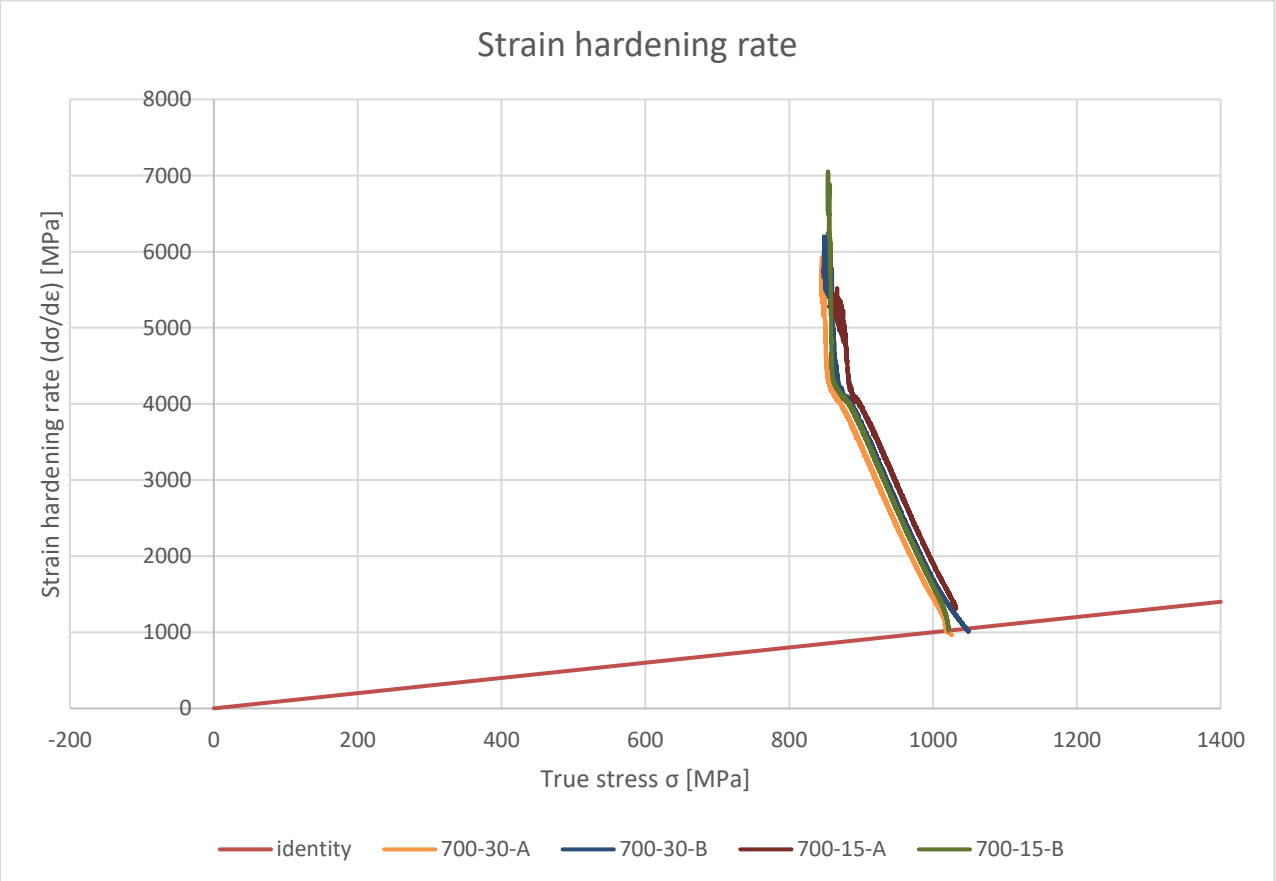

Figure 68: Stain hardening rates for 700-30 and 700-15

The strain hardening is essential to achieve large uniform elongations without necking, this strain hardening is mainly due to the cementite precipitates that act as dislocation obstacles on the ferrite matrix, improving the proprieties of the material.

After failure, the observed fracture surface presented clear signs of necking and voids appearing as holes with “scale” like structure on the surface that can be related to the previously identified Mn inclusions, The void density is compatible along samples. An interesting detail is that the two best performing samples (700-30-B and 700-15-A) have the presence of large ridges and cracks while the remaining samples have none. This can be caused by the energy dissipated by the cracks that did not grew enough to cause a failure.

The dimples size observed on 700-30 and 700-15 are a lot smaller when compared to 750-30 and 750-15 . This is due to the reduced size microstructure of both the cementite and ferrite. A possible mechanism for this ductile fracture is that the voids started nucleating on the cementite grains, either by decohesion or particle break. As cementite particles are very small no conclusion regarding if the inclusions broke or suffered decohesion can be made by observing the possible deposited particles inside the dimples.

According to Shibanuma et al. (**Error! Reference source not found.**) fracture by cleavage is possible by nucleating a crack on the cementite particle that propagates along both the ferrite matrix and the grain boundaries. Even though it is possible no signs of cleavage fracture were observed on any of the samples from 700-30 and 700-15 .

Analyzing the microstructure after the tensile tests, the observed voids nucleated are another indicator of the ductile fracture mechanisms. There is also a difference between 700-30 and 700-15 . While 700-30 had low or no alignment of the grains with the tensile direction, 700-15 had a small alignment of the grains with the tensile direction. This difference had no visible effects on the mechanical proprieties illustrated on the stress / strain curves as both groups do not present a clear benefit against it other as the two best performing samples from the 700ºC groups are one from 700-30 and one from 700-15. These samples are also not perfect coherent on the mechanical proprieties as the failure should have been caused by existing defects on the metal, this justifies why materials with the same composition and heat treatments appears with discrepancies on uniform elongation and ultimate tensile

strength.

Regarding the relation of all the microstructures and their mechanical proprieties. It is reported that both strength (**Error! Reference source not found.**) and toughness (**Error! Reference source not found.**) are improved with decreasing grain size while the ductility is reduced (**Error! Reference source not found.**). The increase on strength and toughness is mainly due to the hindering of dislocations that is favored with smaller grains. The same reasoning is used to justify the decrease in ductility as with more resistance to dislocations the material will withstand more plastic deformation. This duality between increasing all strength, toughness and ductility is also present on defining the optimal grain size of the steel

The shape of the grain is also an important factor. On an article of Abid et al. (**Error! Reference source not found.**)(**Error! Reference source not found.**), it was predicted that equiaxed and elongated martensite grains would improve both strength and ductility (with a larger influence on ductility). A similar morphology to 750-15. This can explain the great combination of proprieties achieved on that sample.

To evaluate the steels' toughness different parameters can be considered. For example, the UTS X TE product, that may not be accurate as a representation of the toughness, and the fracture strain (ε_f) that is more representative for the toughness.

To analyze the fracture stain, the two best samples will be considered 750-15-A and 700-30-B with fracture strains of 0,97 and 1.17 respectively (Table 7). These fracture strains can be considered high as will be discussed.

Hance et al. (**Error! Reference source not found.**) compared AHSS steels of different generations based on the true strain (ε_u) and true fracture strains (TFS) (that require a more precise measurement of the initial and final areas), these values are not very discrepant with the measured uniform elongation and fracture strain. Thus, the Hance diagram (Figure 69) will be utilized as a rough estimate of the quality of the steel. The hence diagram the dashed lines represent the boundaries between the regions of global, balanced, and local formability and the continuous curves are arbitrary the same formability index, iso-F.I ($F.I = \sqrt{\varepsilon_u . TFS}$). Being separated into increasing quality, from poor to excellent.

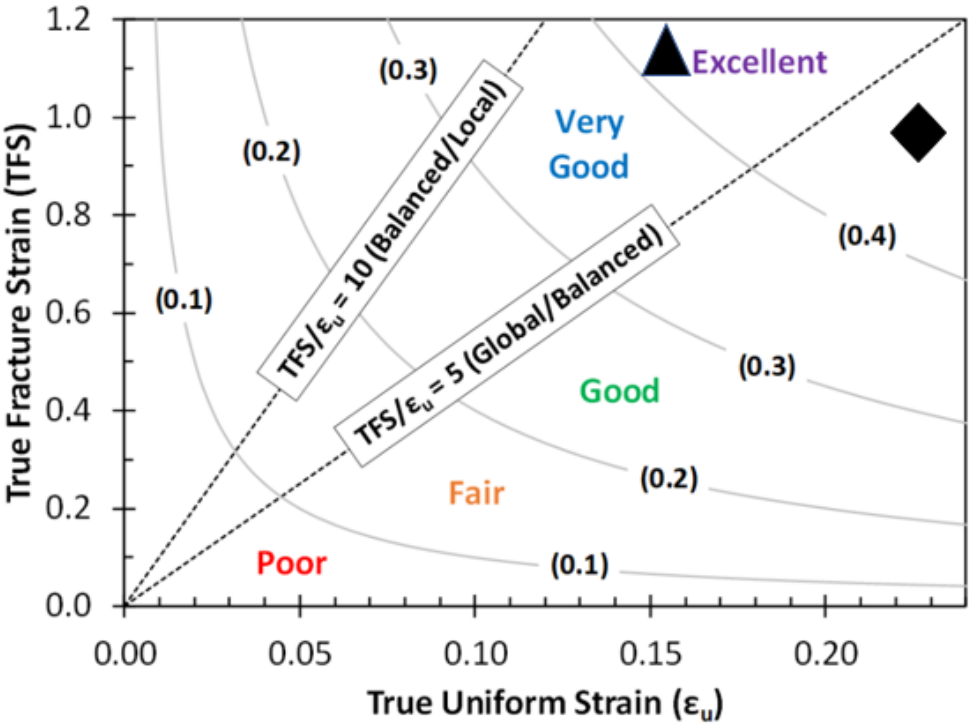

*Figure 69: Hance diagram including the best performing samples (diamond for 750-15-A and triangle for 700-30-B) (modified from (**Error! Reference source not found.**))*

By plotting the proprieties from 750-15-A and 700-30-B into the Hance diagram using the information's from Table 5 and Table 6, 700-15-A would be considered to have an excellent formability index and a global formability. While 700-30-B would be also considered to have an excellent formability index but have a balanced formability.

Another comparison for the fracture strain can be done with the work of Karim et al. (**Error! Reference source not found.**) that found fracture strain in the range of 0.67 up to 1.11 for DP steels. Highlighting the potential and outstanding mechanical proprieties for the analyzed 750-15-A and 700-30-B.

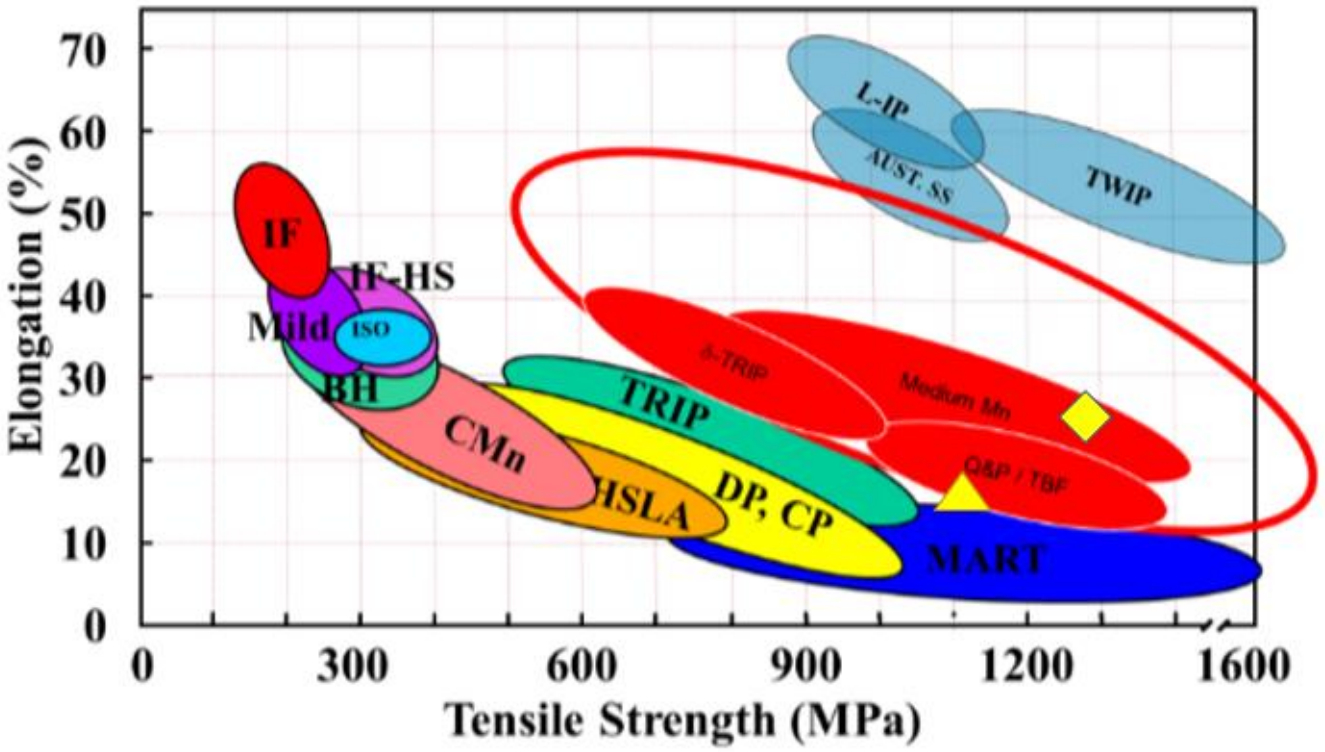

Figure 70: Modified Figure 1 including the best performing sample for each annealing temperature (diamond for 750-15-A and triangle for 700-30-B)

By plotting the proprieties of the best performing samples on Figure 1, one can conclude that the 750-15 have the proprieties of a medium Mn steel and can be considered part of the developing 3rd generation of AHSS (Figure 70), with both high toughness and high strength, this can be expanded for 750-30 if the premature failure cause can be prevented. On the other hand, 700-30 and 700-15 have mechanical proprieties that barely compare to Q&P and TBF steels but can still be considered part of the 3rd generation of AHSS.

700-30 and 700-15 are reliable metals that have good proprieties and can be applied on various industries including the automotive. Further investigation to point the exact reasons the materials from 750-30 and 750-15 had premature failure and preventing it from happening can lead to metals with the mechanical proprieties from 750-15-A and a reliable steel that can be applied on the automotive and petroleum industry.

Chapter 6

Conclusions

The 3rd generation of AHSS have a key role on reducing fuel consumption. This can be achieved by the reducing the weight of vehicles, causing the reduction of greenhouse gases while reducing costs of producing and maintaining then. Sustaining the vehicle's safety is also mandatory and thus, these steels are of great interest for the industry. On the petroleum industry it can lead to cost reduction and time savings on different applications by keeping the material's proprieties and reducing weigth. This generation of the AHSS being developed to combine the once contradictory mechanical proprieties of toughness strength and ductility. Maintaining the production costs low and the easiness of the manufacturing. The challenge is to find the best composition and heat treatment to optimize the desired proprieties for each application. Encouraging studies demonstrated that the gap between the 1st and 2nd AHSS generations can be filled with the 3rd. In this master thesis, the effects of four heat treatment were investigate by evaluating the resulting microstructures, performing tensile tests, observing the fracture surface and the changes on the microstructure after the tensile tests. Following the discussion of the results, the conclusions were:

1. The lower Intercritical temperature for the evaluated composition is between 700°C and 750°C.
2. Large Mn inclusion are present during all stages of the heat treatments and may be a source of voids nucleation, a cause for crack propagation and cause premature failure.
3. A microstructure containing ferrite, bainite and retained austenite can be obtained by annealing at 750° C and following It with a bainitic maintain at 360° C. No conclusive change in proprieties could be evaluated as a function of the holding times.
4. A microstructure containing ferrite and sphere cementite can be obtained by annealing at 700°C and following It with a bainitic maintain

at 360°C. No conclusive change in proprieties could be evaluated as a function of the holding times and without the bainitic maintain a nanoscale ferrite microstructure with nanoscale cementite spheres is obtained.

5. 750-15-A highlights the potential of this material, presenting an ultimate tensile strength of 1327,23 MPa and uniform elongation of 23,11%. An outstanding combination of toughness and strength. Although it is not currently reliable as the other samples annealed at 750° C had premature failures.

6. 700-30-B has a great potential as a material, presenting an ultimate tensile strength of 1051,76 MPa and uniform elongation of 15,15%. The samples annealed at 700° C are reliable, not presenting a huge disparity between samples.

7. All the samples had ductile fracture, but some of them presented a transition to brittle fracture that may have been caused by existing defects or inclusions. It was also observed that samples with cracks or ridges on the fracture surface performed better. While only 750-15-A had a considerable change in microstructure after the tensile tests

8. 750-15-A and 700-30-B have high fracture strains, compatible with the AHSS being developed and have excellent formability index and global and balanced formability respectively.

The obtained results are compatible with the literature for the development of 3rd generation AHSS of various groups and TRIP steels, even with some differences on composition and heat treatments.

Using a temperature below the Intercritical temperature provided an opportunity to evaluate a different type of steel that have interesting proprieties, such as the highest fracture strain calculated on this project. And at the same time evaluate the targeted steel with TRIP effects that have incredible properties in comparison with similar materials.

In the light of this research there are recommendations for following studies. The first is to utilize temperatures above 750°C for the Intercritical annealing. This would allow to evaluate the effect of different temperatures on the annealing process,

on the tensile curves and microstructure, especially on the amount of retained austenite and bainite formed on the bainitic maintain. The inverse is also valid, as using temperatures below 700°C can also be interesting to optimize this steel that has proven to have great proprieties and reliability. Secondly, modifying the composition of the steel, either keeping the same alloying elements and changing their wt% or even adding new alloying elements can be useful to optimize the material's performance for the automotive industry. The final recommendation is to further analyze the fracture to better understand the cause of the premature failures and then prevent it from occurring.

These changes can be the path needed to develop these steels in a way that they combine toughness, strength, ductility, and reliability. The latter is of extremely importance to the automotive industry as its dos does not allow materials that risk the safety of the vehicle

The research presented in this thesis did not find a suitable material for the automotive industry. However, it shows the potential of these steels to be optimized and result into an outstanding metal for various applications. As a result, further research will most probably develop steels with better proprieties. In addiction this research was important to point the issues on these metals and identify recommendations for further studies, contributing to impulse the development of 3rd generations AHSS and contributing to the literature

Bibliography

1. WANG, M.; HUANG, M. X. Abnormal TRIP effect on the work hardening behavior of a quenching and partitioning steel at high strain rate. Acta Materialia, v. 188, p. 551–559, 15 abr. 2020
2. ALLAIN, S. Y. P. et al. In Situ Investigation of the Iron Carbide Precipitation Process in a Fe-C-Mn-Si Q&P Steel. Materials (Basel, Switzerland), v. 11, n. 7, p. E1087, 26 jun. 2018.
3. SUGIMOTO, K.; MUKHERJEE, M. 8 - TRIP aided and complex phase steels In: RANA, R.; SINGH, S. B. (Eds.). . Automotive Steels. [s.l.] Woodhead Publishing, 2017. p. 217–257.
4. ISMAIL, K. et al. Outstanding cracking resistance of fibrous dual phase steels. Acta Materialia, v. 207, p. 116700, 29 jan. 2021
5. ISMAIL, K. et al. Plastic behavior, damage mechanisms and crack propagation resistance in high-toughness Dual-Phase steels, 20 ago. 2020.
6. XIONG, Z. et al. Characterization and Control of the Compromise Between Tensile Properties and Fracture Toughness in a Quenched and Partitioned Steel. Metallurgical and Materials Transactions A, v. 50, n. 8, p. 3502–3513, ago. 2019.
7. A. Pineau, A.A. Benzerga, T. Pardoen, Failure of metals I: Brittle and ductile fracture, Acta Materialia,
8. PINEAU, A.; BENZERGA, A.; PARDOEN, T. Failure of metals III. Fracture and fatigue of nanostructured metallic materials. Acta Materialia, v. 107, 1 ago. 2015.
9. Zhiping Xiong, Pascal J. Jacques, Astrid Perlade, Thomas Pardoen, Ductile and intergranular brittle fracture in a two-step quenching and partitioning steel, Scripta Materialia,
10. XIONG, Z. et al. Ductile and intergranular brittle fracture in a two-step quenching and partitioning steel. Scripta Materialia, v. 157, p. 6–9, 1 dez. 2018.
11. ISMAIL, K. et al. Outstanding cracking resistance of fibrous dual phase steels. Acta Materialia, v. 207, p. 116700, 29 jan. 2021.
12. AYDIN, H. et al. Development of 3rd generation AHSS with medium Mn content alloying compositions. Materials Science and Engineering. A, Structural Materials: Properties, Microstructure and Processing, v. 564, 1 mar. 2013.
13. CAI, Z. et al. Austenite stability and deformation behavior in a cold-rolled transformation-induced plasticity steel with medium manganese content. Acta

Materialia, v. 84, p. 229–236, 1 fev. 2015

14. Phase Transformations, Volume 12 - 1st Edition. Disponível em: <https://www.elsevier.com/books/phase-transformations/banerjee/978-0-08-042145-2>. Acesso em: 29 dez. 2021
15. BLECK, W.; GUO, X.; MA, Y. The TRIP Effect and Its Application in Cold Formable Sheet Steels. steel research international, v. 88, n. 10, p. 1700218, 2017.Mehran Maalekian, The Effects of Alloying Elements on Steels (I), Technische Universität Graz,2007
16. MAALEKIAN, M. The Effects of Alloying Elements on Steels. p. 36, [s.d.].
17. OLSON, G. B.; COHEN, M. A mechanism for the strain-induced nucleation of martensitic transformations. Journal of the Less Common Metals, v. 28, n. 1, p. 107–118, 1 jul. 1972
18. Phase Diagrams, TTT plots & CCT diagrams. Disponível em: <https://callumjodwyer.wixsite.com/beng-project/phase-diagrams>. Acesso em: 25 jun. 2021.
19. Phase Transformations in Steels - 1st Edition. Disponível em: <https://www.elsevier.com/books/phase-transformations-in-steels/pereloma/978-1-84569-970-3>. Acesso em: 25 jun. 2021
20. ZHOU, S. et al. Investigation on High Strength Hot-rolled Plates by Quenching-partitioning-tempering Process Suitable for Engineering. ISIJ International, v. 51, p. 1688–1695, 14 out. 2011
21. Özdemir, Zafer. (2014). Heat treatment effects to the fracture splitting parameters of C70S6 connecting rod. Mechanics. 20. 10.5755/j01.mech.20.3.5384.
22. KOSSAKOWSKI, P. Influence of Initial Porosity on Strength Properties of S235JR Steel at Low Stress Triaxiality. Archives of Civil Engineering, v. 58, p. 293–308, 1 set. 2012
23. González-Velázquez, Jorge. (2018). Elements of Fractography. 10.1007/978-3-319-76651-5_2.
24. YASNIKOV, I.; VINOGRADOV, A.; ESTRIN, Y. Revisiting the Considère criterion from the viewpoint of dislocation theory fundamentals. Scripta Materialia, v. 76, p. 37–40, 1 abr. 2014.
25. MORRIS, J. W. Dislocation-controlled Plasticity of Crystalline Materials: Overview. 2001.
26. Editor(s): K.H. Jürgen Buschow, Robert W. Cahn, Merton C. Flemings, Bernhard

Ilschner, Edward J. Kramer, Subhash Mahajan, Patrick Veyssière, Encyclopedia of Materials: Science and Technology, Elsevier, 2001,

27. UIJL, N. J. D.; CARLESS, L. J. 3 - Advanced metal-forming technologies for automotive applications. In: ROWE, J. (Ed.). . Advanced Materials in Automotive Engineering. [s.l.] Woodhead Publishing, 2012. p. 28–56.
28. E. Doege, T. Hallfeld, Metal Working: Stretching of Sheets, Editor(s): K.H. Jürgen Buschow, Robert W. Cahn, Merton C. Flemings, Bernhard Ilschner, Edward J. Kramer, Subhash Mahajan, Patrick Veyssière, Encyclopedia of Materials: Science and Technology, Elsevier, 2001,
29. SOBOYEJO, W. Mechanical Properties of Engineered Materials. New York: CRC Press, 2002.
30. GRAJCAR, A.; KOZŁOWSKA, A.; GRZEGORCZYK, B. Strain Hardening Behavior and Microstructure Evolution of High-Manganese Steel Subjected to Interrupted Tensile Tests. Metals, v. 8, n. 2, p. 122, fev. 2018.
31. OPIELA, M. et al. Effect of Grain Size on the Microstructure and Strain Hardening Behavior of Solution Heat-Treated Low-C High-Mn Steel. Materials (Basel, Switzerland), v. 13, n. 7, p. E1489, 25 mar. 2020.
32. TRZEPIECIŃSKI, T. Recent Developments and Trends in Sheet Metal Forming. Metals, v. 10, n. 6, p. 779, jun. 2020.
33. Waltl, H., Vette, W. and Griesbach, B. (2007) Tool-Making for Future Car Bodies, IDDRG'2007, 21–23 May, GyĘr, Hungary, pp.31–44.
34. LI, B. L. et al. Microstructural evolution of IF-steel during cold rolling. Acta Materialia, v. 52, n. 4, p. 1069–1081, fev. 2004.
35. AHMAD, E. et al. Effect of cold rolling and annealing on the grain refinement of low alloy steel. IOP Conference Series: Materials Science and Engineering, v. 60, p. 012029, 17 jun. 2014.
36. What is "Cold Rolling" Stainless Steel and Other Metals? | Ulbrich. Disponível em: <https://www.ulbrich.com/blog/what-is-cold-rolling-stainless-steel-and-other-metals/>. Acesso em: 25 jun. 2021.
37. KRIZAN, D. et al. DEVELOPMENT OF THIRD GENERATION ADVANCED HIGH STRENGTH STEELS FOR AUTOMOTIVE APPLICATIONS. 22 nov. 2018.
38. CHANG, Y. et al. An introduction to medium-Mn steel: Metallurgy, mechanical properties and warm stamping process. Materials & Design, v. 94, p. 424–432, 15 mar. 2016.

39. SUGIMOTO, K.; HOJO, T.; KOBAYASHI, J. Critical assessment 29: TRIP-aided bainitic ferrite steels. Materials Science and Technology, v. 33, n. 17, p. 2005–2009, 22 nov. 2017.
40. SUGIMOTO, K. et al. Ductility of 0.1-0.6C-1.5Si1.5Mn Ultra High-strength TRIP-aided Sheet Steels with Bainitic Ferrite Matrix. Isij International - ISIJ INT, v. 44, p. 1608–1614, 1 jan. 2004
41. WANG, L.; SPEER, J. G. Quenching and Partitioning Steel Heat Treatment. Metallography, Microstructure, and Analysis, v. 2, n. 4, p. 268–281, 1 ago. 2013.
42. YI, H. L.; LEE, K. Y.; BHADESHIA, H. K. D. H. Mechanical stabilisation of retained austenite in δ-TRIP steel. Materials Science & Engineering A, v. 18, n. 528, p. 5900–5903, 2011.
43. KAH, P. Efficient Welding Technologies Applicable to HSS Arctic Offshore Structures. [s.d.].
44. RUGGIERI, C. Numerical investigation of constraint effects on ductile fracture in tensile specimens. Journal of the Brazilian Society of Mechanical Sciences and Engineering, v. 26, p. 190–199, jun. 2004.
45. HANZAKI, A. Z.; HODGSON, P. D.; YUE, S. Retained austenite characteristics in thermomechanically processed Si-Mn transformation-induced plasticity steels. Metallurgical and Materials Transactions A, v. 28, n. 11, p. 2405–2414, 1 nov. 1997.
46. JIA, N. et al. Nanoscale spheroidized cementite induced ultrahigh strength-ductility combination in innovatively processed ultrafine-grained low alloy medium-carbon steel. Scientific Reports, v. 7, n. 1, p. 2679, 2 jun. 2017.
47. KUZIAK, R.; KAWALLA, R.; WAENGLER, S. Advanced high strength steels for automotive industry: A review. Archives of Civil and Mechanical Engineering, v. 8, p. 103–117, 31 dez. 2008.
48. KUZIAK, R.; KAWALLA, R.; WAENGLER, S. Advanced high strength steels for automotive industry. Archives of Civil and Mechanical Engineering, v. 8, n. 2, p. 103–117, 1 jan. 2008.
49. ZHAO, J.; JIANG, Z. Thermomechanical processing of advanced high strength steels. Faculty of Engineering and Information Sciences - Papers: Part B, p. 174–242, 1 jan. 2018.
50. Progress in Materials Science - Journal - Elsevier. Disponível em: <https://www.journals.elsevier.com/journals.elsevier.com/progress-in-materials-science>. Acesso em: 29 dez. 2021.

51. CODERMAN, N. J.-. Advanced High Strength Steel (AHSS) for Stronger, Lighter and Safer Cars - Materials and Engineering Resources - MatmatchMaterials and Engineering Resources - Matmatch - Get the latest in materials science and engineering news, educational content and material use cases., 3 jun. 2019. Disponível em: <https://matmatch.com/resources/blog/advanced-high-strength-steel-stronger-lighter-safer-cars/>. Acesso em: 29 dez. 2021
52. YI, H. L.; CHEN, P.; BHADESHIA, H. K. D. H. Optimizing the Morphology and Stability of Retained Austenite in a δ-TRIP Steel. Metallurgical and Materials Transactions A, v. 45, n. 8, p. 3512–3518, 1 jul. 2014
53. SHIRI, S. G. et al. THE FAILIUR ANALYSIS OF Nb-MICROALLOYED δ-TRIP STEEL. p. 15, [s.d.].
54. WANG, J. et al. Tailoring Strength and Ductility of a Cr-Containing High Carbon Steel by Cold-Working and Annealing. Materials, v. 12, n. 24, p. 4136, jan. 2019.
55. ZHAO, J.; JIANG, Z. Thermomechanical processing of advanced high strength steels. Progress in Materials Science, v. 94, p. 174–242, 2018.
56. ZHU, K. et al. The effect of prior ferrite formation on bainite and martensite transformation kinetics in advanced high-strength steels. Acta Materialia, v. 61, n. 16, p. 6025–6036, 1 set. 2013.
57. AN, F.-C. et al. Tailoring cementite precipitation and mechanical properties of quenched and tempered steel by nickel partitioning between cementite and ferrite. Materials Science and Engineering: A, v. 802, p. 140686, 20 jan. 2021.
58. LEE, S.; DE COOMAN, B. C. On the Selection of the Optimal Intercritical Annealing Temperature for Medium Mn TRIP Steel. Metallurgical and Materials Transactions A, v. 44, n. 11, p. 5018–5024, 1 nov. 2013.
59. SHIBANUMA, K.; AIHARA, S.; SUZUKI, K. Prediction model on cleavage fracture initiation in steels having ferrite–cementite microstructures – Part I: Model presentation. Engineering Fracture Mechanics, v. 151, p. 161–180, 1 jan. 2016.
60. MOURITZ, A. P. (ED.). 19 - Fracture toughness properties of aerospace materials. In: Introduction to Aerospace Materials. [s.l.] Woodhead Publishing, 2012. p. 454–468
61. DODD, B.; BODDINGTON, P. The causes of edge cracking in cold rolling. Journal of Mechanical Working Technology, v. 3, n. 3, p. 239–252, 1 jan. 1980. .
62. HANCE, B. Advanced High-Strength Steel (AHSS) Performance Level Definitions and Targets. SAE International Journal of Materials and

Manufacturing, v. 11, n. 4, p. 505–516, 3 abr. 2018.

63. Austenite Martensite Bainite Pearlite and Ferrite structures. Disponível em: <https://www.twi-global.com/technical-knowledge/faqs/faq-what-are-the-microstructural-constituents-austenite-martensite-bainite-pearlite-and-ferrite.aspx>. Acesso em: 30 jul. 2021.
64. MAYR, P. et al. Formation of Delta Ferrite in 9 Wt Pct Cr Steel Investigated by In-Situ X-Ray Diffraction Using Synchrotron Radiation. Metallurgical and Materials Transactions A, v. 41, n. 10, p. 2462–2465, 1 out. 2010.
65. GAO, S. et al. Tensile Deformation of Ultrafine-Grained Fe-Mn-Al-Ni-C Alloy Studied by In Situ Synchrotron Radiation X-ray Diffraction. Crystals, v. 10, n. 12, p. 1115, dez. 2020.
66. LI, W.-L.; LI, J. C. M. The effect of grain size on fracture toughness. Philosophical Magazine A, v. 59, n. 6, p. 1245–1261, 1 jun. 1989.
67. MORRIS JR., J. W. The influence of grain size on the mechanical properties of steel. 1 maio 2001.
68. LIANG, N. et al. Effect of grain structure on Charpy impact behavior of copper. Scientific Reports, v. 7, n. 1, p. 44783, 17 mar. 2017.
69. ABID, N. H.; ABU AL-RUB, R. K.; PALAZOTTO, A. N. Computational modeling of the effect of equiaxed heterogeneous microstructures on strength and ductility of dual phase steels. Computational Materials Science, v. 103, p. 20–37, 1 jun. 2015.
70. ABID, N. H.; ABU AL-RUB, R. K.; PALAZOTTO, A. N. Micromechanical finite element analysis of the effects of martensite morphology on the overall mechanical behavior of dual phase steel. International Journal of Solids and Structures, v. 104–105, p. 8–24, 1 jan. 2017.

Universidade de São Paulo

Engenharia de Petróleo – Escola Politécnica

Número: 9835602 USP **Data: 22/11/2021**

DEVELOPMENT OF 3RD GENERATION STEEL COMBINING HIGH TOUGHNESS AND STRENGTH FOR PETROLEUM AND AUTOMOTIVE APPLICATIONS

Rodrigo Gianni Ferreira

Orientador: Prof. Pascal Jacques

Artigo Sumário referente à disciplina PMI3349 – Trabalho de Conclusão de Curso II
Este artigo foi preparado como requisito para completar o curso de Engenharia de Petróleo na Escola Politécnica da USP. Template versão 2021v01.

Abstract

Weight reduction was Always an objective to the automotive industry to reduce production costs and fuels consumption. The petroleum industry is also avid for new developments as it is always looking for the cutting-edge developments on materials to be used. These are the motivations to develop the 3rd generation advanced high strength steels (AHSS) to combine high toughness strength and ductility.

The developed materials presented an outstanding potential to combine the desired proprieties, having interesting proprieties and two main microstructures related to the annealing temperature, one containing ferrite, bainite and retained austenite (presenting TRIP effects) for 750°C and the other containing ferrite and cementite for 700°C. The steels presented remarkable mechanical proprieties such as an ultimate tensile stress up to 1327,23 MPa and uniform elongation up to 23,11%.

Resumo

A redução do peso sempre foi um objetivo para a indústria automotiva, a fim de reduzir custos de produção e consumo de combustíveis. A indústria do petróleo também e avida por novas desenvolvimento já que está sempre à procura de matérias de ponta para serem utilizados. Deste modo, motivando a indústria a desenvolver os metais avançados de alta resistência de terceira geração (AHSS do inglês) combinando tenacidade, resistência e ductilidade.

Os materiais desenvolvidos apresentaram um excepcional potencial para combinar todas essas propriedades desejadas, tendo propriedade interresantes e duas principais microestruturas relacionadas a temperatura de recozimento, uma contendo ferrita, bainita e austenita retida (apresentando efeitos TRIP) para 750°C, e outra contendo ferrita e cementita para 700°C. Os metais apresentaram propriedades mecânicas notáveis como uma tensão de tração máxima de até 1327,23 Mpa e um alongamento uniforme de até 23,11%.

1. Introduction

The weight of vehicles is directly related to fuels consumption and the emission of greenhouse gasses, as reducing the weight reduces the fuel consumption on an average on 4,9% for each 10% reduction on the total weight . Steels are the most utilized material on cars, applied on doors, chassis, and support beans and therefore are the first target to weight reduction. But reducing the amount of steel on a vehicle comes with safety problem, a decrease of 100 kg can cause an increase of the safety risk of 3 to 4,5% . This incentivizes the development of more efficient steels that can stand the same load with smaller amounts of material and therefore, reduce weight while maintaining the vehicle’s safety.

Improving the metal's proprieties can also be of use to the petroleum industry for many applications, such as drill pipes, drill collars, drill bits or any other application that benefits from high resistance and weight reduction. These proprieties combined could reduce costs and facilitated the maneuver od the equipment on the drilling sites. Culminating on time savings, that is a main target on the industry

Toughness and strength are generally correlated on mild steels and conventional high strength steels (HSS. With increasing elongations, the metal present lower tensile strength and with increasing tensile strength the maximum elongation is reduced. This causes optimization problems as different types of steels will be best suited for each application, materials with high total elongations can be utilized on deep drawing manufacturing but the produced parts cannot be utilized for applications that demand higher toughness such car crashes. To fulfil the need of an easy to shape steel that can also be utilized for high strength applications the AHSS can be used to optimize both once contradictory proprieties. Three AHSS family can be separated on three generations.

The 1st generation AHSS is includes Dual-Phase steels (DP), transformation induced plasticity steels (TRIP), complex phase steel (CP) and martensitic steel (MS). These steel types mainly present more than one phase, and its proprieties results from the combination of the advantages of each phase

The 2nd generation AHSS includes the Twinning Induced Plasticity steels (TWIP) , Nano-TWIP, Duplex and Triplex steels. These steels present outstanding mechanical properties, with both high total elongation and tensile strength. But their Mn content is very high, exceeding 15 Wt% causing then to be considerably more expensive and therefore economically unviable for the automotive industry.

The 3rd generation of AHSS is the ongoing development and is targeting to fill the gap between the 1st and 2nd generations while maintaining an economically viable price. The 3rd generation include the medium Mn steels, TRIP-aided Bainitic Ferrite TBF) , quenching and partitioning steel (Q&P) and δ-TRIP steels.

The goal of this thesis is to investigate the effects of heat treatments and compositions on final microstructure of a 3rd generation steel and its influence on the final mechanical proprieties on the steel and possibly obtain strain hardening with the aid of transformation induced plasticity (TRIP). Targeting the best compromise between toughness, ductility, and strength.

2. Methodology

The study presented here investigated the resulting microstructure on a medium manganese steel with high carbon content and silicon that was submitted to a full austenization at 1000 °C and quenching, followed by Intercritical annealing at either 750 °C or 700 °C for 5 minutes and finally a bainitic maintain at 360 °C using a lead bath for either 15 or 30 minutes. SEM observations were performed to observe the microstructure, succeeded by tensile tests to measure the mechanical proprieties, finally fractography and damage observations were made to evaluate the fracture mechanism and calculate the fracture strain. The composition of the metal is shown on table 1.

Table 1 – Composition of the steel.

Element	Cr	Cu	Fe	Mn	Ni	Si	C^{tot}
%wt	0.01	0.01	96.5	1.45	0.02	1.42	0.48

3. Heat treatments and experiments

3.1. Heat treatments

The Samples were separated in 6 groups, with the details of holding times and temperatues described on table 2. The four groups with the complete heat treatment were each one divided on groups A and B.

Table 2 – Sumary of heat treatments

Intercritical annealing temperature [˚C]	Intercritical annealing holding time [min]	Lead bath temperature [˚C]	Lead bath holding time [min]	group letter	Group name
750	5	360	30	A	750-30
		360	30	B	
750	5	360	15	A	750-15
		360	15	B	
700	5	360	30	A	700-30
		360	30	B	
700	5	360	15	A	700-15
		360	15	B	
750	5	---	---	---	750-00
700	5	---	---	---	700-00

3.2. Experiments

3.2.1. Tensile test

To evaluate the proprieties such as, uniform elongation, ultimate tensile stress, and yield strength of the heat-treated metals, two tensile specimens from each the four groups with complete heat treatments with target dimensions of 110x6x1 mm were machined. For the tensile test, a Zwick/Roell tensile tester was utilized with speed of 1 mm/min. By coupling the information acquired on the tensile tests it is possible to perform a fractography on the SEM to calculate the fracture strain and even observe the changes in microstructure caused by the tensile test.

3.2.2. Scanning Electron Microscope (SEM)

The characterization of the material's microstructure was done by using the SEM after careful polishing following the specified methods for steel. The images were obtained by using the secondary electrons signal (SE2), 15 Kv of electron high tension (ETH) and rolling direction of images represented on the horizontal axis. The SEM was also utilized to evaluate the fracture surface and damage observations

3.2.3. X-Ray Diffraction (XRD)

To determine the material's composition, the XRD was utilized with a cobalt source and angles between 26° and 120°. Also using the database is possible to identify the phases based on the observed peaks.

4. Results

This section targets to show the resulting microstructures before and after the tests, the materials proprieties obtained at the tensile test as well as the way the metal suffered fracture.

4.1. Tensile tests

The information obtained during the tensile tests are plotted on Figure 1 and Figure 2 as engineering stress/strain curves and true stress/strain curves, respectively.

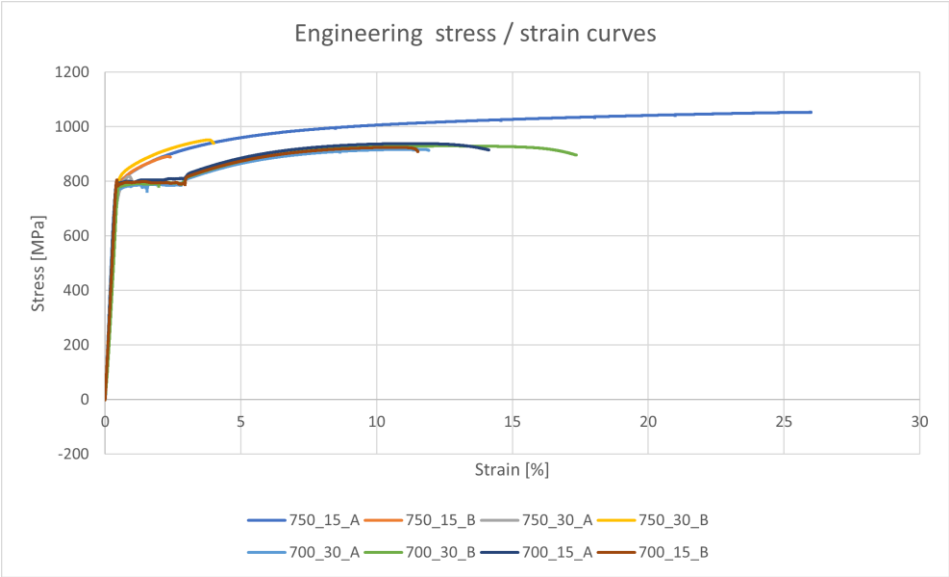

Figure 1 - Experimental engineering stress-strain curves of the steels

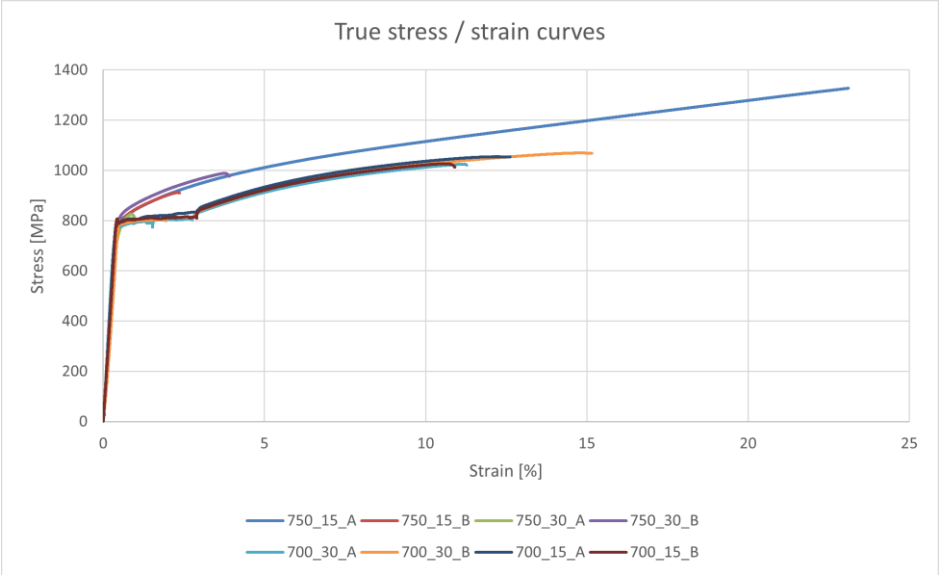

Figure 2 - Experimental true stress-strain curves of the steels

From the curves it is possible to extract some of the material properties of each sample. Ultimate tensile stress, yield strength and uniform elongations are presented on Table 3

Table 3 – Properties of tensile test samples

	ultimate tensile stress [MPa]	yield strength [MPa]	uniform elongation [%]	Product UTS X UE [Mpa . %]
750-30-A	805.21	760.81	0.99	800.68
750-30-B	976.46	811.28	3.92	3829.14
750-15-A	1327.23	799.25	23.11	30672.47
750-15-B	909.96	777.69	2.37	2157.51
700-30-A	1021.84	804.17	11.27	11514.70
700-30-B	1051.76	806.17	15.15	15938.50
700-15-A	1044.51	807.14	12.62	13178.35
700-15-B	1012.97	808.20	10.90	11041.13

From thse results it is possible to determine that the best performing samples are the 750-15-A and 700-30-B. Therefore, fot the following results these are the samples that will be more deeply described.

4.2. Microstructures, Fracture and Damage

By using the SEM it was possible to obtain the microstructures of the samples, with the microstructures oh samples 750-15 and 700-30 shown on Figure 3. On samples 750-15 it is possible to observe a lamellar structure with two different phases That were confirmed to be ferrite and austenite by and XDR. But 700-30 present very similar lamellar shaped grains with spheres at the grain boundaries, the XDR was also used to characterize the phases present on this samples and conclude that the grains are ferrite, and the spheres are cementite.

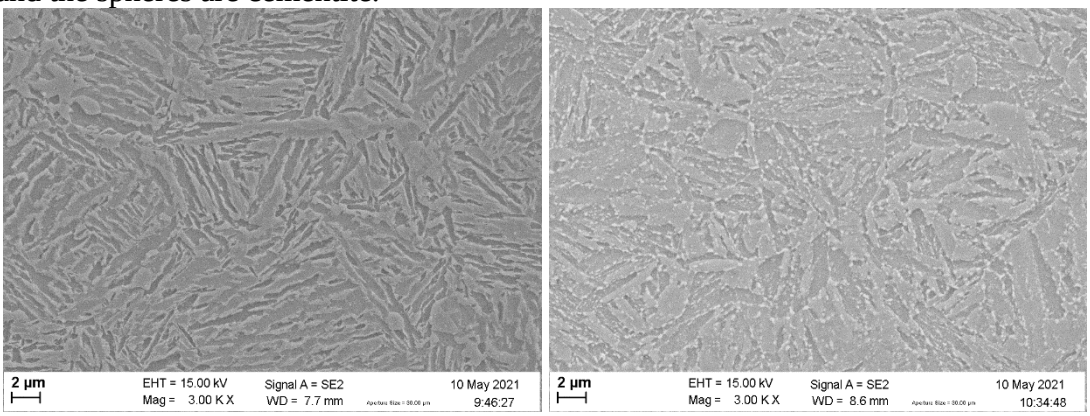

Figure 3 - Microstructures for 750-15 (left) and 700-30 (right)

On 750-15 that was annealed at 750°C a possible route for the formation of the microstructure is that during the Intercritical annealing, ferrite and austenite were formed keeping the fibrous structure from the martensite, after that, during the bainitic maintain, the carbon present in the C-rich austenite diffuses and forms ferrite and cementite (forming the bainite) while the austenite gets its carbon content reduced, stabilizing it into retained austenite.

For sample 700-30 a possible route is that the martensite started transforming at the grain boundaries into ferrite and cementite and assumed this structure after quenching.

When comparing to similar studies, it was concluded that the fibrous structure indeed improved the materials properties, increasing the product UTS X UE and therefore, that the step of fully austenizing and quenching to form a martensite substructure to produce a final product with that structure can contribute for an improvement on the mechanical properties.

After the tensile tests were performed, fracture and damage observations were made, a fracture surface analysis was made (shown in Figure 4). And by measuring the strain on each direction, the fracture strain could be calculated and are shown on Table 4.

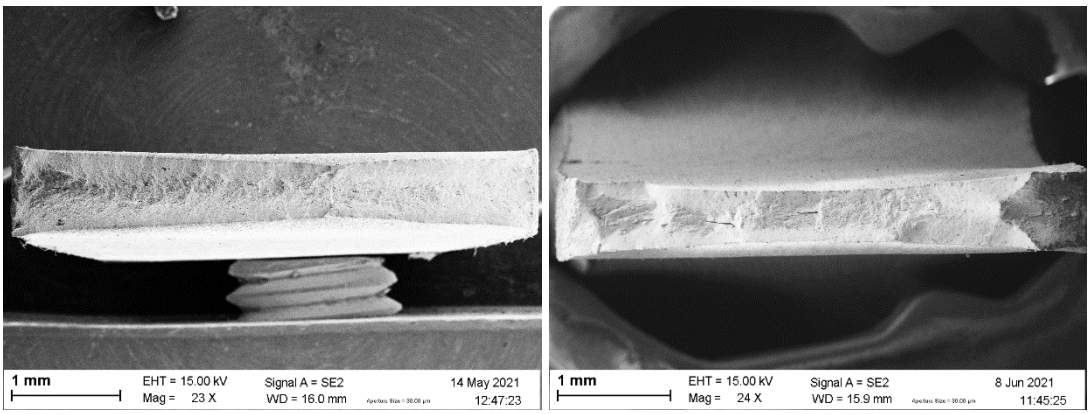

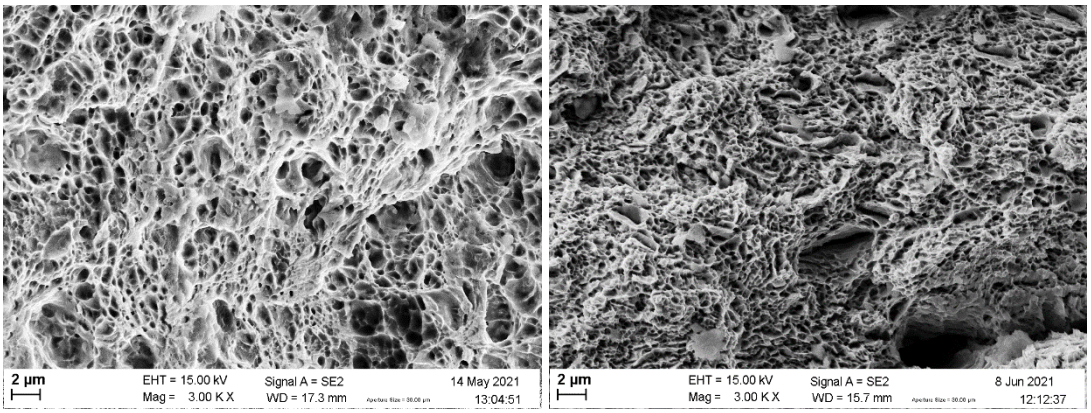

Figure 4 – Fracture surfaces for 750-15-A (left) and 700-30-B (right)

750-15–A was the best performing sample, and it can be observed that its fracture was purely ductile, with a considerable necking and a fracture creating a 45° angle slant . This sample also presents porosities that are slightly increased on the sample's center, but the samples is still consistent through the width. The observed dimples are on average 1 micron in diameter ,again consistent with the lamellas thickness.

The sample 700-30-B presented similar void density and size when compared to the sample annealed at 750 °C, the main difference is on the dimples size that ate on average 0,7 microns on diameter.

Table 4 – Calculate fracture strain

	Ef [-]
750 15 A	0.970858
700 30 B	1.172651

Both samples presented considerably high fracture strain when compared to the literature, highlighting the outstanding potential of these metals.

Also utilizing the SEM, the microstructure near the fracture surface was evaluated to identify damage and changes in microstructure caused by the tensile test as shown on Figure 5.

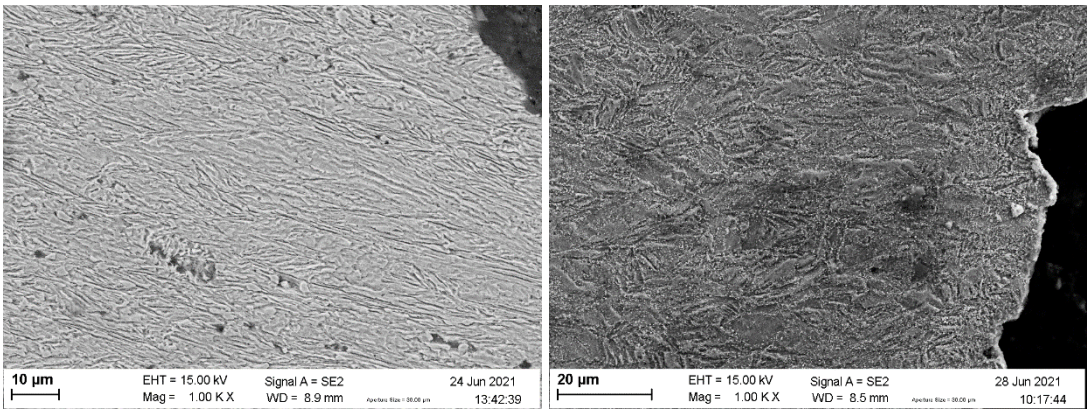

Figure 5 – Microstructures after the tensile test for 750-15-A (left) and 700-30-B (right).

Sample 750-15-A presents voids nucleated near the fracture surface, that are not present far from that region, and a high grain alignment with the tensile direction. This characterizes a large change on the original microstructure. This is coherent as this is the best performing sample on the tensile test because

the alignment sets the weak points to void nucleation (grain boundaries) on a perpendicular direction with the tensile direction.

Sample 700-30-B had voids nucleating near the fracture surface but with minor alignment of the grains with the tensile direction or changes on the microstructure.

With the information obtained on the tensile tests, it is possible to plot the elongation versus the tensile strength on both discussed metals to compare then with the existing 3rd generation AHSS (shown on figure 6).

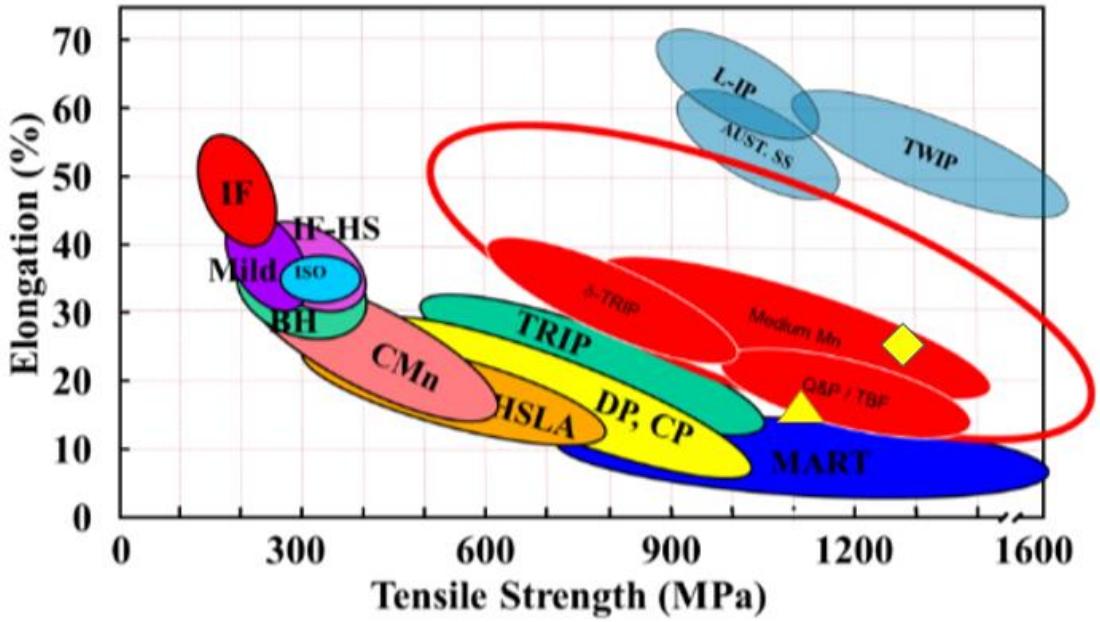

Figure 6 – Mechanical proprieties of steels with highlighted area for 3rd generation steels development (modified from Krizan et al.) including the best performing sample for each annealing temperature (diamond for 750-15-A and triangle for 700-30-B)

By plotting the properties of the best performing samples on Figure 6, one can conclude that the 750-15 have the properties of a medium Mn steel and can be considered part of the developing 3rd generation of AHSS, with both high toughness and high strength. On the other hand, 700-30 and have mechanical properties that barely compared to Q&P and TBF steels but can still be considered part of the 3rd generation of AHSS.

5. Conclusions

The obtained metals are compatible with the literature for the development of 3rd generation AHSS, presenting a great combination of once contradictory mechanical properties of toughness strength and ductility. This study also concluded that the fibrous morphology in fact improves the mechanical properties on the evaluated metals.

750-15-A highlights the potential of this material, presenting an ultimate tensile strength of 1327,23 MPa and uniform elongation of 23,11%. An outstanding combination of toughness and strength. While 700-30-B has a great potential as a material, presenting an ultimate tensile strength of 1051,76 MPa and uniform elongation of 15,15%.

6. References

Progress in Materials Science, Volume 94, 2018, Pages 174-242, ISSN 0079-6425, https://doi.org/10.1016/j.pmatsci.2018.01.006.

D. Krizan, K. Steineder, S. Kaar, T. Hebesberger: Development of third generation advanced high strengthsteels for automotive applications, 19th International Conference Transfer 2018, Trencianske Teplice,Slovakia, 2018. (PDF) PHYSICAL METALLURGY OF BATCH ANNEALED MEDIUM-MN STEELS FOR AUTOMOTIVE APPLICATIONS. Available from: https://www.researchgate.net/publication/337323898_PHYSICAL_METALLURGY_OF_BATCH_ANNEALED_MEDIUM-MN_STEELS_FOR_AUTOMOTIVE_APPLICATIONS [accessed Jun 27 2021].

Karim Ismail, Astrid Perlade, Pascal J. Jacques, Thomas Pardoen, Outstanding cracking resistance of fibrous dual phase steels, Acta Materialia, Volume 207, 2021

Yi, H.L., Chen, P. & Bhadeshia, H.K.D.H. Optimizing the Morphology and Stability of Retained Austenite in a δ-TRIP Steel. Metall Mater Trans A 45, 3512–3518 (2014). https://doi.org/10.1007/s11661-014-2267-4

Xiong Zhiping, Jacques Pascal J., Perlade Astrid, Pardoen, Thomas, 2020/07/01,On the sensitivity of fracture mechanism to stress concentration configuration in a two-step quenching and partitioning steel, International Journal of Fracture

Jia, N., Shen, Y.F., Liang, J.W. et al. Nanoscale spheroidized cementite induced ultrahigh strength-ductility combination in innovatively processed ultrafine-grained low alloy medium-carbon steel. Sci Rep 7, 2679 (2017). https://doi.org/10.1038/s41598-017-02920-9

F.-C. An, J.-J. Wang, S.-X. Zhao, C.-M. Liu, Tailoring cementite precipitation and mechanical properties of quenched and tempered steel by nickel partitioning between cementite and ferrite, Materials Science and Engineering: A, Volume 802, 2021, 140686, ISSN 0921-5093, https://doi.org/10.1016/j.msea.2020.140686.